

**PREPARATION OF INDIUM  
TELLURIDE THIN FILMS FOR DEVICE  
APPLICATIONS**

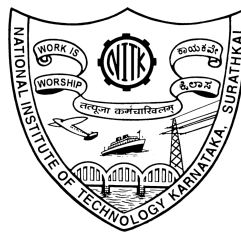
Thesis

Submitted in partial fulfilment of the requirements for the degree  
of

**DOCTOR OF PHILOSOPHY**

by

**VALLEM SOWJANYA**



**DEPARTMENT OF PHYSICS  
NATIONAL INSTITUTE OF TECHNOLOGY  
KARNATAKA,  
SURATHKAL, MANGALORE -575025**

**July, 2019**

## **DECLARATION**

*by the Ph.D. Research Scholar*

I hereby *declare* that the Research Thesis entitled **“Preparation of indium telluride thin films for device applications”** Which is being submitted to the National Institute of Technology Karnataka, Surathkal in partial fulfilment of the requirements for the award of the Degree of **Doctor of Philosophy in Physics** is a *bonafide report of the research work carried out by me*. The material contained in this Research Synopsis has not been submitted to any University or Institution for the award of any degree.

Vallem Sowjanya  
(**Reg.No.:145065PH14F04**)  
Department of Physics

Place: NITK-Surathkal

Date:

## CERTIFICATE

This is to *certify* that the Research thesis entitled **Preparation of indium telluride thin films for device applications** submitted by **Vallem Sowjanya** (Register Number:**145065PH14F04**) as the record of the research work carried out by her, is *accepted as the Research Thesis submission* in partial fulfilment of the requirements for the award of degree of **Doctor of Philosophy**.

Research Guide(s)

Prof. Kasturi V. Bangera

(Signature with Date and Seal)

Chairman - DRPC

(Signature with Date and Seal)

## ACKNOWLEDGEMENT

I would like to express my sincere thanks to numerous people who have helped and supported during my Ph.D.

Foremost, I wish like to express my gratitude to Prof. (Mrs.) Kasturi V. Bangera who has helped and encouraged in all stages of my Ph.D. work with great patience and immerse care. Her guidance helped me a lot in all the time of research and thesis writing. Similar profound goes to Prof. G. K. Shivakumar, who has given valuable suggestions and advices to explore my knowledge.

Besides my advisor, I would like to thank the members of RPAC Dr. Ajith A. K. and Dr. Vidya Shetty. K, for their insightful comments and encouragement.

I am grateful to National Institute of Technology Karnataka and Ministry of Human Resource Development (India) for favourable working environment and financial assistance.

I would like to thank my research colleagues, Dr. Santhosh T.C.M, Dr. Veena E, Mr. Biswajit Barman, Mr. Bharath S. P., Miss. Subhasmitha ray and Dr. Shashidhar for their help, encouragement and best wishes.

My sincere thanks to HOD, all faculty members, staff and research students of Physics department for their support throughout my work.

My heart-felt gratitude to Dr. Murali Reddy G. and Prof. Shreedhara Reddy P, who are my mentors and encouraged me to step into research.

I owe my special thanks to my sibling Mr. Vijay kumar Reddy V., my parents Santi Reddy and Indira Devi, for their continuous support and encouragement during this study and throughout the life which made me to focus on goals and dreams. I would like to thank my husband Mr. Raviteja Reddy S, for support and encouragement.

There are many persons to whom I would like to express my gratitude. Although, I did not mention their names here, their help will never be forgotten.

Vallem Sowjanya



## ABSTRACT

The main objectives of this thesis work are to attain device quality of indium telluride ( $\text{In}_2\text{Te}_3$  and  $\text{InTe}$ ) thin films using thermal evaporation technique and to evaluate the suitability of these films for device applications. The key motivation point to this investigation is that these materials are exhibiting similar type of structures, band gaps, lattice constants and chemically compatible with traditional semiconductors such as III-V, II-VI and VI group compounds. The annealing temperature played a major role to get mono-phased and stoichiometric  $\text{In}_2\text{Te}_3$  and  $\text{InTe}$  films. Hence, all the films were prepared at different substrate temperatures and annealed at optimized temperature and variations in the properties of these films were reported. The optical band gap and electrical conductivity of  $\text{In}_2\text{Te}_3$  films were found to be  $0.99 \pm 0.02$  eV and  $10^{-1} \Omega^{-1}\text{cm}^{-1}$  respectively. Moreover, these films have shown 90% of transmittance in IR region. The optical band gap of  $\text{InTe}$  films was varied from 1.61 eV to 1.42 eV with an increase in the substrate temperature from 298 K to 473 K. The electrical conductivity of  $\text{InTe}$  films was found of the order of  $10^1 \Omega^{-1}\text{cm}^{-1}$ . The absorption coefficient of  $\text{InTe}$  films was found to be of the order of  $10^6 \text{cm}^{-1}$ . The optical properties accompanied with electrical properties of indium telluride films makes them suitable for absorbent layer in photovoltaic cells.

Thermoelectric properties need specific requirements such as high seebeck coefficient with good electrical conductivity and low thermal conductivity. Accordingly, growth parameters were optimized by varying substrate temperature and thickness to investigate the thermoelectric properties. The  $\text{In}_2\text{Te}_3$  films shown good thermoelectric properties when compared with  $\text{InTe}$  films with maximum thermoelectric power of  $27 \mu \text{W m}^{-1} \text{K}^{-2}$  at 450 K. To enhance thermoelectric power, various dopants such as Bi,  $\text{Sb}_2\text{Te}_3$ , Al, Sb, Se and Te were added in the range of 1-7 at% separately. The 3 % Se doping enhanced the power factor of  $\text{In}_2\text{Te}_3$  films by 14 times which in turn 4.7 times greater than  $\text{Sb}_2\text{Te}_3$  films. Finally, heterojunctions of n-Si/ $\text{In}_2\text{Te}_3$  and n-Si/ $\text{InTe}$  were fabricated and interface properties were studied to understand the performance of indium telluride in opto-electronic devices. Among all diodes, as-deposited n-Si/ $\text{In}_2\text{Te}_3$

heterojunction had higher rectification ratio of 61.2 at  $\pm 5V$  with affordable barrier heights of 0.11 eV which allows easy carrier transport across the barrier.

Keywords: Indium telluride, thermal evaporation, doping, thermoelectric properties and heterojunctions.

## CONTENTS

	<b>Page No.</b>
<b>CHAPTER 1 INTRODUCTION</b>	
1.1 Thin film technology .....	1
1.2 Compound semiconductors .....	2
1.3 III-VI compound semiconductors (Indium telluride) .....	4
1.4 Literature review .....	7
1.5 Scope and objectives .....	13
<b>CHAPTER 2 EXPERIMENTAL METHODS AND CHARACTERIZATION</b>	
2.1 Preparation technique .....	15
2.1.1 Physical methods .....	15
2.1.2 Chemical methods .....	20
2.2 Thickness measurement methods .....	23
2.3 Characterisation .....	25
2.3.1 Structural and compositional characterization .....	25
2.3.2 Electrical Characterization .....	28
2.3.3 Optical Characterization .....	30
<b>CHAPTER 3 OPTIMIZATION AND PROPERTIES OF INDIUM TELLURIDE THIN FILMS</b>	
3.1 Introduction .....	32
3.2 Structure and composition of the source materials .....	33
3.3 Preparation of In <sub>2</sub> Te <sub>3</sub> thin films .....	35
3.3.1 Growth conditions of In <sub>2</sub> Te <sub>3</sub> thin films .....	35

3.3.2 Optimisation of growth parameters for stoichiometric In <sub>2</sub> Te <sub>3</sub> films .....	36
3.3.3 Effect of substrate temperature on the properties of In <sub>2</sub> Te <sub>3</sub> films .....	39
3.4 Preparation of InTe thin films .....	43
3.4.1 Growth conditions of InTe thin films .....	43
3.4.2 Optimisation of growth parameters for stoichiometric InTe films .....	43
3.4.3 Effect of substrate temperature on the properties of InTe films .....	45

## **CHAPTER 4 THERMOELECTRIC PROPERTIES OF INDIUM TELLURIDE THIN FILMS**

4.1 Introduction .....	51
4.2 Thermoelectric properties of In <sub>2</sub> Te <sub>2</sub> thin films .....	53
4.2.1 Growth conditions and optimisation .....	53
4.2.2 Structural and thermoelectric properties of In <sub>2</sub> Te <sub>3</sub> films...	54
4.3 Thermoelectric properties of doped In <sub>2</sub> Te <sub>3</sub> thin films .....	59
4.3.1 Growth conditions of doped In <sub>2</sub> Te <sub>3</sub> thin films .....	59
4.3.2 Bi doped In <sub>2</sub> Te <sub>2</sub> thin films .....	60
4.3.3 (a) Sb <sub>2</sub> Te <sub>3</sub> doped In <sub>2</sub> Te <sub>2</sub> thin films .....	64
(b) Sb <sub>2</sub> Te <sub>3</sub> alloyed In <sub>2</sub> Te <sub>2</sub> thin films.....	67
4.3.4 Al doped In <sub>2</sub> Te <sub>2</sub> thin films .....	71
4.3.5 Sb doped In <sub>2</sub> Te <sub>2</sub> thin films .....	75
4.3.6 Se doped In <sub>2</sub> Te <sub>2</sub> thin films .....	79
4.3.7 Te doped In <sub>2</sub> Te <sub>2</sub> thin films .....	83
4.4 Thermoelectric properties of doped InTe thin films .....	87
4.4.1 Growth conditions and optimisation .....	87
4.4.2 Structural and thermoelectric properties of InTe films .....	87

## **CHAPTER 5 Si-In<sub>2</sub>Te<sub>3</sub> AND Si-InTe THIN FILM HETEROJUNCTIONS**

5.1 Introduction .....	91
5.2 Si-In <sub>2</sub> Te <sub>3</sub> heterojunction .....	92
5.2.1 Optimisation of growth conditions .....	92
5.2.2 I-V-T characteristics of Si-In <sub>2</sub> Te <sub>3</sub> heterojunction .....	93
5.3 Si-InTe heterojunction .....	99
5.3.1 Optimisation of growth conditions .....	99
5.3.2 I-V-T characteristics of Si-InTe heterojunction .....	99

## **CHAPTER 6 SUMMARY AND CONCLUSIONS**

6.1 Summary of the present work .....	105
6.2 Conclusions of the present work .....	105
6.2.1 Stoichiometric and mono-phased indium telluride thin films.....	105
6.2.2 Thermoelectric properties of indium telluride thin films.	106
6.2.3 Junction properties of Si-indium telluride interface.....	109
6.3 Scope for the future work .....	110

<b>REFERENCES</b> .....	111
-------------------------	-----

## **PUBLICATIONS**

## **CURCULUM VITAE**

## LIST OF FIGURES

	<b>Page No.</b>
<b>Figure 2.1</b> Schematic diagram of thermal evaporation system.....	16
<b>Figure 2.2</b> Photographs of thermal evaporation systems used to deposit, (a) $\text{In}_2\text{Te}_3$ films and (b) InTe films.....	17
<b>Figure 2.3</b> A representative image for cross sectional SEM image for 350 nm thickness film.....	24
<b>Figure 2.4</b> RIGAKU x-ray diffractometer .....	25
<b>Figure 2.5</b> ZEISS field emission scanning electron microscope .....	27
<b>Figure 2.6</b> Schematic diagram of the thermo emf measurement set up.....	30
<b>Figure 2.8</b> Shimadzu UV-VIS-NIR spectrophotometer.....	31
<b>Figure 3.1</b> XRD patterns of powdered bulk (a). $\text{In}_2\text{Te}_3$ and (b). InTe materials.....	34
<b>Figure 3.2.</b> EDAX spectra of bulk $\text{In}_2\text{Te}_3$ and InTe powers.....	35
<b>Figure 3.3</b> X-ray diffractogram of as-deposited films at different substrate temperatures .....	36
<b>Figure 3.4</b> X-ray diffractogram of films deposited at 423 K and annealed at different temperatures.....	36
<b>Figure 3.5.</b> Photograph of $\text{In}_2\text{Te}_3$ films deposited at 423 K and annealed at 573 K for 2h.....	38
<b>Figure 3.6</b> XRD patterns of annealed (573 K (1h)) $\text{In}_2\text{Te}_3$ thin films at different substrate temperatures.....	39
<b>Figure 3.7.</b> FESEM images of annealed $\text{In}_2\text{Te}_3$ thin films deposited at (a) 298 K, (b) 373 K, (c) 423 K and (d) 473 K substrate temperatures.....	39
<b>Figure 3.8</b> (a). I-V characteristic curves and (b). Plot of $\ln R$ verses $1/T$ of $\text{In}_2\text{Te}_3$	

films deposited at different substrate temperatures and annealed at 573 K for 1h....	41
<b>Figure 3.9 (a).</b> Transmittance spectra,	
<b>(b).</b> Variation in absorption co-efficient with photon energy and	
<b>(c).</b> Tauc's plot of In <sub>2</sub> Te <sub>3</sub> thin films deposited at different substrate	
temperatures and annealed at 573 K for 1h.....	42
<b>Figure 3.10.</b> XRD patterns of InTe films at different substrate temperature.....	44
<b>Figure 3.11.</b> XRD patterns of InTe films grown at 473 K and annealed at	
different temperatures for different durations .....	44
<b>Figure 3.12.</b> XRD patterns of InTe thin films grown at different substrate	
temperature and annealed at 523 K for 1h.....	46
<b>Figure 3.13.</b> FESEM images of annealed (523K 1h) InTe thin films grown at	
different substrate temperatures.....	46
<b>Figure 3.14. (a).</b> I-V curve of stoichiometric InTe films	
<b>(b).</b> lnR versus inverse temperature plots of InTe films deposited at different	
Substrate temperatures and annealed at 523 K for 1 h.....	48
<b>Figure 3.15. (a).</b> Transmittance as a function of wavelength	
<b>(b).</b> Tauc's plots and	
<b>(c).</b> Absorption coefficient as a function of energy for InTe thin films.....	49
<b>Figure 4.1</b> Plot of thermo emf as a function of temperature difference of In <sub>2</sub> Te <sub>3</sub>	
films grown at different conditions.....	53
<b>Figure 4.2</b> XRD patterns of In <sub>2</sub> Te <sub>3</sub> thin films grown at different substrate	
temperatures .....	54
<b>Figure 4.3</b> Surface micrographs of indium telluride films prepared at different	
substrate temperatures.....	55
<b>Figure 4.4 (a)</b> Variation in thermo emf with temperature difference	
<b>(b).</b> Plot of thermoelectric power versus hot end temperature,	
<b>(c)</b> Variation in electrical conductivity with inverse temperature and	

(d) Variation of power factor with temperature for films deposited at different substrate temperature.....	57
<b>Figure 4.5 (a)</b> Plot of thermo emf versus temperature difference,	
(b). Temperature dependent electrical conductivity for different thickness films and	
(c). Power factor of different thickness films as function of temperature.....	58
<b>Figure 4.6</b> XRD patterns of Bi doped $\text{In}_2\text{Te}_3$ thin films deposited at 423 K.....	60
<b>Figure 4.7</b> FESEM micrographs of Bi doped $\text{In}_2\text{Te}_3$ thin films.....	61
<b>Figure 4.8</b> EDAX spectra of Bi-1 films.....	62
<b>Figure 4.9 (a).</b> Variation in thermo emf with temperature difference,	
(b). Plot of thermoelectric power versus hot end temperature,	
(c). Electrical conductivity as function of inverse temperature and	
(d). Variation of power factor with temperature, of Bi doped $\text{In}_2\text{Te}_3$ films.....	63
<b>Figure 4.10</b> XRD patterns of $\text{Sb}_2\text{Te}_3$ doped $\text{In}_2\text{Te}_3$ films deposited at 423 K .....	64
<b>Figure 4.11</b> FESEM micrographs of $\text{Sb}_2\text{Te}_3$ doped $\text{In}_2\text{Te}_3$ thin films.....	65
<b>Figure 4.12 (a).</b> Variation in thermo emf with temperature difference,	
(b). Plot of thermoelectric power versus hot end temperature,	
(c). Electrical conductivity as function of inverse temperature and	
(d). Variation of power factor with temperature, of $\text{Sb}_2\text{Te}_3$ doped $\text{In}_2\text{Te}_3$ films .....	66
<b>Figure 4.13</b> XRD patterns of $\text{Sb}_2\text{Te}_3$ alloyed $\text{In}_2\text{Te}_3$ films deposited at 423 K Substrate temperature .....	68
<b>Figure 4.14</b> FESEM micrographs of $\text{Sb}_2\text{Te}_3$ alloyed $\text{In}_2\text{Te}_3$ thin films.....	69
<b>Figure 4.15 (a).</b> Variation in thermo emf with temperature difference,	
(b). Plot of thermoelectric power versus hot end temperature,	
(c) Variation in electrical conductivity with inverse temperature and	
(d) Variation of power factor with temperature of $\text{Sb}_2\text{Te}_3$ alloyed $\text{In}_2\text{Te}_3$ films.....	70
<b>Figure 4.16.</b> XRD patterns of Al doped $\text{In}_2\text{Te}_3$ films deposited at 423 K.....	71
<b>Figure 4.16</b> FESEM micrographs of Al doped $\text{In}_2\text{Te}_3$ thin films.....	72



<b>Figure 4.17 (a).</b> Variation in thermo emf with temperature difference,	
<b>(b).</b> Plot of thermoelectric power versus hot end temperature,	
<b>(c).</b> Electrical conductivity as function of inverse temperature and	
<b>(d).</b> Variation of power factor with temperature, of Al doped $\text{In}_2\text{Te}_3$ films.....	74
<b>Figure 4.18</b> XRD patterns of Sb doped $\text{In}_2\text{Te}_3$ thin films deposited at 423 K substrate temperature.....	75
<b>Figure 4.19</b> FESEM micrographs of Sb doped $\text{In}_2\text{Te}_3$ thin films.....	76
<b>Figure 4.20.</b> Representative elemental of mapping to uniform distribution of dopants (Sb-1 films).....	77
<b>Figure 4.21 (a).</b> Variation in thermo emf with temperature difference,	
<b>(b).</b> Plot of thermoelectric power versus hot end temperature,	
<b>(c).</b> Electrical conductivity as function of inverse temperature and	
<b>(d).</b> Variation of power factor with temperature, of Sb doped $\text{In}_2\text{Te}_3$ films.....	78
<b>Figure 4.22</b> XRD patterns of Se doped $\text{In}_2\text{Te}_3$ thin films deposited at 423 K Substrate temperature.....	80
<b>Figure 4.23</b> FE-SEM micrographs of Se doped $\text{In}_2\text{Te}_3$ thin films .....	80
<b>Figure 4.24 (a)</b> Variation in thermo emf with temperature difference,	
<b>(b)</b> Plot of thermoelectric power versus hot end temperature,	
<b>(c)</b> Electrical conductivity as a function of inverse temperature and	
<b>(d)</b> Power factor versus temperature plot, of Se doped $\text{In}_2\text{Te}_3$ films.....	82
<b>Figure 4.25.</b> XRD patterns of Te doped $\text{In}_2\text{Te}_3$ thin films deposited at 423 K.....	83
<b>Figure 4.26</b> FE-SEM micrographs of Te doped $\text{In}_2\text{Te}_3$ thin films.....	84
<b>Figure 4.27 (a).</b> Variation in thermo emf with temperature difference,	
<b>(b).</b> Plot of thermoelectric power versus hot end temperature,	
<b>(c).</b> Electrical conductivity as function of inverse temperature and	
<b>(d).</b> Variation of power factor with temperature, of Te doped $\text{In}_2\text{Te}_3$ films.....	86
<b>Figure 4.28 (a).</b> Thermo emf as a function of temperature difference,	

(b). Variation in thermoelectric power with temperature,	
(c). Temperature dependent conductivity and	
(d) Power factor as a function of temperature of InTe films deposited at different substrate temperature and annealed at 523 K for 1 h.....	88
<b>Figure 5.1</b> Illustration of fabricated Si-In <sub>2</sub> Te <sub>3</sub> or Si-InTe heterojunction structure....	93
<b>Figure 5.2.</b> XRD patterns of n-Si/p-In <sub>2</sub> Te <sub>3</sub> thin films.....	94
<b>Figure 5.3</b> FE-SEM images of n-Si/p-In <sub>2</sub> Te <sub>3</sub> thin film.....	95
<b>Figure 5.4</b> I-V-T curve of n-Si/p-In <sub>2</sub> Te <sub>3</sub> thin films.....	96
<b>Figure 5.5</b> ln (I) versus voltage curve in forward bias at room temperature.....	97
<b>Figure 5.6</b> The plots of current versus square of voltage at room temperature for (a) as-deposited and (b) annealed Si/In <sub>2</sub> Te <sub>3</sub> thin film diodes.....	98
<b>Figure 5.7</b> Richardson plot of Si-In <sub>2</sub> Te <sub>3</sub> junction.....	98
<b>Figure 5.8.</b> XRD patterns of (a) As-deposited at 473 K and (b) Annealed at 473 K for 1 h, n-Si/p-InTe thin films.....	100
<b>Figure 5.9</b> FESEM images of n-Si/p-InTe thin films.....	101
<b>Figure 5.10</b> Temperature dependent I-V curve of (a). as-deposited and (b). annealed n-Si/p-InTe thin films.....	101
<b>Figure 5.11</b> ln (I) versus voltage curve of (a). as-deposited at 473 K and (b). annealed at 473 K for 1 h in forward bias at room temperature.....	102
<b>Figure 5.12</b> Current as a function of square of voltage at (a) 303 K and (b) 373 K of (a) As-deposited and (b) annealed Si/InTe diodes.....	103
<b>Figure 5.13</b> Richardson plot of (a) as-deposited at 473 K and (b) annealed at 473 K for 1 h of Si-InTe junction.....	104
<b>Figure 6.1</b> Statistics of improvement in power factor of doped In <sub>2</sub> Te <sub>3</sub> films.....	108

## LIST OF TABLES

	<b>Page No.</b>
<b>Table 1.1</b> Some traditional semiconductors with their transition type and band gap... 3	3
<b>Table 1.2</b> III-VI compounds with their transition type and band gap..... 5	5
<b>Table 1.3</b> (a) Some bulk properties of In <sub>2</sub> Te <sub>3</sub> materials and (b) Some bulk properties of InTe material..... 6	6
<b>Table 2.1</b> Materials brands and purity..... 22	22
<b>Table 3.1</b> Elemental composition of powdered bulk source materials..... 35	35
<b>Table 3.2</b> Variation in composition of In <sub>2</sub> Te <sub>3</sub> thin films with substrate temperature. 37	37
<b>Table 3.3</b> Composition of In <sub>2</sub> Te <sub>3</sub> thin films at different annealing conditions..... 38	38
<b>Table 3.4.</b> Composition and grain size of annealed In <sub>2</sub> Te <sub>3</sub> thin films..... 40	40
<b>Table 3.5.</b> The resistivity, activation energy and optical band gap of In <sub>2</sub> Te <sub>3</sub> thin films..... 41	41
<b>Table 3.6</b> Compositional analysis of InTe thin films..... 47	47
<b>Table 3.7</b> Activation energy and optical band gap of InTe thin films..... 49	49
<b>Table 4.1</b> Variation in the composition of as-deposited films at different substrate temperatures..... 56	56
<b>Table 4.2</b> Composition of Bi doped In <sub>2</sub> Te <sub>3</sub> thin films..... 61	61
<b>Table 4.3</b> Composition of Sb <sub>2</sub> Te <sub>3</sub> doped In <sub>2</sub> Te <sub>3</sub> thin films..... 65	65
<b>Table 4.4</b> Composition of Sb <sub>2</sub> Te <sub>3</sub> alloyed In <sub>2</sub> Te <sub>3</sub> thin films..... 69	69
<b>Table 4.5</b> Elemental composition of Al doped In <sub>2</sub> Te <sub>3</sub> thin films..... 73	73
<b>Table 4.6</b> Elemental composition of Sb doped In <sub>2</sub> Te <sub>3</sub> films..... 77	77
<b>Table 4.7</b> Elemental composition of Se doped In <sub>2</sub> Te <sub>3</sub> thin films ..... 81	81

<b>Table 4.8</b> Elemental composition of Te doped $\text{In}_2\text{Te}_3$ thin films.....	85
<b>Table 5.1</b> Compositional analysis of $\text{In}_2\text{Te}_3$ thin films on Si wafer.....	93
<b>Table 5.2</b> Rectification ratio of as-deposited and annealed Si/ $\text{In}_2\text{Te}_3$ heterojunction..	96
<b>Table 5.3</b> Compositional analysis of InTe thin films on Si wafer.....	100
<b>Table 5.4</b> Rectification ratio of as-deposited and annealed Si/InTe heterojunction...	102

## NOMENCLATURE

### ABBREVIATIONS

Ag	Silver
Al	Aluminium
Bi	Bismuth
Sb	Antimony
Se	Selenium
Te	Tellurium
In <sub>2</sub> Te <sub>3</sub>	Indium telluride
InTe	Indium mono-telluride
Sb <sub>2</sub> Te <sub>3</sub>	Antimony telluride
RF	Radio frequency
CVD	Chemical vapour deposition
PVD	Physical vapour deposition
AC	Alternative Current
DC	Direct current
MBE	Molecular beam epitaxy
PLD	Pulse laser deposition
TFT	Thin film transistor
XRD	X-ray diffraction
SEM	Scanning Electron Microscopy
FESEM	Field Emission Scanning Electron Microscopy

EDAX	Energy Dispersive Analysis of X-ray
EDS	Energy Dispersive Spectroscopy
IR	Infra-red
NIR	Near infra-red
Vis	Visible
UV	Ultra Violet
I-V	Current- Voltage
C-V	Capacitance-Voltage
n-	n-type
p-	p-type
SCLC	Space Charge Limited Conduction
TED	Thermionic-emission diffusion model
TE	Thermoelectric
PF	Power Factor
RR	Rectification Ratio

#### **SYMBOLS AND UNITS**

nm	nanometre
$\mu\text{m}$	micrometre
eV	Electron volt
$\mu\text{V}$	microvolt
mW	milliwatt
h	hour
D	Grain size

a, b & c	lattice constants
d	Inter-planar distance
$2\theta$	Bragg angle
$\sigma$	Conductivity
$\rho$	Resistivity
$\alpha$ -	Alpha phase
$\beta$ -	Beta phase
n	Carrier concentration
R	Resistance
T	Temperature
$E_g$	Band gap
$E_a$	Activation energy
at. %	Atomic percentage
h $\nu$	Photon energy
$k_z$	Boltzmann constant
Å	Angstrom
K	Kelvin
A	Ampere
cm	centimetre
m	metre
min	Minute
$\lambda$	Wavelength
V	Voltage

$\Omega$	ohm
S	Seebeck coefficient
s	Second
$\theta$	Angle
$\epsilon_0$	Permittivity of vacuum
$\epsilon_r$	Relative permittivity
$\nu$	Frequency
ZT	Figure of merit



## CHAPTER 1

### INTRODUCTION

*Overview:*

*This chapter describes a brief introductory information about thin film technology, compound semiconductors specially about III-VI compounds (indium telluride) and its importance. Further, the literature survey about indium telluride material in both bulk and thin film form (in brief) are discussed. The possible research gaps are identified from the literature review which are mentioned in the scope. Finally, the objectives of present investigations are drawn from the scope.*

#### **1.1 Thin film technology**

Thin film science and technology is playing an important role in the development of devices ranging from energy efficient display devices to energy harvesting and energy storage devices such as solar cell, sensor, memory, battery, super-capacitor, etc. Thin film is a state of the material in which conductivity becomes a function of thickness. Typical thickness extends from fractions of a nanometre to several micrometers. Generally, thin films are used to improve surface properties of the solid materials. Thin films have properties that can be different from that of their corresponding bulk properties. A film is considered as thin, as long as its surface properties are different from its bulk behaviour. Transmission, reflection, absorption, hardness, abrasion resistance, permeation and electrical behaviour are some of the properties of a bulk material surface that can be improved by using a thin film form. They have a larger surface to volume ratio, hence the surface and near surface characteristics decide the properties of the thin film. As a result, thin film properties not only rely on the thickness of the film, but also on the nature of substrate upon which the films are grown and deposition parameters used in the fabrication of thin films. Thin film fabrications are carried out by depositing the required material in the atomistic deposition over the required substrate, which may result in either single crystalline, polycrystalline or amorphous structure depending on the deposition conditions. Thin film technology has the potential to engineer the various properties such as surface morphology, surface

roughness, porosity and crystalline size. These advantages in this film assist in the development of new products and minimize the wastage as in conventional manufacturing techniques.

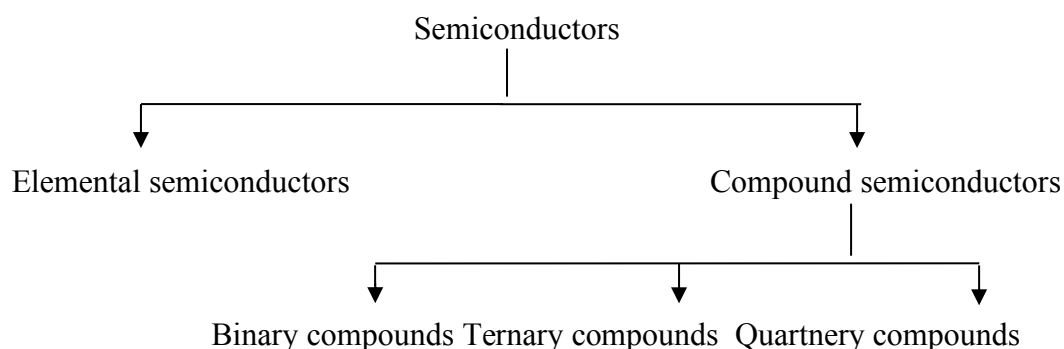
## 1.2 Compound semiconductors

The semiconductors became more important because of their sustainable applications in almost all branches of industry and areas of daily life. Due to low mobile carrier concentrations, the observation and interpretation of electronic process are easier in semiconductors when compare to metals and other crystals. This is the reason behind the vast usage of semiconductors in many applications.

The semiconductor thin films have been the basis of development in a wide variety of diverse modern technologies. Some of these include high speed transistor, solar cell, solid state lighting, sensors, information storage devices, etc. From past several decades, the research work in this field has been highly supported by such technological application.

Semiconductors can be classified in several ways. Based on constituent atoms in it, semiconductors are available in two forms namely elemental and compound semiconductors.

In elemental semiconductor, all the constituent atoms are of same kind, whereas a compound semiconductor is composed of atoms of two or more different elements. The hierarchy of compound semiconductors is shown below,



The scope of materials which can be classified as compound semiconductors is vast and covers the entire periodic table. It includes IV-IV, II-IV, I-V, II-V, III-V, I-VI, II-VI, III-VI, V-VI, I-VII, I-III-VI, I-IV-VI, I-V-VI and II-III-V compounds. However, because of the excessive developing cost of these materials as high quality semiconductors, most of these compounds are still in a primitive state of development when compared with Ge or Si. But the only compounds which have been developed to the state of significant commercial applications are found in the III-V and II-VI semiconductor groups of materials. Some of the traditional compound semiconductors and transition type with band gap are mentioned in table 1.1.

**Table 1.1** Some traditional semiconductors with their transition type and band gap

Type of Semiconductor	Material	Type of transition	Band gap (eV)
Elemental	C	Indirect	5.47
	Ge	Indirect	0.78
	Si	Indirect	1.12
	Sn	Direct	0.08
III-V	GaAs	Direct	1.42
	InAs	Direct	0.36
	InSb	Direct	0.17
	GaP	Indirect	2.26
	GaN	Direct	3.36
	InN	Direct	0.7
IV-IV	SiC	Indirect	2.99
II-VI	ZnO	Direct	3.35
	CdSe	Direct	1.7
	ZnS	Direct	3.68

Many researchers have investigated in detail about the properties of binary compounds of III-V, II-VI, and I-VII type which having crystalline structures of zinc blend or wurtzite. There is a limited investigated group of semiconductors which also have a zinc blend or wurtzite structure namely III-VI compound semiconductors. The III-VI compounds are chemically compatible with the traditional semiconductor materials and they exhibit similar band gaps. The III-VI compounds have many distinct structural, optical and electric properties that are peculiar with respect to traditional group IV, III-V or II-VI materials. This combination of these features of III-VI compounds makes a significant ascendancy as new device materials.

### **1.3 III-VI compound semiconductors (Indium telluride)**

III-VI semiconductors comprise of two basic principal stoichiometries,

1.  $A^{III}-B^{VI}$  compounds
2.  $A_2^{III}-B_3^{VI}$  compounds

The  $A^{III}B^{VI}$  compound exhibits a layered structure with weak bonding between covalently bonded B-A-A-B layers (A= Ga, In; B= S, Se, Te). The adjacent layers of the compounds are coupled with Vander walls force and exhibiting weak bonding between covalently bonded layers. The layered crystal structure results in strong optical and electrical anisotropy. In addition to this, the layered  $A^{III}B^{VI}$  compounds became attractive because of their high nonlinear optical coefficient in the infrared region. These features make them suitable candidates for second harmonic generation materials.

The  $A_2^{III}B_3^{VI}$  compounds exhibit a defect zinc blende or wurtzite structure with one-third of the cation sites vacant. Thus  $A_2^{III}B_3^{VI}$  can be doped to a higher level than the other conventional tetrahedral level of vacancies. This causes a deviation in the electronic state impurities and electrical neutrality accommodated by these defects which results the semiconducting properties remain unchanged even at significant impurity concentration. The crystal structures of these materials also explain the high

stability for radiation with regards to a number of parameters such as optical constants in the infrared region (Ohuchi et al. 1999).

Both forms of these materials are possible novel materials for electronic or optoelectronic devices. Some of the III-VI compounds with their transition type and band gap have mentioned in table 1.2

**Table 1.2** III-VI compounds with their transition type and band gap

Type of Semiconductor	Material	Type of transition	Band gap (eV)
III-VI	Gallium sulfide	Direct	2.5-3.4
	Gallium selenide	Direct	2-2.6
	Gallium telluride	Direct	1-1.2
	Indium sulfide	Direct	2-2.4
	Indium selenide	Direct	1.2-1.3
	Indium telluride	Direct	1.03-1.23

Among these compounds, indium telluride with direct band gap energy found its applications in gas sensors, pressure transducers, photo-voltaic, electrochemical solar cell devices, switching and memory devices.

The commonly occurring stoichiometries of indium telluride are  $\text{In}_2\text{Te}_3$ ,  $\text{InTe}$ ,  $\text{In}_3\text{Te}_4$ ,  $\text{In}_7\text{Te}_{10}$ , etc. The formation of particular stoichiometry mainly depends on the temperature and pressure under the process of material synthesis. However,  $\text{InTe}$  and  $\text{In}_2\text{Te}_3$  are stable than other stoichiometries according to phase diagram of binary indium telluride compound reported by Grochowski et al. Some basic properties of  $\text{In}_2\text{Te}_3$  and  $\text{InTe}$  are tabulated below,

**Table 1.3 (a)** Some bulk properties of In<sub>2</sub>Te<sub>3</sub> materials

<b>Property</b>	<b>Parameters</b>
Structure	Cubic with lattice parameters a= b=c= 18.45 Å JCPDS:16-0445
Molar mass	612.436 g/mol
Density	5.76 g/cm <sup>3</sup>
Melting point	940 K
Band gap	0.94-1.2 eV
Type of transition	Direct
Type of conductivity	p-type

**Table 1.3 (b)** Some bulk properties of InTe materials

<b>Property</b>	<b>Parameters</b>
Structure	Tetragonal with lattice parameter a=b=8.437 Å, c=7.139 Å JCPDS: 07-0112
Molar mass	242.418 g/mol
Density	6.34 g/cm <sup>3</sup>
Melting point	969 K
Optical Band gap	1.16 eV
Type of transition	Direct
Type of conductivity	p-type

## 1.4 Literature review

The III-VI semiconductors are owing the interest in various research domains due to its peculiar properties. The properties of III-VI materials have been mostly investigated in the bulk crystal form. In spite of its good electrical and optical properties, implementation of these materials in practical applications is limited by their poor mechanical and thermal properties. The mechanical properties of the materials can be strengthening by the thin film form which can makes them potential for device applications. Among III-VI materials, indium telluride is paying a special interest because of its attractive electrical and optical properties along with stoichiometric defects which makes them suitable for opto-electronic devices and thermoelectric applications. However, the properties of indium telluride mainly depend on the parametrisation of growth condition due to the formation of different stoichiometries under varies pressures and temperatures.

The outcome results of  $\text{In}_2\text{Te}_3$  crystals revealed the attractive properties of material. Reportedly, direct optical band gap of  $\text{In}_2\text{Te}_3$  crystals ranges from 0.94 to 1.2 eV whereas,  $\sim 1.16$  eV for InTe. The electrical conductivity of  $\text{In}_2\text{Te}_3$  crystal is  $\sim 6.94 \times 10^{-6} (\Omega\text{-cm})^{-1}$  whereas,  $\sim 60 (\Omega\text{-cm})^{-1}$  for InTe crystals. The optical properties of these materials accompanied with electrical properties make them potential for opto-electronic applications. In addition,  $\text{In}_2\text{Te}_3$  material is consisting a large number of stoichiometric defects in its cation lattice due to the valance mismatch between indium and tellurium. These defects are uniformly distributed in  $\alpha\text{-In}_2\text{Te}_3$  phase (cubic lattice constant 18.4860 Å) whereas, non-uniformly distributed in  $\beta\text{-In}_2\text{Te}_3$  phase (cubic lattice constant 6.1580 Å). The phase of  $\text{In}_2\text{Te}_3$  depends on the cooling process of crystal growth technique, if the material gradually cools to room temperature then it gives  $\alpha\text{-In}_2\text{Te}_3$  phase otherwise, the quenching takes place which produces the  $\beta\text{-In}_2\text{Te}_3$ . Among these phases, the  $\alpha\text{-In}_2\text{Te}_3$  phase is widely suggested for applications. Furthermore, Wang et al. (2016) reported the tenable nonlinear absorption response due to the existence of defect density states which makes them promising material for ultrafast nonlinear optical devices. However, aforementioned the bulk form of these materials have poor mechanical properties hence the thin films form is most suggested form for

device applications. The literature survey on indium telluride thin films has given below.

Barua and Goswami (1970) were the first to investigate the structural properties of vacuum deposited  $\text{In}_2\text{Te}_3$  thin films which deposited on glass, NaCl crystals and mica. The deposits were essentially found to be  $\beta$ - phase  $\text{In}_2\text{Te}_3$ .

Krishna Sastry and Jayarama Reddy (1980) prepared InTe thin films using flash evaporation technique. They observed amorphous nature in room temperature deposited films whereas crystalline structure at 573 K substrate temperature and also an increase in mobility with substrate temperature. In addition, they found the weak dependency of thermoelectric power of these films on temperature.

De Purkayastha et al. (1981) observed an optimum substrate temperature of 453 K for the preparation of  $\alpha$ - $\text{In}_2\text{Te}_3$  thin films by electron beam evaporation and corresponding hole mobility of these films was found to be  $48 \text{ cm}^2 \text{ V}^{-1} \text{ s}^{-1}$ .

Mathur et al (1981) observed an irreversible change in electrical conductivity above the temperature of 525 K in polycrystalline n-type  $\text{In}_2\text{Te}_3$  thin films which were prepared by thermal evaporation method. The authors also noticed hall mobility values of the films were independent of the temperature.

Dawar et al. (1982) thermally deposited silver-sapphire- $\text{In}_2\text{Te}_3$  thin films and investigated the field effect properties in the temperature ranging from 77 K to 295 K. The positive gate field of transistor had increased the carrier density and reduced the mobility whereas opposite effect had observed in negative gate field which was explained on the basis of charge carrier accumulation and depletion at the interface of insulator and semiconductor.

Mathur et al. (1982) later studied the DC electrical conductivity and hall effect of  $\beta$ - $\text{In}_2\text{Te}_3$  thin films obtained by direct thermal evaporation on sapphire substrates in the temperature ranging from 77 K to 295 K. Measurements of DC conductivity and hall coefficient revealed that mobility of these films was found to be constant ( $112 \text{ cm}^2 \text{ V}^{-1} \text{ s}^{-1}$ ) up to 220K and decreased later.



Rousina and Shivakumar (1987) investigated the variation in electrical conductivity of InTe thin films prepared by thermal evaporation in the temperature ranging from 300 K to 400 K. They determined two activation energies 0.45 and 0.096 eV for low and high temperature regions respectively. The high temperature value of the activation energy is twice the low temperature activation energy due to the presence of an interfacial inversion layer at the semiconductor-metal contact.

Rousina and Shivakumar (1988) obtained stoichiometric InTe thin films from non-stoichiometric bulk composition using vacuum evaporation method. They observed an increase in indium with substrate temperature whereas, reduction in indium at annealing temperature above 473 K.

Rousina and Shivakumar (1988) investigated the photo-induced effect on the rectification behaviour of Al/Al<sub>2</sub>O<sub>3</sub>/n-InTe/Bi sandwich structures obtained by thermal evaporation technique. They found that the rectification ratio is higher in the illuminated case than dark.

Rousina and Shivakumar (1988) studied I-V characteristics for metal-InTe-metal (metal: Cu, In, Sb and Al) prepared by thermal evaporation method. They found that the resistance offered by these metal contacts increased in the order of copper, indium, antimony, and aluminium. They also investigated the I-V characteristics for Al-InTe-In sandwich from which they concluded that Al is a blocking contact to show good rectification properties.

Rousina and Shivakumar (1989) investigated the properties of Ni/p-InTe schottky barrier deposited by thermal evaporation technique. Authors reported both barrier height and work function of these films as 0.62 eV and 5.03 eV respectively.

Rousina and Yousefi (1990) investigated optical properties of In<sub>2</sub>Te<sub>3</sub> thin films obtained by thermal evaporation in the temperature of 300-600 K. The authors observed that transparent energy region in the films deposited above 400 K was different from as-deposited films.

Zahab et al. (1990) prepared polycrystalline  $\beta$ - In<sub>2</sub>Te<sub>3</sub> thin films by vacuum thermal evaporation technique on glass substrates followed by appropriate annealing. They

found an energy gap of these films was between 1.1-1.18 eV by conducting electrical, optical and photoconductivity measurements in the temperature range 300-600 K.

Afifi et al. (1996) investigated switching phenomenon in amorphous  $\text{In}_2\text{Te}_3$  thin films by thermal evaporation technique which revealed that these films were typical for memory switch. Authors observed an exponential decrease in switching voltage when temperature raises from 298 K to 373 K and also reported the values of switching voltage activation energy and conduction activation energy.

Hegab et al. (1998) studied the effect of annealing on optical properties of  $\text{In}_2\text{Te}_3$  thin films prepared by thermal evaporation technique. The authors observed that annealed films shown an increase in energy gap with annealing temperature. They found that transition of these films from amorphous to the polycrystalline structure at 523 K substrate temperature. Also, refractive index and absorption index values determined for as-deposited films in the wavelength ranges 500-2500 nm.

Emziane et al. (1999) prepared  $\alpha\text{-In}_2\text{Te}_3$  polycrystalline thin films by thermal evaporation of In and Te layers on glass and  $\text{SnO}_2$  coated substrates. The optimum annealing temperature and duration to get stoichiometric films found by these authors were 663 K and 30 min respectively.

Afifi et al. (2000) investigated the effect of annealing on the AC conductivity and the dielectric properties of  $\text{In}_2\text{Te}_3$  thin films obtained by thermal evaporation technique in the frequency ranges 100-100K Hz and in the temperature ranges 303-373 K. The AC conduction activation energy of these films was reported as 0.065 eV for as-deposited films and decreased with annealing temperature. Authors observed that both dielectric constant and dielectric loss increased with temperature and decreased with frequency.

Seyam (2001) investigated dielectric properties of stoichiometric  $\text{In}_2\text{Te}_3$  thin films obtained by thermal evaporation technique in the frequency range of  $10^2\text{-}10^5$  Hz at temperature from 300 K to 400K. Relaxation time was found to be decreased with increase in temperature. Both capacitance and loss tangent were found to be decrease with increasing frequency and increased with increasing temperature.

Lakshminarayana et al. (2002) observed variation in thermoelectric power with an inverse thickness of p-type  $\alpha$ - $\text{In}_2\text{Te}_3$  thin films obtained by flash evaporation method at substrate temperature of 473 K. They observed that thermoelectric power is independent of substrate temperature in these films.

Guettari et al. (2003) reported the electrical and optical properties of  $\text{In}_x\text{Te}_y$  thin films which were prepared using co-evaporation method. The well oriented and mono-phase  $\alpha$ - $\text{In}_2\text{Te}_3$  films were attained at 500 K substrate temperature with slight tellurium deficiency on their surface. These films were p-type with very low conductivity of order  $\sim 10^{-6} \Omega^{-1} \text{cm}^{-1}$  and optical band gap was approximated to 1.2 eV.

Desai et al. (2005) prepared stoichiometric  $\alpha$ - $\text{In}_2\text{Te}_3$  thin films on glass substrates at 473 K and  $\beta$ - $\text{In}_2\text{Te}_3$  films on NaCl substrates at 523 K by flash evaporation method from  $\alpha$ - $\text{In}_2\text{Te}_3$  bulk. These authors investigated an effect of substrate temperature on the composition, crystallinity and crystallite size of  $\text{In}_2\text{Te}_3$  films.

Desai et al. (2005) conducted an experiment to investigate the sensitivity of carbon dioxide gas on the  $\text{In}_2\text{Te}_3$  thin film obtained by flash evaporation. They found that the sensitivity of films increases with an increase in the concentration of  $\text{CO}_2$  gas. Authors concluded from their experiments that the  $\text{In}_2\text{Te}_3$  thin films are useful in monitoring  $\text{CO}_2$  concentration.

Desai et al. (2005) investigated strain sensitivity of  $\text{In}_2\text{Te}_3$  thin films prepared on mylar substrates by flash evaporation technique. They observed linear variation in change of resistance of these films with both tensile and compressive strains. They also found higher gauge factor and good temporal stability of films. So, authors finally concluded that these films are suitable to use as strain gauges in transducer applications.

Desai et al. (2006) reported ohmic (Ag, Sn, In and Zn) and non-ohmic (Al) contacts to the p-type  $\text{In}_2\text{Te}_3$  thin films obtained by flash evaporation method. They investigated the influence of substrate temperature on the conduction activation energy and the optical band gap of these films. The investigation revealed that both activation energy and the optical energy gap of films were decreased up to 473 K. Finally, authors concluded that the  $\text{In}_2\text{Te}_3$  films deposited at 473 K with a direct optical energy gap of 1 eV are suitable as absorbers in thin solar cells.

Perananthm et al. (2006) observed amorphous nature in as-deposited indium telluride films, tetragonal structure in 523 K annealed films and orthogonal structure in films annealed at 673 K which were grown by vacuum evaporation technique. They observed an indirect allowed transition with an optical energy gap in the range of 0.82-1.14 eV.

Matheswaran et al. (2010) investigated dielectric properties of vacuum evaporated InTe bilayer thin films. Their observations revealed that capacitance and dielectric constant of films decreases with increase in frequency whereas, loss factor increases with increase in frequency. Also found that when temperature increases, the temperature coefficient of capacitance also increases and temperature coefficient of permittivity decreases.

Desai et al. (2011) observed the temperature dependence of I-V and C-V experimental data of Al/p-In<sub>2</sub>Te<sub>3</sub> schottky diode fabricated on glass substrate by flash evaporation method in the range of 303-335 K. Authors concluded from I-V characteristics that the contacts are non-uniform due to the presence of some low special barrier inhomogeneities at metal-semiconductor interface.

Matheswaran et al. (2012) investigated the thickness dependent structural and optical properties of In/Te bilayer thin films prepared by thermal evaporation and annealing at 523 K in Ar atmosphere for half an hour. Authors observed that the films structure was a mixed phase of In<sub>2</sub>Te<sub>3</sub> and In<sub>2</sub>Te<sub>5</sub> whereas In<sub>2</sub>Te<sub>3</sub> phase was dominant at lower thickness. Crystallite size of the films was found to be improved with an increase in thickness whereas optical band gap decreased.

Sathymoorthy et al. (2012) prepared the  $\alpha$ -In<sub>2</sub>Te<sub>3</sub> single crystal thin films from In/Te bilayer using thermal evaporation method followed by post-irradiation with 100 MeV Si ions at different fluence ( $1 \times 10^{13}$  to  $5 \times 10^{13}$  /cm<sup>2</sup>). The optical analysis of this films revealed the optical band gap of  $1.1 \pm 0.5$  eV and refractive index of  $\sim 3.3$  of the films which had shown a small improvement in the films properties than previous reports.

Matheswaran et al. (2013) studied the effect of 130 MeV Au ion irradiation on CO<sub>2</sub> gas sensing of In<sub>2</sub>Te<sub>3</sub> thin films prepared by thermal evaporation method. Potentially, the In/Te thin films which were irradiated with 130 MeV Au ions at  $3 \times 10^{13}$  ions/cm<sup>2</sup> flux

shown better sensing properties to CO<sub>2</sub> gas. The response time of these films was reported as 15-20 s for 1000 ppm of CO<sub>2</sub> gas.

Yuan et al. (2018) prepared good crystalline Ti doped InTe thin films in nitrogen atmosphere at 723 K annealing temperature using magnetron co-sputtering method. The optical band gap of InTe films was increased from 1.56 to 1.85 eV with increased Ti doping concentration. The authors observed the nonlinear absorption coefficients due to the broadening of optical band gap. The films shown the dynamic response time due to the surface defect density which traps the carriers. In addition, the carrier life of films can be adjusted by Ti dopant.

Literature review reveals that many of the authors investigated basic structural, electrical, optical properties and effect of temperature on these properties of indium telluride thin films. Still there is an ambiguity in properties of few reports due to the existence of these films in combination of different stoichiometries. Hence, optimization of deposition parameters plays a major role in obtaining the mono-phased films. The response time of the indium telluride thin films for nonlinear optical device is very less due to surface defect density which in turn acts as trapping centres for carriers. However, the investigations on thermoelectric properties and schottky barrier properties of indium telluride thin films are comparatively very less.

### **1.5 Scope and objectives**

Indium telluride films have direct band gap of 1.1 eV which is an attractive feature for solar cell applications. These films have very good sensing properties to monitor CO<sub>2</sub> gas with good temporal stability and quick response time in nano seconds. Indium telluride films have high gauge factor and hence are useful as strain gauges in transducer applications. Additionally, due to the large number of intrinsic defects ( $\sim 5.5 \times 10^{21} \text{ cm}^{-3}$ ), the defect states are useful to tune the non-linear optical absorption coefficients which makes them suitable for optical limiting applications. Finally, indium telluride exhibits radiation stability in electrical and optical properties which had been examined up to  $10^{18}$  fast neutrons per cm<sup>2</sup> (Volovichev et al. 1998). Hence

these material may have a scope to implement in applications in the vicinities of nuclear reactors.

Indium telluride has good electrical conductivity ( $\sim 0.66 \Omega^{-1} \text{ m}^{-1}$ ) and less thermal conductivity ( $\sim 1 \text{ W m}^{-1} \text{ K}^{-1}$ ) which are suitable properties for thermoelectric applications. Despite of its attractive features to exhibit good thermoelectric properties, the reports on this topic are still under meagre. In order to exploit indium telluride in any opto-electronic devices, the electrical properties of interface have to be understood which can ensure the device performance. But investigations on the interface properties of these films were studied with metals such as Bi, Al and Ni. Hence the present work focuses on a detailed study on the effect of doping and annealing on the properties of indium telluride thin film and suitability of indium telluride thin films for thermoelectric power generation. Along with this, the heterojunction of indium telluride with Si is also investigated.

Objectives:

1. To optimize the growth conditions to get homogeneous and stoichiometric indium telluride thin films.
2. To find the effect of deposition parameters on the structural, electrical and optical properties of prepared films.
3. To investigate the effect of annealing on structural and electrical properties of deposited films.
4. To investigate the effect of doping on structural and electrical properties of indium telluride films.
5. Suitability of indium telluride thin films for thermoelectric power generator and hetero junction applications.

## CHAPTER 2

### EXPERIMENTAL METHODS AND CHARACTERISATION

Overview:

*This chapter explains the methods which were used for cleaning the substrates, technique chosen to grow the films, characterisation techniques and working formulae used to estimate structural, electrical, optical and thermoelectric properties. In addition to this, the basic principles of various methods are described and illustration of setup/ system were depicted for required methods.*

#### **2.1 Preparation of the thin films**

There is a wide choice of deposition methods available to prepare thin films. These techniques are broadly classified into physical methods and chemical methods. The distinction between the physical and chemical methods mainly relies on the way the film deposits on the substrate. Basically, mechanical or electro-mechanical process takes place in physical methods, whereas chemical reaction occurs among the contents in chemical methods.

##### **2.1.1 Physical methods**

(a) Physical vapour deposition

(i) Thermal evaporation technique

Thermal evaporation technique is one of the commonly used vacuum deposition method in which an electrical energy is supplied to heat a boat or filament which in turns heats a deposition material to an evaporation point. The vaporised material transports through the vacuum and finally condense on the substrate in the form of thin film. This process can be performed at high vacuum level to avoid reaction between the vapours and atmospheric atoms or molecules. At this high vacuum, the mean free path of vapour atoms is of the same order that of the dimension of vacuum chamber. Hence,

particles can travel in straight line path from the evaporation source to the substrate. The schematic representation of thermal evaporation unit is shown in figure 2.1.

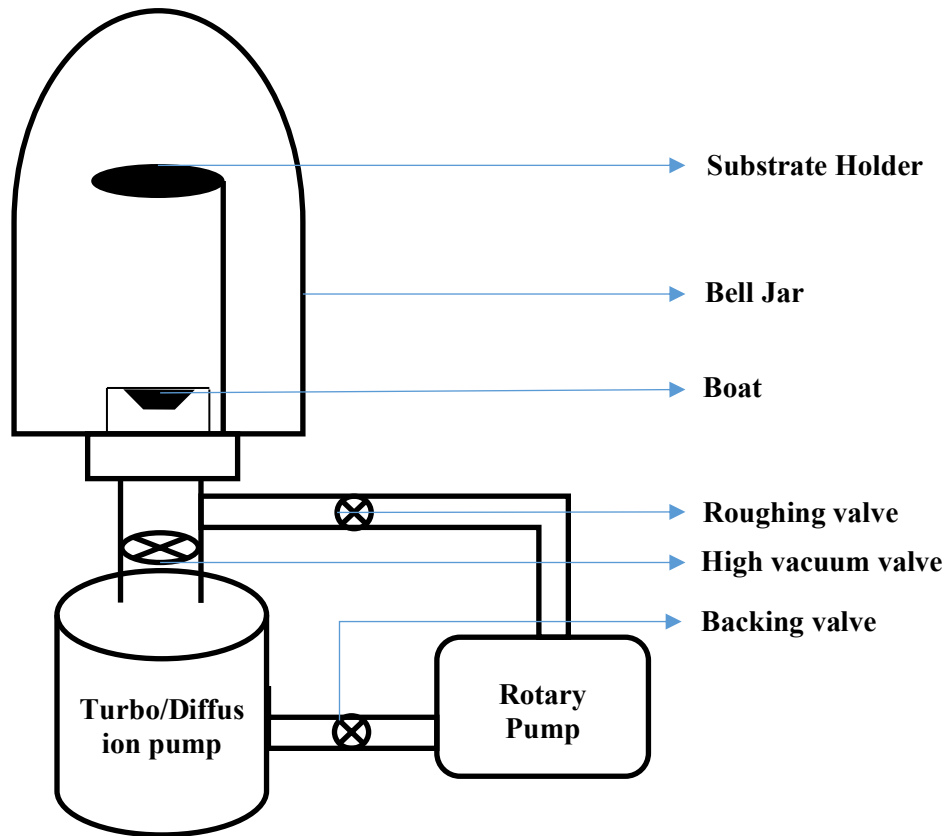


**Figure 2.1** Schematic diagram of thermal evaporation system.

Advantages of thermal evaporation method:

- Excellent purity of films
- High deposition rates

Wide range of materials including metals, organic and inorganic polymers can be deposited using this method



Disadvantages of thermal evaporation method:

- Less adhesion between substrate and the material to be deposited. Hence, requires special substrate preparation techniques.
- Not suitable for materials which decompose while heating and hence requires careful control of deposition parameters.



**Figure 2.2** Photographs of thermal evaporation systems used to deposit, (a).  $\text{In}_2\text{Te}_3$  films and (b). InTe films.

#### (ii) Pulsed laser deposition

Pulsed laser deposition or laser ablation is one of the method used to deposit thin films in which a high power pulsed laser beam is irradiated inside the vacuum chamber to strike the target of source material. A quartz lens is used to tune the power density of

the laser pulse. At particular power density of laser pulse, the source material vaporises from the target and deposits on substrate in the form of thin film. This whole process is carried out in ultra-high vacuum or in the oxygen atmosphere which is commonly used to get oxide films.

The physical phenomena of laser on target and film growth are quite complex. When laser pulse is absorbed by the target, the energy is initially converted into electronic excitation and then into thermal, chemical and mechanical energy which results in evaporation, ablation and plasma formation. The ejected species expand into the surrounded vacuum in the form of a plume containing many energetic species including atoms, molecules, electrons, ions, clusters and molten globules before depositing on the typically hot substrate. The spatial distribution of the plume is depending on the background pressure inside the deposition chamber. These high energetic species ablated from the target are bombarding the substrate surface and may cause damage to the surface by sputtering of atoms from the surface and may also cause defect formation in the deposited films. The sputtered species from substrate and the particles emitted from the target form a collision region which act as a source for condensation of particles. The point at which the condensation rate is high enough to reach a thermal equilibrium, the film starts to grow on the substrate.

Advantages of pulsed laser deposition method:

- Can deposit thin film of same composition as that of the target

Disadvantages of pulsed laser deposition method:

- It is difficult to achieve large area uniformity.

(iii) Molecular beam epitaxy

In molecular beam epitaxy, the substrate is placed in ultra-high vacuum and source materials are evaporated from elemental sources. The evaporated molecules or atoms flow as a beam and deposit on the substrate. Once the atoms reach the substrate, they move by surface diffusion until they reach a thermodynamically favourable location to form bonding with respect to the substrate. In this process, the molecules of source material will dissociate to atomic form and fix at a favourable site. The deposition rate

of films is very low in this method when compared with other methods. The substrate used in this method is cleaned with argon ion bombardment to remove the undesired oxides and impurities on the top layers of the substrate. Further, the substrate is subjected to annealing to heal any damage caused by the ion irradiation. After the cleaning process, the substrate enters into the growth chamber through sample exchange load lock. The effusion cell contains the source material in the elemental form of very high purity and is heated to evaporation point. This results in a transport of molecules in the ultra-high vacuum chamber and impinge on the hot substrate surface. On the substrate, the molecules will diffuse and eventually incorporate into the growing film.

Advantages of molecular beam epitaxy method:

- The fine control on the vacuum chamber environment and on the quality of the source material allows a much higher purity films.

Disadvantages of molecular beam epitaxy method:

- A great technological effect is required to produce systems that yield the desired quality, uniformity of the films

(b) Sputtering:

In this method, the surface of solid material is irradiated with high energetic positive ions which transforms momentum to the surface atoms and results in the ejection of atoms from the surface of the material. The atoms ejected from surface will be deposited on the substrate to form a thin film. The energetic particles which causes the sputtering may be due to ions or neutral atoms or neutral electrons or protons. But most of the sputtering applications are done by the irradiation of ions. The sputtering yield basically depends on the bombarded solid material, its structure and composition, incident ion characteristics and finally on experimental geometry. If the bombardment of energetic particles results no reaction between the cathode and particles, then it is called as physical sputtering. Several aspects have been employed to deposit thin films using sputtering which includes D.C. bias sputtering, R.F sputtering, A.C. asymmetric bias sputtering, ion plating and getter sputtering. For these sputtering options the

required ambient pressure is in the order of  $10$  to  $10^{-2}$  Torr. In spite of good adhesion and high uniform thickness of the films, the sputtering yield reduces at lower pressures due to decrease in the density of bombarding ions.

### **2.1.2 Chemical methods**

In chemical methods, the fluid precursors are used to deposit thin films on the substrates. The fluid precursor can reach the substrate either in gas phase or liquid phase which chemically decomposes in the vicinities of the substrate and finally forms the required material in the thin film form.

(a) Chemical vapour deposition:

Reportedly, the chemical vapour deposition (CVD) is successfully employed to grow the high quality semiconducting films. In this technique, the volatile compound is made to thermally decompose or reach with other gases (or vapours) to produce a non-volatile reaction resulted compound on the substrate. The nature of decomposition can vary based on various factors such as pyrolysis, halide disproportion, hydrogen reduction and chemical reaction between volatile metal halides and vapours of different elements used in precursor which are finally leading to the deposition of semiconducting compounds on the substrate.

(b) Spray pyrolysis:

In spray pyrolysis method, the films are formed on the preheated substrates. the precursor is a solution, prepared with soluble salts of required compound. This solution is converted into droplets through the nozzle and spray in the deposition chamber with the help of a carrier gas. The carrier gas plays a significant role in the pyrolytic reaction process. When these droplets move nearer to the pre-heated substrate, a thermally induced chemical reaction takes place between droplets of different chemical species. This results in the formation of required products on the surface of the substrate. In this technique, doping can be done easily by dissolving the required amount of dopant into spray solution. After the deposition, the substrates are allowed to cool to the room

temperature. The main drawback of this method is that a large number of small droplets evaporate and do not contribute in the formation of the required film.

However, each and every method has its own limitations. The preference for a particular deposition technique depends on several aspects such as material to be deposited, limitations imposed by the substrate, specific application, deposition rate and purity of the final film required for specific applications.

In case of indium chalcogenides, the compound forms in different stoichiometries under variable pressure and temperature. Therefore, the evaporated films are the mixture of at least two phases further which can cause ambiguity in properties of material. Hence, a special attention needs to be taken about growth technique and handling parameters required to attain mono-phased films. In order to study the properties of indium telluride thin films, the basic requirements are minimized defects, mono-phase and optimum orientation of crystallites.

Thermal evaporation is one of the physical method in which the deposition parameters such as substrate temperature, residual pressure and deposition rate can be controlled. In this method the deposition takes place inside the high vacuum of order  $10^{-6}$  Torr. Therefore, the average mean free path of vapours can be around 1 m which is larger than chamber dimension (12" dia.), hence particles will follow the straight line path and form the films in more directional manner, and purity of the films can be maintained. Hence, to deposit indium telluride thin films, thermal evaporation method is selected.

The soda lime glass is an inexpensive material having amorphous nature with high melting point. Additionally, they have capability to hold the polycrystalline thin films up to some moderate conditions of thickness, substrate temperature, annealing temperature and annealing duration which again depends on the material properties. Hence, the soda glass slides were used as substrate material. An adhesion of the material to the substrate is basically depends on the matching of lattice constants, if lattice constants of films varies with respect to the substrate, causes the mismatch between the thermal expansion coefficients (TEC) of substrate and material. Such variations in TEC results the peel off of film from the substrate. The thermal expansion coefficients of

soda lime glass and materials using in this investigation are varying in the order from  $10^{-6}$  to  $10^{-5}$  /K. Hence, due to this one order variations in thermal expansion coefficients, the substrate can hold the material up to some moderate temperature which in turn vary from material to material. However, in present investigation, the good quality of pure  $\text{In}_2\text{Te}_3$  films observed up to 573 K annealing temperature for 1h duration, whereas for  $\text{InTe}$  about 523 K annealing point up to 2h duration. In case of doping, the quality of films attained at different conditions which is discussed in results and discussion section.

In order to get better quality films, and study the properties of indium telluride thin films, the synthesis was carried out by evaporating the pellets of source materials using molybdenum boat in the vacuum ranging from  $10^{-5}$  to  $10^{-6}$  torr using thermal evaporation technique. The deposition rate was changed according to requirement in the range of 4-11 nm/S and source to substrate distance was varied from 11 cm to 12 cm. The purity and brand names of all dopants and base materials are mentioned in table 2.1. To study the diode properties, the p-n junction was made with Si for both  $\text{In}_2\text{Te}_3$  and  $\text{InTe}$  films. In order to remove oxide layer, the silicon (Si) wafers were dipped in diluted hydrofluoric acid (HF) of 1 % concentration in distilled water for 2 minutes. Annealing was carried out in air using muffle furnace was used for post annealing treatment of the samples in air. The deposition conditions were optimized by varying substrate temperature annealing temperature and annealing duration.

**Table 2.1** Materials brands and purity

<b>Material Name and symbol</b>	<b>Brand</b>	<b>Purity</b>
Indium telluride ( $\text{In}_2\text{Te}_3$ )	ACI Alloys, Inc, USA	99.999 %
Indium telluride ( $\text{InTe}$ )	ACI Alloys, Inc, USA	99.999%
Bismuth (Bi)	SRL, India	99.5%
Antimony telluride ( $\text{Sb}_2\text{Te}_3$ )	Alfa Aesar, Russia	99.999%
Aluminium (Al)	Alfa Aesar, US	99.9995%
Antimony (Sb)	Himedia, India	99.9%
Selenium (Se)	Sigma-Aldrich, china	99.999%
Tellurium (Te)	Sigma-Aldrich, Japan	99.99%

## 2.2 Thickness measurement method

There are many methods to measure the thickness of the films, most of such methods are quartz crystal microbalance, surface profilers, interferometry, gravimetric method and through cross section image of scanning electron microscope (SEM).

(i) Quartz crystal microbalance:

The quartz is a piezo-electric material which is useful to measure and monitor the thickness ( $T_f$ ) of the films. The amount of material deposited ( $\Delta m$ ) on the surface of quartz crystal can be quantified by monitoring the change in resonant frequency ( $\Delta f$ ) by using equation,

$$\Delta f = -\frac{2nf_0^2}{\sqrt{\rho_q\mu_q}} \frac{\Delta m}{A}$$
$$T_f = \frac{\Delta m}{A\rho_f} \longrightarrow (2.1)$$

Where,  $f_0$  is an oscillation frequency at the fundamental mode,  $n$  is overtone number,  $A$  is active surface area of quartz crystal resonator,  $\mu_q$  and  $\rho_q$  are shear modulus ( $2.947 \times 10^{11} \text{ gcm}^{-1}\text{s}^{-2}$ ) and density ( $2.648 \text{ g/cm}^3$ ) of quartz, respectively and  $\rho_f$  is the density of the deposited film.

Since the frequency is a function of temperature, this method is not useful at higher temperatures.

(ii) Multiple-beam interferometry

The multiple-beam interferometry is part of optical method in which a reflected ray from the surface of film and reflected ray from the interface of film and substrate are brought together to produce interference patterns. The measurement of fringe width ( $x$ ) and fringe shift ( $\Delta x$ ) can allow to estimate thickness of the film using,

$$T_f = \left(\frac{\Delta x}{x}\right) \frac{\lambda}{2} \longrightarrow (2.2)$$

where,  $\lambda$  is wavelength of the incident light.

In this method both films and substrate should be more reflective.

(iii) Gravimetric method:

Herein, the thickness of the films ( $T_f$ ) usually depends on mass of film and the density of material adapted from bulk ( $\rho$ ). The mass of the films ( $m_f$ ) can be taken from the difference in mass of substrate before deposition ( $m_o$ ) and after deposition ( $m_a$ ). By scaling the area of film to be deposited, the working formula is,

$$T_f = \frac{m_f}{\rho A} \longrightarrow (2.3)$$

In present study the gravimetric method has been used and further verified by SEM cross section image. Since the density of films has taken from bulk, there might be error in film thickness values. Hence, SEM cross section images were recorded for 10 samples and error was countered from gravimetric method.

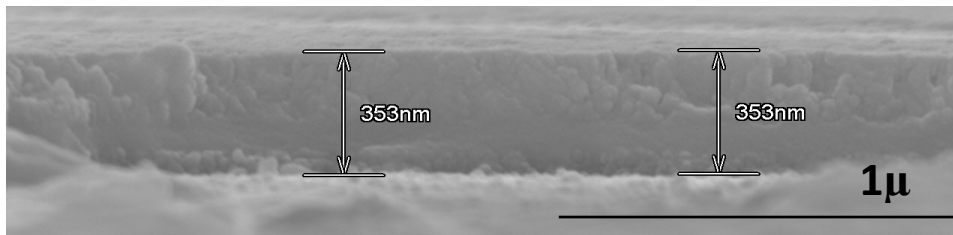


**Figure 2.3** A representative image for cross sectional SEM image for 350 nm thickness film.

The average error in thickness measurement was estimated to be 5% ( $\pm 10$  nm of 350 nm) of thickness measured from gravimetric method.



## 2.3 Characterization

### 2.3.1 Structural and compositional characterization

X-ray diffraction (XRD) is a powerful non-destructive technique to characterize solid materials. X-rays are generated in cathode ray tube from the heated filament to produce electrons, as well as accelerate the electrons towards a target by applying a voltage, and bombarding the target material with electrons. When electrons have sufficient energy to liberate inner shell electrons of target material, characteristic spectra will produce. It provides information on structures, phases, preferred crystal orientations and other structural parameters such as average grain size, crystallinity, strain and crystal defects. X-ray diffraction peaks are produced by constructive interference of monochromatic beam of x-rays scattered at specific angles from each set of lattice planes in a sample. The peak intensities are determined by the distribution of atoms within the lattice. Consequently, the x-ray diffraction gives fingerprint pattern due to periodic and unique atomic arrangement in a given material.



**Figure 2.4** RIGAKU x-ray diffractometer.

X-ray diffraction of the films were recorded by x-ray diffractometer (RIGAKU MINI FLUX-600 model) using  $\text{Cu K}_\alpha$  radiation in  $2\theta$  ranging from  $20^\circ$  to  $65^\circ$ .

The grain size can be calculated by the formula,

$$\text{Grain size } D = \frac{0.94 \lambda}{\beta \cos \theta} \longrightarrow (2.4)$$

where  $\lambda$  = wavelength of Cu  $k_{\alpha}$  line (1.54059 Å)

$\beta$  = full width at half maxima value and

$\theta$  = Bragg's angle

The lattice parameters can be calculated by using the formula

$$d_{hkl} = \frac{1}{\sqrt{\frac{h^2}{a^2} + \frac{k^2}{b^2} + \frac{l^2}{c^2}}} \longrightarrow (2.5)$$

where  $d$  = inter planar distance,  $h, k, l$  - miller indices and  $a, b, c$  – lattice Constants

The scanning electron microscope is a type of electron microscope that builds up the images of sample surface point by point in a time sequence by scanning it with a high-energy beam of electrons in a raster scan pattern. The electrons interact with the atoms that makes the sample to produce signals that contain information about the sample's surface topography, composition and properties. A direct observation of microstructure as well as the investigation of morphology can be made using the scanning electron microscope (SEM). SEM generate images using secondary electron and back-scattered electron (BSE) detectors. SEM is a powerful instrument which permits the characterization of heterogeneous materials and surfaces on a local scale. In the present investigations SEM is used in its most common mode, the emissive mode. In this mode the secondary electrons emitted from the specimen are collected. It is especially suitable for obtaining information concerning the surface region of the specimen.

The EDS detector collects the characteristic x-rays of different elements. The x-ray photon first creates a charge pulse in detector. This charge pulse is then converted into a voltage pulse whose amplitude reflects the energy of detected x-ray. Finally, this

voltage pulse produces an energy spectrum which is useful to determine the abundance of specific elements. A typical EDS spectrum is portrayed as a plot of x-ray count versus energy (in KeV). Energy peaks correspond to the various elements in the sample. Energy dispersive x-ray spectroscopy can be used to find the chemical composition of materials which is under a spot of size about few microns and to create element composition maps over a much broader raster area. These capabilities together provide fundamental compositional information for a wide variety of materials, including polymers and metals.



**Figure 2.5** ZEISS field emission scanning electron microscope.

The chemical composition of the films was confirmed by energy dispersive analysis of X-rays (EDAX) (OXFORD, CLASS ONE SYSTEM model). Composition is rounded off to one decimal place and an estimated maximum error of  $\pm 0.5$  at % was assumed. Field emission scanning electron microscope (FESEM) (CARL ZEISS model) was used to capture surface image of the films.

### 2.3.2 Electrical characterization

If an electronic conductor or semiconductor is connected to voltage source, then it results in a current. Current-voltage curves of an electrical device or component are set of graphical curves which are used to define its operation within an electrical circuit. If the I-V curve is linear and symmetric then contact is said to be ohmic. If I-V curve is non-linear and asymmetric then the contact is said to be non-ohmic. An ideal ohmic contact is one in which the voltage drop across the junction is zero. The metal-semiconductor junction will show ohmic nature when the barrier to the electron flow between metal and semiconductor is small and easy to overcome even at small voltages.

To determine the electrical properties of semiconductor material, the nature of contact with semiconductor needs to be checked. In this investigation, the ohmic contacts were made by the evaporation of high purity silver onto the films under vacuum. The ohmic nature of the contacts is verified by current- voltage characteristics.

DC two probe method is used to measure the electrical resistivity as well as activation energy of prepared thin films. In this method, resistivity is computed by measuring the resistance across the sample by passing a current through it. The resistivity of film at constant temperature is calculated by the formula,

$$\rho = \frac{RA}{L} \longrightarrow (2.6)$$

where A is an area of cross section of the film and L is the length.

Activation energy  $E_a$  of film can be calculate using the resistance values at different temperatures (298-473 K) by using relation,

$$R = R_0 \exp\left(\frac{E_a}{kT}\right) \longrightarrow (2.7)$$

where k is Boltzmann constant and T represents the temperature in absolute scale.

In order to check the suitability of indium telluride to diode, the heterojunction made with Si. The typical rectification nature of a p-n junction is studied through I-V characteristic curves. Generally, in p-n junction, the I-V characteristics depends on thermionic emission in interface region of low doping profile material whereas, on

tunnelling current in high doping profile material. However, the mostly used model is thermionic emission diffusion model in which the relation between voltage and current denoted by equation 2.8.

$$I = I_s \left\{ \exp \left( \frac{qV}{\eta kT} - 1 \right) \right\} \longrightarrow (2.8)$$

At higher voltages equation 2.8 can be written into,

$$I = I_s \left\{ \exp \left( \frac{qV}{\eta kT} \right) \right\}$$

Where,  $I_s$  indicates reverse saturation current,  $q$  is elementary charge,  $\eta$  represents ideality factor,  $k$  is Boltzmann's constant and  $T$  is the temperature. The equation for reverse saturation current is,

$$I_s = A^* T^2 \left\{ \exp \left( - \frac{q\phi_b}{kT} \right) \right\} \longrightarrow (2.9)$$

Here,  $A^*$  is Richardson's constant and  $\phi_b$  is barrier height.

Hence, equation 2.8 have been used to estimate ideality factor to understand the conduction mechanism whereas equation 2.9 is used to estimate the barrier height.

In the present study, a lab designed experimental setup (Figure. 2.6) has been used to investigate the thermoelectric properties of both  $\text{In}_2\text{Te}_3$  and  $\text{InTe}$  films. The experimental setup consists of two aluminum clamps to hold the sample in which one of the clamp was connected to the heater. Here, the sample size (Indium telluride thin film) was maintained such that the length-to-width ratio as 5.5 and the ohmic contacts at the both ends of the thin film were made with silver (thermal evaporation method). To maintain the temperature gradient in sample, the heater temperature was raised gradually. The temperature indicators with thermocouple were connected to the hot and cold ends of the sample to monitor the maintained temperature gradient. This temperature gradient induces the thermo emf in the sample and it can be explained as follows: at the hot probe, the thermal energy of the majority carrier is higher than at the cold probe, hence carriers will tend to diffuse away from the hot probe driven by the temperature gradient. As they diffuse away from the hot probe, they leave behind the oppositely charged immobile donor atoms, which results in a current flow towards the

hot probe and the magnitude of voltage across two ends will give the generated thermo emf values. The thermo emf of the prepared films was measured in the temperature gradient range of 5-170 K. Further, the current flow towards hot probe for p-type material and away from the hot probe for n-type material, this allows to find the material type.

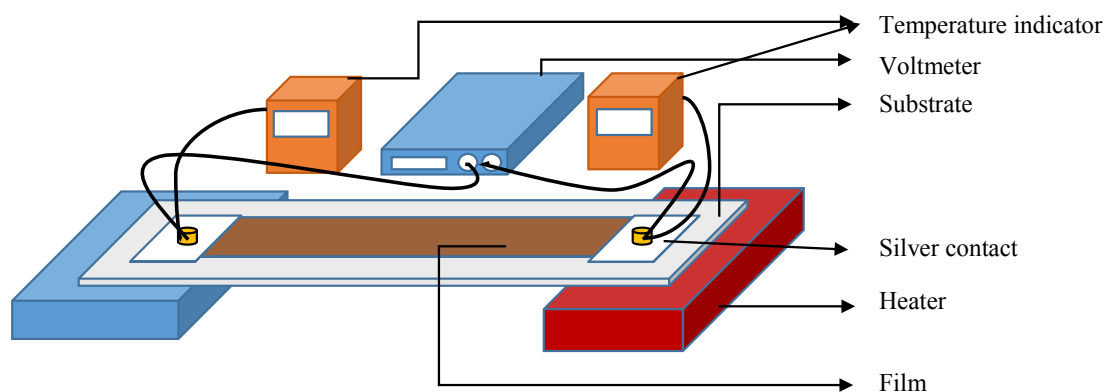


**Figure 2.6** Schematic diagram of the thermo emf measurement set up.

Thermoelectric power of material can be measured using formula,

$$S = \frac{\Delta V}{\Delta T} \longrightarrow (2.10)$$

where  $\Delta V$  = voltage difference

$\Delta T$  = temperature difference

### 2.3.3 Optical characterization

Optical analysis is a non-destructive technique which explores the change in intensity, energy, phase, direction or polarization of the light wave after interaction with the object being studied.

Spectrophotometry (UV-VIS-NIR) is one of the most basic methods to investigate the properties of materials through their interaction with light which is useful to measure an intensity of light reflected, transmitted or absorbed by that material. The material absorbs light when the incident photons create atomic or charge in movements in the

material. If we measure that absorption as a function of photon energy, we can get an insight into its electronic and atomic structure. We have to note the morphology, stress, temperature, contact with other materials, etc. All these defects may affect the materials phonons and electrons transitions and will modify the materials absorption capability of light in many cases. This phenomenon allowing us to know more about the material's properties through the measurement of its absorption spectrum, all these variables must be controlled or monitored while performing the measurements.



**Figure 2.8** Shimadzu UV-VIS-NIR spectrophotometer.

The optical absorption spectra of indium telluride films were recorded using a spectrophotometer (SHIMADZU UV-3600) in the wavelength range of 500-2500 nm.

Absorption coefficient formula

$$\alpha(\nu) = \frac{A(h\nu - E_g^{opt})^r}{h\nu} \longrightarrow (2.11)$$

where, A= constant,  $E_g^{opt}$ = optical energy gap,  $h\nu$  is energy of incident photon and r = power which characterizes the type of the optical transition process. The parameter 'r' has value ½ for direct allowed transition and the value 2 for the indirect allowed transition. The usual method for determination of optical band gap involves a graph of  $(\alpha h\nu)^{1/r}$  against  $h\nu$ . The linearity of  $(\alpha h\nu)^{1/r}$  versus  $h\nu$  plot indicates the existence of the allowed type of transition.

## CHAPTER 3

### OPTIMISATION AND PROPERTIES OF INDIUM TELLURIDE THIN FILMS

Overview:

*This chapter describes the process followed to get stoichiometric and mono-phased indium telluride films from the structural and compositional confirmation. The optimisation process reveals that the annealing temperature plays an important role to achieve mono-phased and stoichiometric films. Hence, the structural, electrical and optical properties of  $\text{In}_2\text{Te}_3$  and  $\text{InTe}$  films are investigated at optimised annealing temperature by varying the substrate temperature. The parameters such as lattice constants, activation energy, resistivity/conductivity, optical band gap and absorption coefficient have been reported for mono-phased  $\text{In}_2\text{Te}_3$  and  $\text{InTe}$  films.*

#### 3.1 Introduction

In order to understand the properties of a material, investigation should start with optimising the growth conditions to attain stoichiometric and mono-phased films at which the extrinsic defects are considered to be minimum. Since the indium telluride exists in different stoichiometries such as  $\text{In}_2\text{Te}_5$ ,  $\text{In}_2\text{Te}_3$ ,  $\text{InTe}$ ,  $\text{In}_7\text{Te}_{10}$  and  $\text{In}_3\text{Te}_4$  at various pressures and temperature, a precise control on growth condition is essential. To get stoichiometric indium telluride films, different methods are reported. Emziane et al (1999) had used thermal evaporation method to grow  $\text{In}_2\text{Te}_3$  films. They varied the annealing temperature and duration to obtain the mono-phase and stoichiometry of the films and optimised annealing temperature at 663 K (30 min) on  $\text{SnO}_2$  coated glass substrates (Emziane et al. 1999). Guettari et al. (2003) attained mono-phased and nearly stoichiometric ( $\pm 1$  at. %) films at 500 K substrate temperature by co-evaporation of In and Te (Guettari et al. 2003). Desai et al. (2005) prepared  $\text{In}_2\text{Te}_3$  films by flash evaporation method on glass substrates and obtained stoichiometry at 473 K substrate temperature (Desai et al. 2005). Matheswaran et al. (2012) prepared single-phase and



non-stoichiometric  $\text{In}_2\text{Te}_3$  films from In/Te bilayer by irradiation of 130 MeV Au ion flux of  $1 \times 10^{13}$  ions/cm<sup>3</sup> (Matheswaran et al. 2012).

Whereas for InTe, Rousina and Shivakumar (1987) had grown stoichiometric films from non-stoichiometric bulk compound with excess of In using thermal evaporation technique but the type of substrate used in this investigation was not mentioned (Rousina and Shivakumar 1988). Peranatham et al. (2007) reported stoichiometry of InTe films at 523 K annealing temperature, but these films are exhibiting optical band gap of  $\text{In}_2\text{Te}_3$  (~1) (Peranatham et al. 2007). Intermediately, there are many reports on indium telluride thin films in which some reported about stoichiometry of the films and others mentioned only the phases involved in it (Afifi et al. 1996; Hegab et al. 1998; Krishna Sastry and Jayarama Reddy 1983; Kumar and Rao 2011; De Purkayastha et al. 1980; Sastry and Reddy 1980). In case of indium telluride, the compound forms in different stoichiometries under variable pressure and temperature. Therefore, the evaporated films are mixture of at least two phases which can cause ambiguity in properties of material. Hence there is a compulsion to study electrical and optical properties of mono-phased InTe in thin film form for further usage in micro-electric devices. In this chapter, the growth parameters such as substrate temperature, annealing temperature and annealing duration have been varied to attain stoichiometry in both  $\text{In}_2\text{Te}_3$  and InTe thin films.

### 3.2 Structure and composition of source materials

In order to know the structure and composition of source materials, the powdered  $\text{In}_2\text{Te}_3$  and InTe precursors are subjected to XRD and EDAX analysis. Figure 3.1 shows the powder XRD patterns of bulk  $\text{In}_2\text{Te}_3$  and InTe. Diffractogram of both  $\text{In}_2\text{Te}_3$  and InTe are indexed using cubic  $\alpha\text{-In}_2\text{Te}_3$  (JCPDS card No: 00-033-1488) and tetragonal InTe (JCPDS Card No:01-071-0109) diffraction data, respectively. The estimated lattice parameter of  $\text{In}_2\text{Te}_3$  is 18.4782 Å which is very close to the standard data (18.4860 Å). In  $\text{In}_2\text{Te}_3$  compound, the peaks correspond to (5 1 1), (8 2 2), (9 3 3) and (12 0 0) planes located at  $2\theta$  of 25.2, 41.42, 49.05 and 60.12° respectively, and dominant along  $\text{In}_2\text{Te}_3$  (5 1 1) planes. Whereas InTe is also exhibiting multi-peaks and predominant along (2

2 0) plane located at  $2\theta$  of  $29.88^\circ$ . The calculated lattice parameters are  $8.4513 \text{ \AA}$  and  $7.1852 \text{ \AA}$  which are matching well with standard values ( $a=8.4540 \text{ \AA}$  and  $c=7.1520 \text{ \AA}$ ).

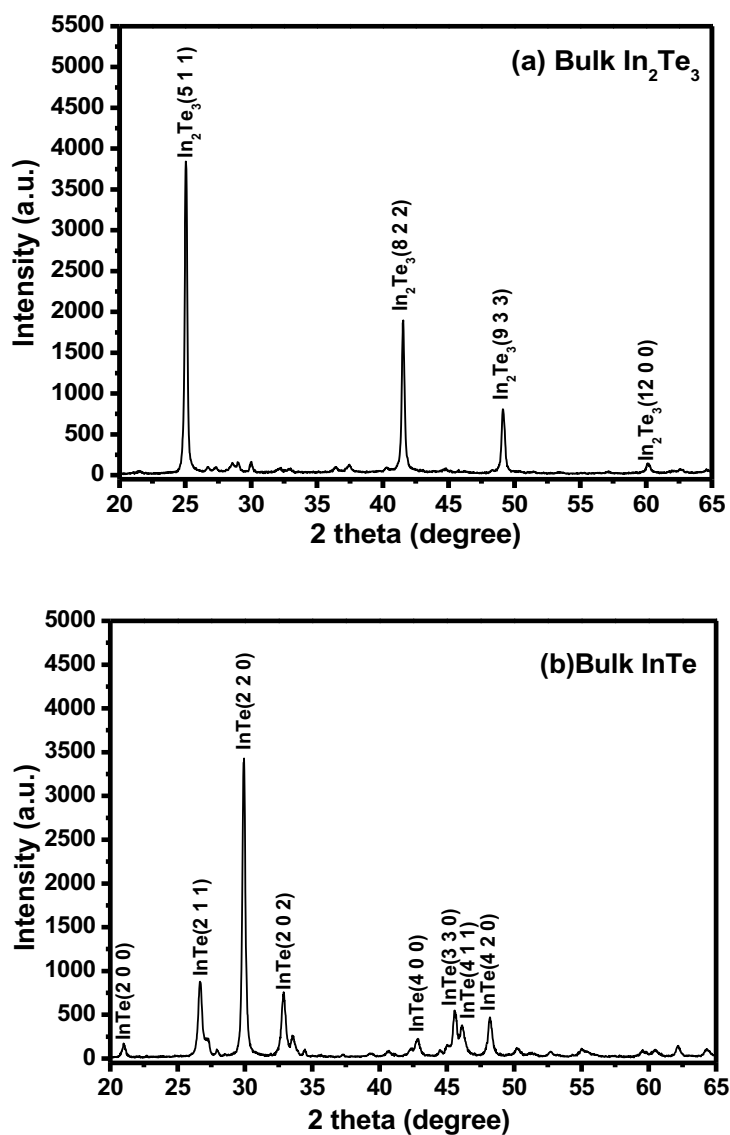


**Figure 3.1** XRD patterns of powered bulk (a).  $\text{In}_2\text{Te}_3$  and (b).  $\text{InTe}$  materials.

Figure 3.2 shows the EDAX spectra of  $\text{In}_2\text{Te}_3$  and  $\text{InTe}$  compounds. The composition of elements presented in this compounds are tabulated in table 3.1. In  $\text{In}_2\text{Te}_3$ , the composition is nearer to stoichiometric ratio (2/3) whereas  $\text{InTe}$  compound is having an excess amount of In. With this basic analysis of source compounds we have initiated our investigation on the growth and optimisation of  $\text{In}_2\text{Te}_3$  and  $\text{InTe}$  thin films.

**Table 3.1** Elemental composition of powdered bulk source materials

Compound	Elemental composition (at.%)	
	In	Te
In <sub>2</sub> Te <sub>3</sub>	40.6	59.4
InTe	51.6	48.4

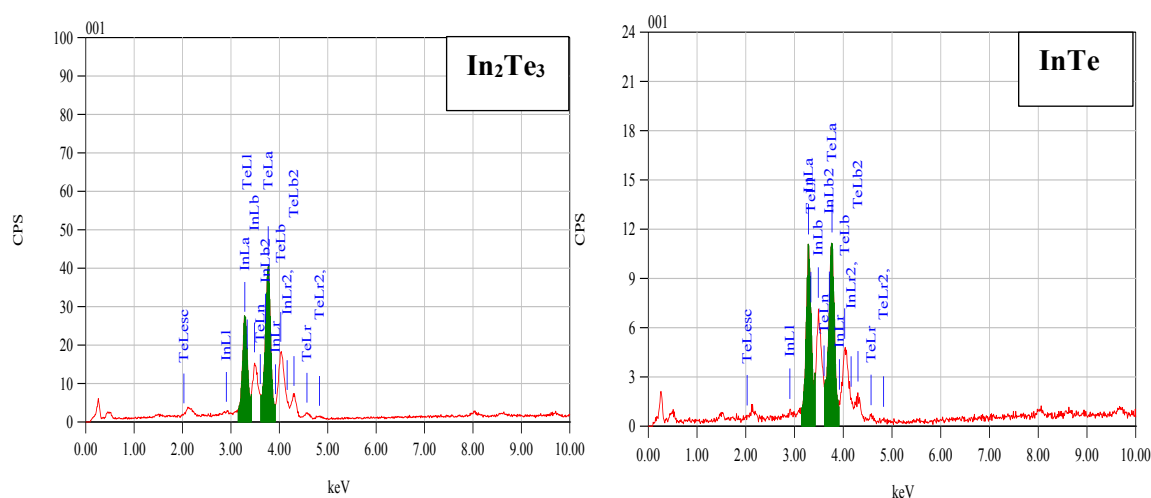


**Figure 3.2** EDAX spectra of bulk In<sub>2</sub>Te<sub>3</sub> and InTe powders.

### 3.3 Preparation of In<sub>2</sub>Te<sub>3</sub> thin films

#### 3.3.1 Growth conditions of In<sub>2</sub>Te<sub>3</sub> thin films

The In<sub>2</sub>Te<sub>3</sub> thin films were grown on soda lime glass substrates using thermal evaporation technique. The pre-deposited soda lime glass substrates were thoroughly cleaned by three step process, initially by dipping them in chromic acid for 24 h to remove impurities on the top layer of the substrate, then washed them with liquid detergent, and finally ultrasonicated with acetone. For each deposition, a substrate of 7.5 x 2.5 cm<sup>2</sup> dimension was used. The residual pressure inside the chamber was maintained at ~ 5x10<sup>-6</sup> torr. The distance between the substrate to source was optimised to 12 cm. A molybdenum boat (200 A) was used to evaporate the source material

(99.999% pure  $\text{In}_2\text{Te}_3$  pellets) and the current was gradually increased up to 52 A, further maintained constant throughout the deposition. The thickness of the films was maintained around  $350 \pm 10$  nm. The deposition rate was maintained to 4.2 nm/s. While optimising the deposition parameters, the substrate temperature of the films was varied from 298 K to 473 K whereas, annealing temperature and duration were varied from 373 K to 573 K and 1 h to 3 h, respectively. The electrical properties of the  $\text{In}_2\text{Te}_3$  films were investigated in the temperature range of 305 K to 453 K. The current-voltage characteristics of the films were investigated in the voltage range of -5 V to +5 V.

### 3.3.2 Optimisation of growth parameters for stoichiometric $\text{In}_2\text{Te}_3$ thin films

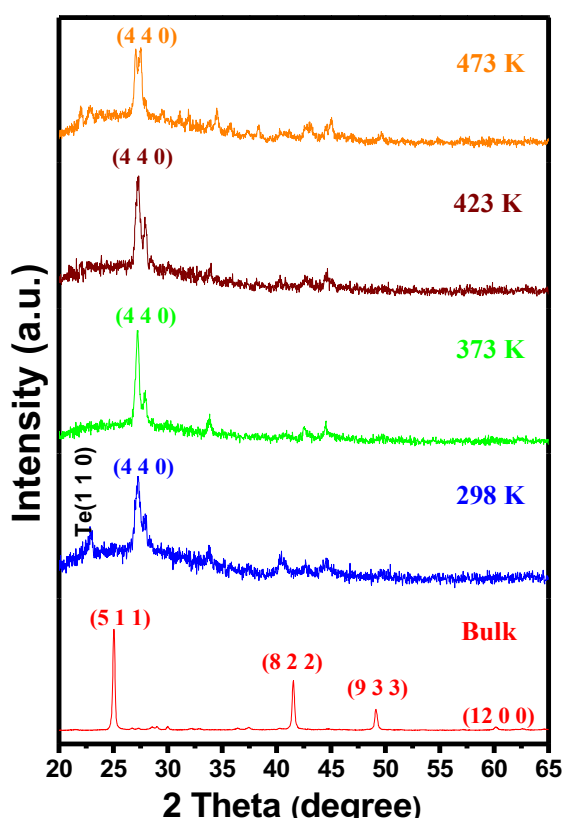


**Figure 3.3** X-ray diffractogram of as-deposited films at different substrate temperatures.

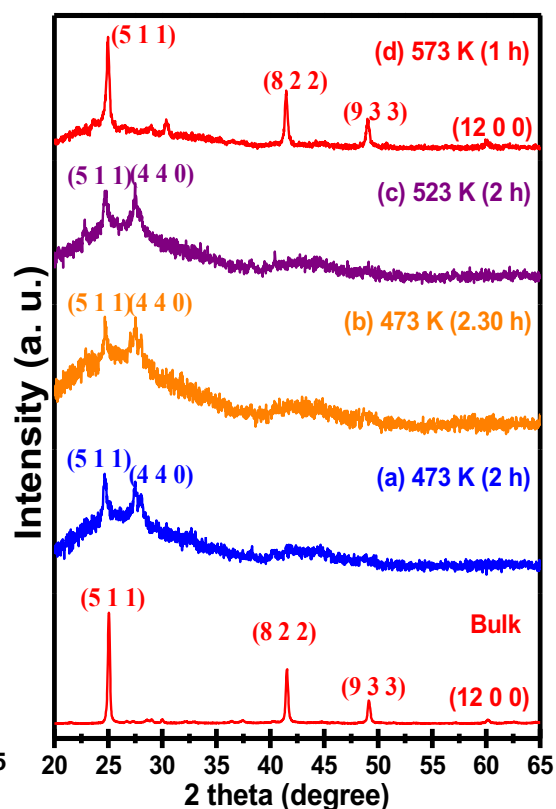


**Figure 3.4** X-ray diffractogram of films deposited at 423 K and annealed at different temperatures.

The films deposited at different substrate temperatures ranging from 298 K to 473 K are subjected to both XRD and EDAX studies. Figure 3.3 shows the XRD patterns of the as-deposited films at different temperatures. XRD patterns are indexed on the basis of cubic  $\text{In}_2\text{Te}_3$  JCPDS data, the same data card which used to index the precursor bulk compound is used. The as-deposited films are polycrystalline in nature with preferred orientation along (4 4 0) direction. The films deposited at 298 K are having an additional peak corresponding to hexagonal Te (1 1 0) at  $2\theta$  of  $23.02^\circ$  (JCPDS data No. 01-078-2312) which disappeared for the films deposited at 373 K substrate temperature. It is also observed that XRD patterns of bulk precursor powder and as-deposited films are dissimilar.

**Table 3.2** Variation in composition of  $\text{In}_2\text{Te}_3$  thin films with substrate temperature

Substrate temperature (K)	Composition ( at.%)	
	In	Te
298	47.2	52.8
373	45.5	54.5
423	45.6	54.4
473	44.7	55.3

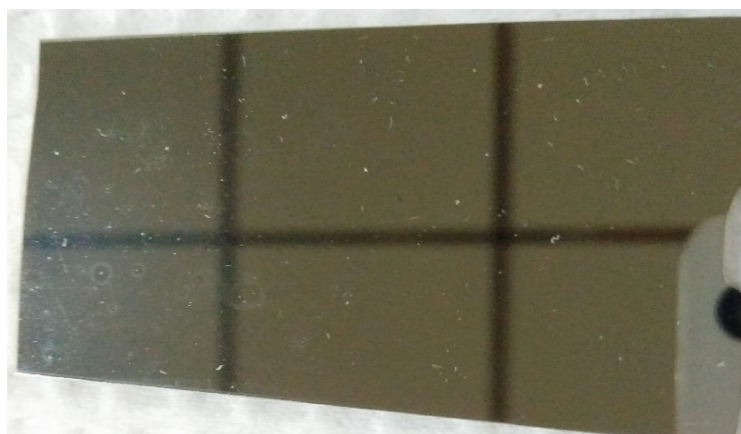
EDAX analysis shown in table 3.2 revealed that the as-deposited films have relatively higher In:Te ratio when compared to the stoichiometric ratio (40:60) of  $\text{In}_2\text{Te}_3$  as they are rich in indium. It has been observed that the crystallinity of the films deteriorates when the films are deposited at a substrate temperature of 473 K. Hence, the films deposited at 423 K are selected for further analysis.

Figure 3.4(a), 3.4(b) show the diffraction patterns of films deposited at 423 K followed by post-annealing at 473 K for 2 h and 2:30 h, respectively, whereas figure 3.4(c) shows the XRD pattern of films annealed at 523 K for 2 h. In contrast to the as-deposited films, the annealed films show a decrease in the intensity of (4 4 0) peak and the appearance of (5 1 1) peak. Table.3.3 summarizes the effect of annealing temperature and duration on the composition of  $\text{In}_2\text{Te}_3$  thin films. Irrespective of annealing duration, the films annealed at 473 K and 523 K are found to be non-stoichiometric and indium rich.

**Table 3.3** Composition of  $\text{In}_2\text{Te}_3$  thin films at different annealing conditions

Annealing temperature and duration of 423 K deposit $\text{In}_2\text{Te}_3$ thin films	Composition (at%)	
	In	Te
473 K for 2 h	42.9	57.1
473 K for 2:30 h	44.2	55.8
523 K for 2 h	42.7	57.3
573 K for 1 h	40.9	59.1
573 K for 2 h	40.2	59.8

Figure 3.4(d) shows the diffraction pattern of a film deposited at 423 K and annealed at 573 K for 1 h. These films show good crystallinity with strong (5 1 1), (8 2 2), (9 3 3) and (12 0 0) peaks which are matching well with the standard data. Compositional analysis of these films revealed that films are nearly stoichiometric. Although, the films annealed for 2 h have better composition, but the quality and crystallinity of the films are found to be diminished (Figure 3.5). Hence, the films deposited at 423 K followed by post annealing treatment at 573 K for 1 h are suggested as better quality films.



**Figure 3.5** Photograph of  $\text{In}_2\text{Te}_3$  films deposited at 423 K and annealed at 573 K for 2h.

### 3.3.2. Effect of substrate temperature on the properties of $\text{In}_2\text{Te}_3$ films at constant annealing temperature

Structural properties:

From above analysis, one can observe that the optimised annealing temperature is 573 K. Hence, the effect of annealing on  $\text{In}_2\text{Te}_3$  films was investigated at 573 K by varying the substrate temperature.  $\text{In}_2\text{Te}_3$  thin films deposited at 298 K, 373 K, 423 K and 473 K substrate temperatures are annealed at 573 K for 1 h to investigate structural, electrical and optical properties. The XRD patterns of the annealed films are shown in figure 3.6. All films are polycrystalline in nature and contained diffractions from (5 1 1), (8 2 2), (9 3 3) and (12 0 0) planes which matches well with the XRD pattern of powdered source material. The lattice constant of the films is estimated to be 18.478 Å using equation 2.6 which matches well with the standard data.

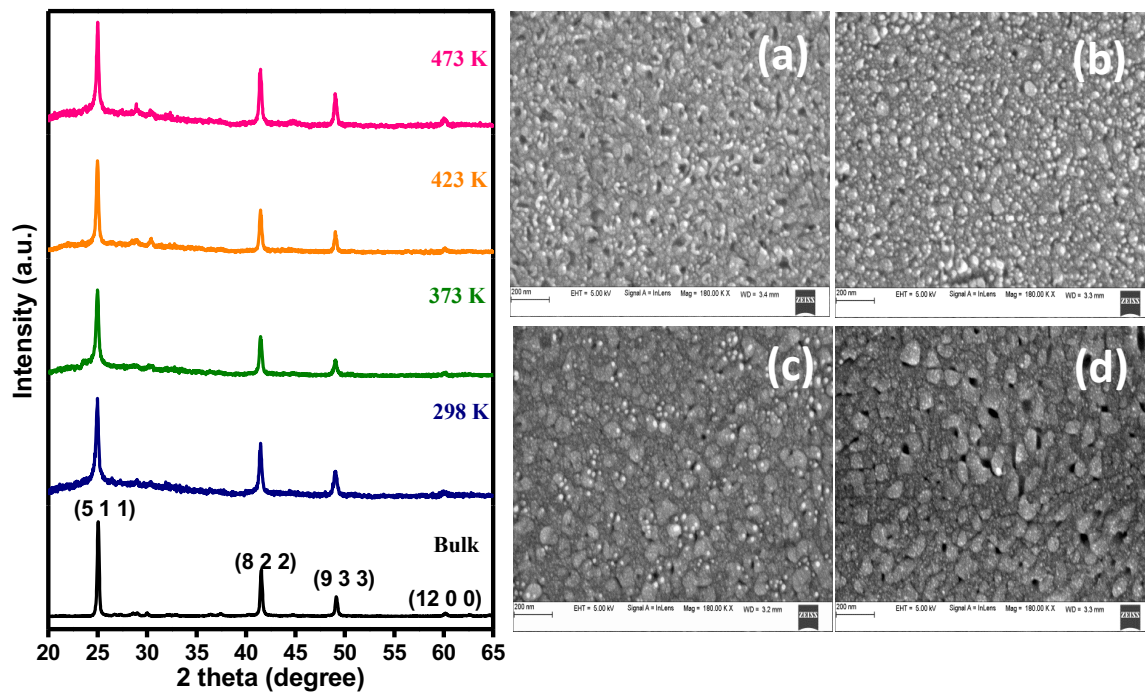


**Figure 3.6** XRD patterns of annealed (573 K (1h))  $\text{In}_2\text{Te}_3$  thin films at different substrate temperatures.

**Figure 3.7** FESEM images of annealed  $\text{In}_2\text{Te}_3$  thin films deposited at (a). 298 K, (b). 373 K, (c). 423 K and (d). 473 K substrate temperatures.

The FESEM images of these  $\text{In}_2\text{Te}_3$  thin films shown in figure 3.7 demonstrates the granular structure. It can also be seen that the grain size increases proportionally with the substrate temperature. Inter-granular gaps are originated in all films and are more accent in 473 K deposited films. Table.3.4 shows the variation of composition and grain size of annealed  $\text{In}_2\text{Te}_3$  films with the substrate temperature. The films are having almost same composition regardless of the substrate temperature with indium (In) and tellurium (Te) atomic percentages as  $41.26 \pm 0.34$  and  $58.61 \pm 0.4$ , respectively. However, the films deposited at 423 K are nearly stoichiometric.

**Table 3.4** Composition and grain size of annealed  $\text{In}_2\text{Te}_3$  thin films

Substrate temperature of the films annealed at 573 K for 1h (K)	Atomic percentage of elements (at.%)		Grain size (nm)
	In	Te	
298	41.6	58.4	29.32
373	41.7	58.3	30.04
423	40.9	59.1	34.28
473	41.0	59.0	36.65

Electrical properties:

The electrical studies have been carried out by making silver contacts on films using thermal evaporation unit. The symmetric nature of I-V curves in figure 3.8(a) represents the ohmic nature of silver to the films which in turn offers negligible voltage drop across the interface of silver and  $\text{In}_2\text{Te}_3$  films. To know the type of majority carrier, the films are subjected to thermo-electric probe analysis (Hot probe) which reveals that both as-deposited and annealed films are p-type.



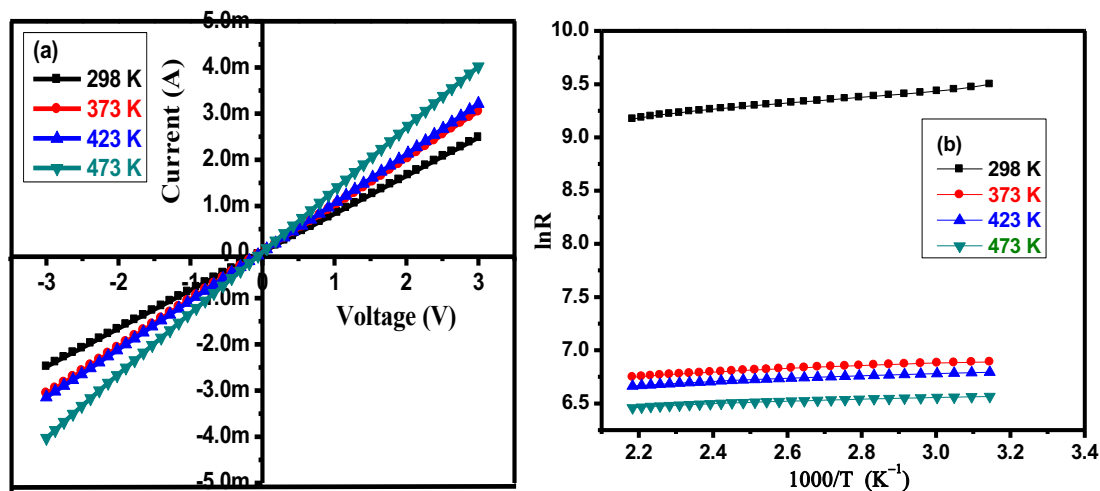


**Figure 3.8 (a).** I-V characteristic curves and **(b).** Plot of ln R versus 1/T of In<sub>2</sub>Te<sub>3</sub> films deposited at different substrate temperatures and annealed at 573 K for 1h.

The electrical resistivity of the annealed films is estimated at room temperature from the slope of I-V curves (Figure 3.8(a)). The electrical resistivity of the films is found to be decreased with an increase in the substrate temperature which might be due to the increase in grain size. Figure 3.8(b) shows the plot of variation in ln R with inverse temperature (Arrhenius plot of R(T)). The thermal activation energy of the prepared films is determined from the slope of Arrhenius plots which is found to be  $0.01 \pm 0.005$  eV. Table 3.5 shows the variation in resistivity, activation energy and optical band gap of annealed In<sub>2</sub>Te<sub>3</sub> thin films with substrate temperature.

**Table 3.5.** The resistivity, activation energy and optical band gap of In<sub>2</sub>Te<sub>3</sub> thin films

Substrate temperature of In <sub>2</sub> Te <sub>3</sub> films annealed at 573 K for 1h (K)	Resistivity at Room temperature ( $\Omega$ -cm)	Activation energy (eV)	Optical band gap (eV)
298	0.423	0.015	0.99
373	0.343	0.012	1.01
423	0.33	0.011	0.98
473	0.263	0.009	0.97

Optical properties:

Figure 3.9(a) represents transmittance spectra of annealed  $\text{In}_2\text{Te}_3$  films. Higher transmittance is observed in the near IR region for all annealed films (maximum of 90 % at 1500 nm wavelength). Figure 3.9(b) shows the variation in absorption co-efficient ( $\alpha$ ) with photon energy of the films in visible range. The absorption co-efficient of the prepared films in the visible range is of the order of  $10^5 \text{ cm}^{-1}$ .

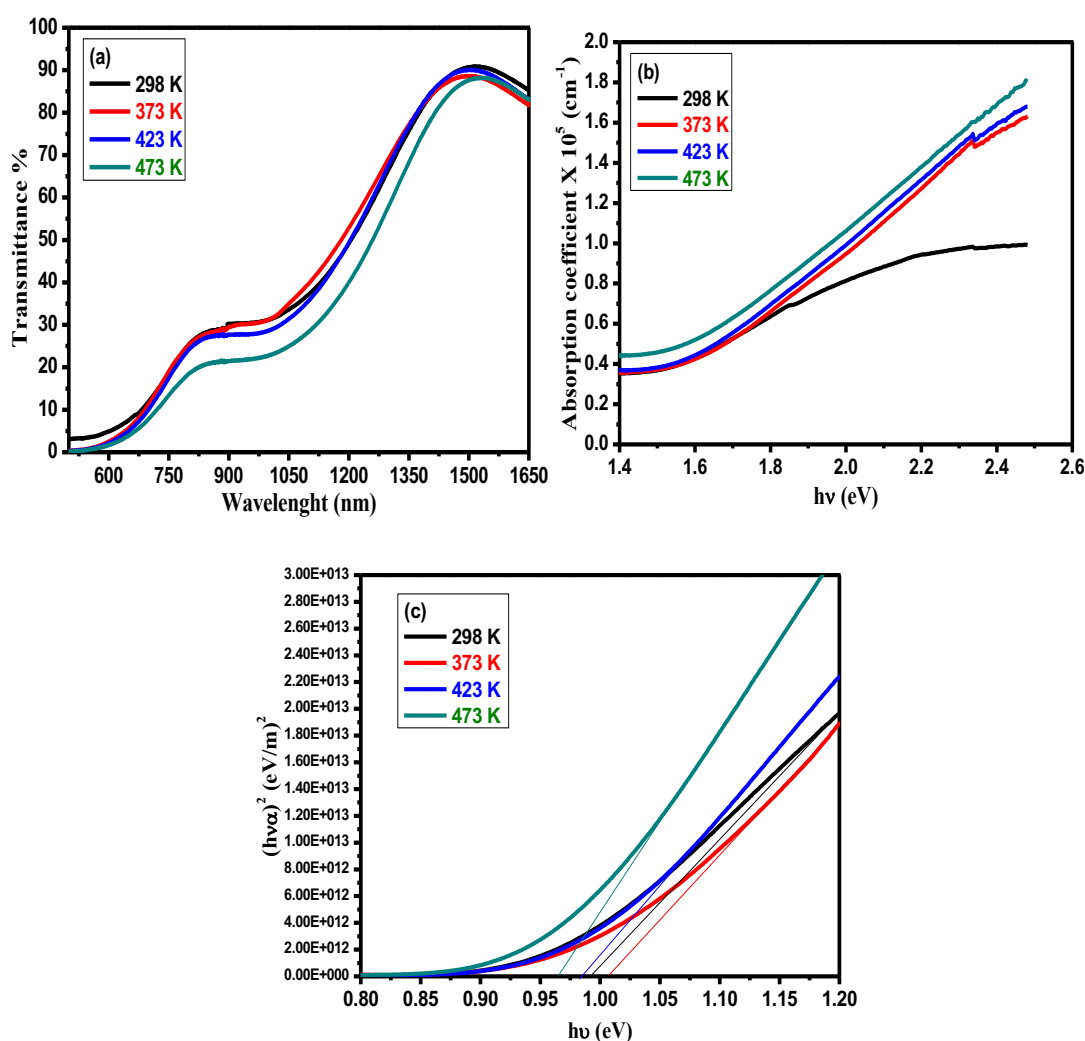


**Figure 3.9 (a).** Transmittance spectra, **(b).** Variation in absorption co-efficient with photon energy and **(c).** Tauc's plot of  $\text{In}_2\text{Te}_3$  thin films deposited at different substrate temperatures and annealed at 573 K for 1h.

Figure 3.9(c) shows the variation in  $(h\nu\alpha)^2$  with photon energy in the range of 0.8 to 1.2 eV. The direct band gap of  $\text{In}_2\text{Te}_3$  films is estimated by extrapolating linear portion of Tauc's plots to energy axis which is found to be  $0.99 \pm 0.02$  eV regardless of applied substrate temperature.

### **3.4 Preparation of InTe thin films**

#### **3.4.1 Growth conditions of InTe thin films**

The InTe thin films were deposited on glass substrates of  $7.5 \times 2.5 \text{ cm}^2$  dimension using thermal evaporation technique. Prior to the deposition, the glass substrates were dipped in chromic acid for 24h and washed with liquid detergent and acetone. To evaporate the source material (InTe pellets with 99.999 % purity) a 100 A molybdenum boat has been used. An electrical supply to boat is gradually increased up to 52 A and further kept it constant throughout the deposition. The residual pressure of the deposition chamber has been maintained below  $10^{-5}$  torr. The source to substrate distance was maintained constant at 11 cm. The thickness of the InTe films was maintained constant of about  $300 \pm 10$  nm. The substrate temperature was varied from 305 K to 453 K and annealing temperature from 473 K to 573 K for duration of 1 h to 2 h. The I-V characteristics of stoichiometric InTe films were investigated in the voltage of range - 5 V to +5 V.

#### **3.3.2 Optimisation of growth parameters for stoichiometric InTe thin films**

To get stoichiometric and mono-phased InTe thin films, the investigation is initiated by varying substrate temperature. Figure 3.10 shows the XRD patterns of InTe films deposited at different substrate temperature. Here, all films are showing polycrystalline nature and exhibiting the mixed phase of InTe and  $\text{In}_2\text{Te}_3$ . All as-grown films are predominantly oriented along  $\text{In}_2\text{Te}_3$  (4 4 0) plane except the films growth at 423 K in which  $\text{In}_2\text{Te}_3$  (5 3 1) is dominant. However, the contribution of  $\text{In}_2\text{Te}_3$  phase is dominant in as-deposited films whereas, InTe peaks are having very small intensity. In

order to fix the substrate temperature for further analysis, all as-deposited films are subjected to compositional analysis.

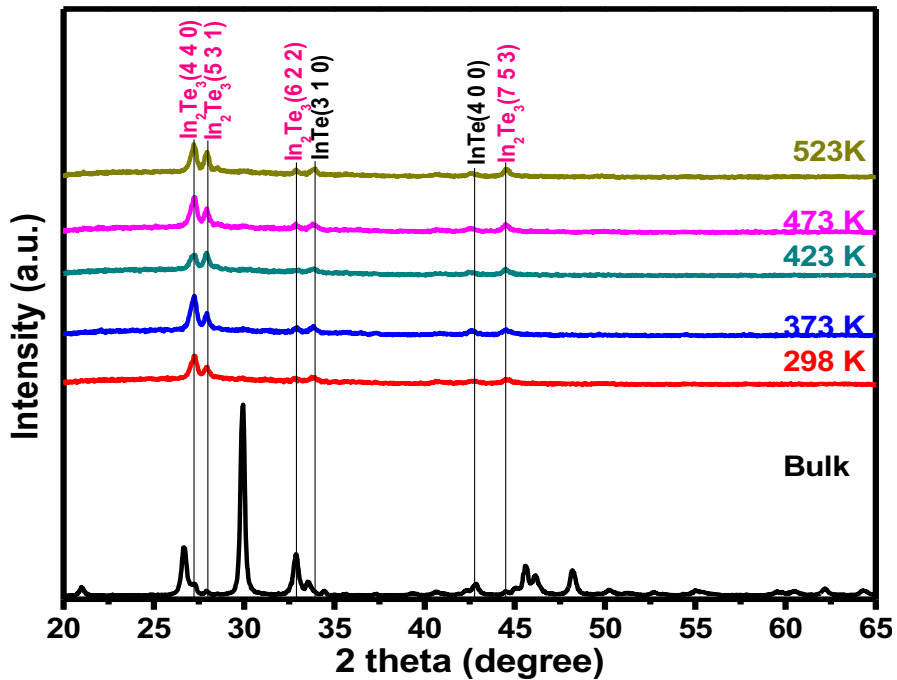


Figure 3.10 XRD patterns of InTe films at different substrate temperature.

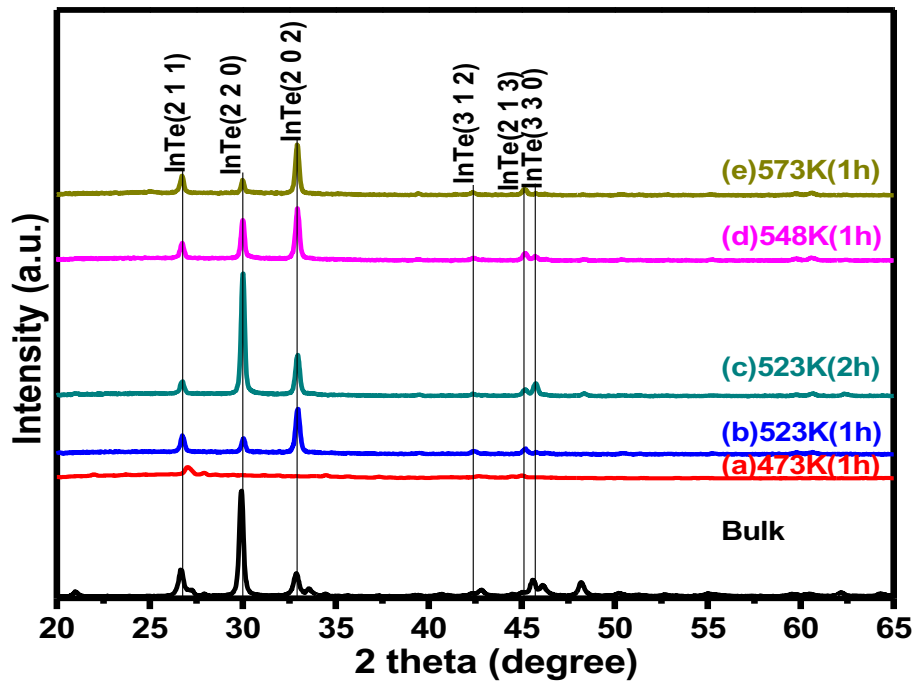


Figure 3.11 XRD patterns of InTe films grown at 473 K and annealed at different temperatures for different durations.

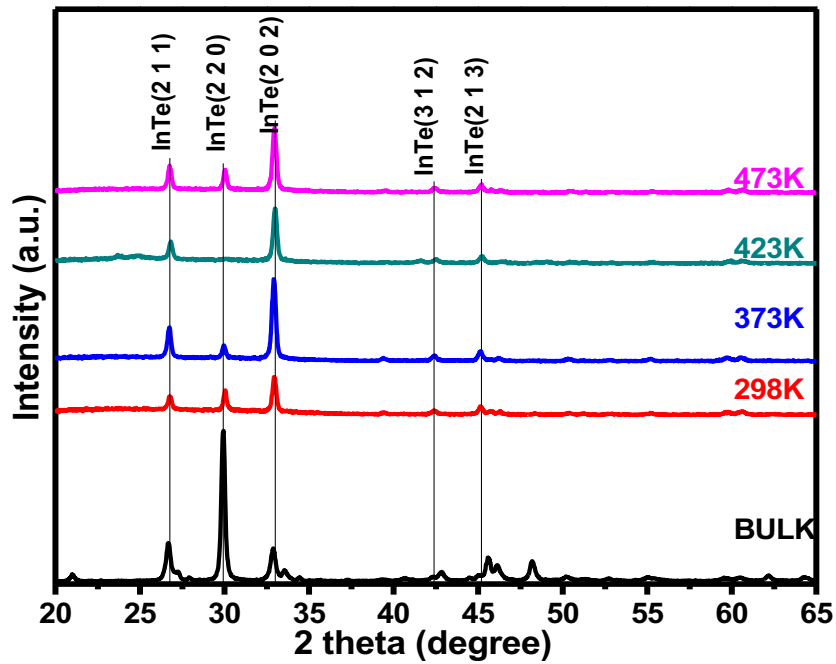
The details of elemental compositions are given in table 3.5 which is revealed that all as-deposited films are indium rich. Among all as-deposited films, the films deposited at 473 K are nearer to stoichiometric InTe, but exhibiting the mixed phase of In<sub>2</sub>Te<sub>3</sub> and InTe. Hence the films deposited at 473 K are selected for post-annealing treatment.

Figure 3.11 shows the XRD patterns of InTe films grown at 473 K and annealed at different annealing temperatures and durations. Figure 3.11(a) represents diffraction pattern of InTe films annealed at 473 K for 1h. Even though films are annealed at 473 K, they retained in the mixed phase of In<sub>2</sub>Te<sub>3</sub> and InTe. Further increase in annealing temperature leads to formation of single phase InTe films. Irrespective of annealing duration, the films annealed at 523 K and above 523 K (Figure 3.11(b-e)) are mono-phased tetragonal InTe films. The increase in annealing duration enhances the peak intensity. The EDAX analysis of annealed films reveals that the films grown at 473 K and annealed 523 K for 1h are stoichiometric films with In and Te atomic percentage of 49.93 and 50.07, respectively. Hence, the optimised annealed temperature to get mono-phase InTe films is 523 K for 1h which is adapted for further investigation to study the electrical and optical properties by varying the substrate temperature.

### **3.4.3 Effect of substrate temperature on properties of InTe films at constant annealing temperature**

Structural properties:

Figure 3.12 indicates the diffraction patterns of InTe films grown at different substrate temperature and annealed at 523 K for 1h. Irrespective of applied substrate temperature, all films are mono-phased and predominant along tetragonal InTe (2 0 2) plane. The XRD patterns of all these films are matching with bulk as well as with standard data. The compositional analysis of these films showed that all films are nearly stoichiometric (In 49.60±0.50 at. % and Te 50.40±0.50 at.%). From the XRD data, the estimated lattice parameters of annealed films are a =b= 8.4363 Å and c = 7.1129 Å which are matching well with standard data (standard a = 8.4540 Å and c = 7.1520 Å).



**Figure 3.12** XRD patterns of InTe thin films grown at different substrate temperature and annealed at 523 K for 1h.

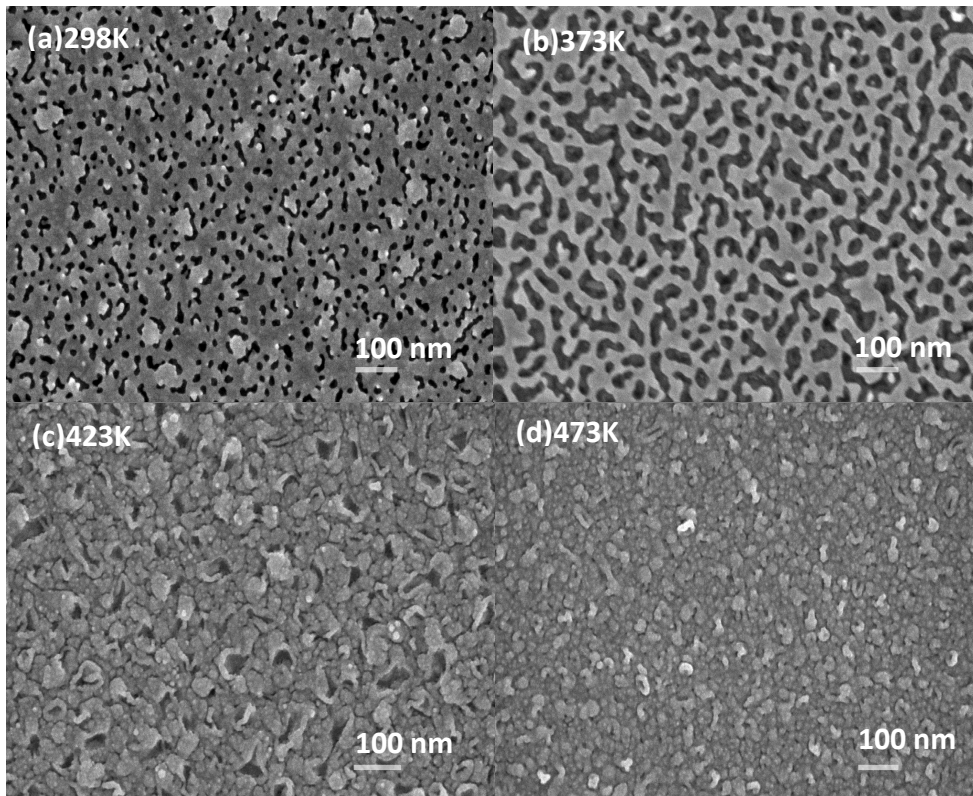


**Figure 3.13** FESEM images of annealed (523K 1h) InTe thin films grown at different substrate temperatures.

Figure 3.13 shows the FESEM micrographs of annealed InTe films deposited at different substrate temperatures. FESEM images of the films deposited at 298, 373, 423 and 473 K indicate distinct morphologies. Room temperature deposits as seen in figure 3.13(a), shows a flake like morphology with porous top layer which might be due to the high rate of deposition of Te since vapour pressure is higher than that of indium. Figure 3.13(b) represents the annihilation of flakes portions and further increase in substrate temperature resulted in the unclear grain formation with inter grain gaps (figure 3.13(c)). Finally, the morphology of films deposited at 473 K (figure 3.13(d)) reveals the complete rearrangement of grains and also reduction in the inter-grain gaps. However, the substrate temperature significantly influences the uniformity of InTe films. The intergrain gaps are found to be decreased with an increase in the substrate temperature and reasonably uniform films are obtained at 473 K substrate temperature.

**Table 3.6** Compositional analysis of InTe thin films

Temperature (K)		Elemental composition (at.%)	
Substrate temperature	Annealing temperature	In	Te
Bulk	-	51.6	48.4
298	-	51.8	48.2
373	-	52.5	47.5
423	-	51.9	48.1
473	-	50.8	49.2
298	523 (1h)	50.4	49.6
298	523 (2h)	49.9	50.1
373	523 (1h)	49.6	50.4
423	523 (1h)	49.2	50.8
<b>473</b>	<b>523 (1h)</b>	<b>49.9</b>	<b>50.1</b>
523	523 (1h)	50.3	49.7
523	523 (2h)	50.1	49.9
523	548 (1h)	51.4	48.6
523	573 (1h)	50.7	49.3

Electrical properties:

To investigate the electrical properties, the silver contacts are made on InTe films and verified ohmic nature using I-V plots. The silver contacts are showing ohmic behaviour with InTe films in figure 3.14 (a). Figure 3.14 (b) represents Arrhenius plots of resistance R(T). The linearity of  $\ln R$  versus inverse temperature graph indicates the semiconducting behaviour. The thermal activation energy of InTe films are determined from the slopes of figure 3.14 (b). The thermal activation energy is found to be minimum (Table 3.7) for the films grown at 423 K substrate temperature which can be expected due to larger grain size (Figure 3.13). The estimated electrical conductivity of stoichiometric InTe films is found around  $15.612 \Omega^{-1} \text{ cm}^{-1}$  at room temperature which is comparatively higher than the reported value of  $2.5 \times 10^{-2} - 4 \times 10^{-2} \Omega^{-1} \text{ cm}^{-1}$  at  $T = 298 \text{ K}$  for evaporated thin films (Madelung et al. 1998). The type of conductivity of the InTe films is confirmed by hot probe method which revealed that p-type conductivity.

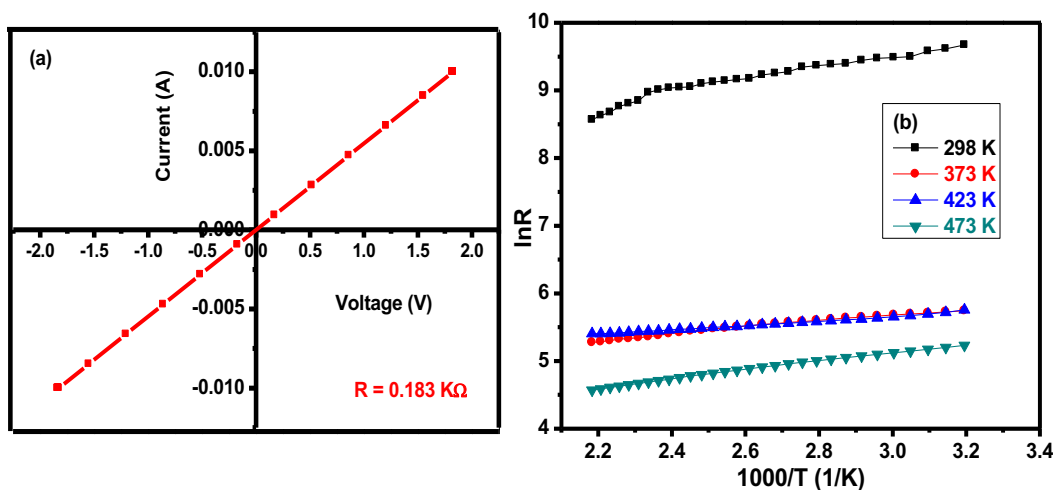


**Figure 3.14 (a).** I-V curve of stoichiometric InTe films **(b).**  $\ln R$  versus inverse temperature plots of InTe films deposited at different substrate temperatures and annealed at 523 K for 1 h.

Optical properties:

The transmission spectra of InTe films are depicted in figure 3.15(a) and showing higher transmittance (65- 80 %) in NIR region. To estimate optical energy gap of the



obtained films, the Tauc's plots has been plotted which reveals that the films are direct band gap semiconductors.

**Table 3.7** Activation energy and optical band gap of InTe thin films

Substrate temperature of InTe films annealed at 523 K for 1h (K)	Activation energy (eV)	Optical band gap (eV)
298	0.0805	1.61
373	0.0565	1.60
423	0.0280	1.58
473	0.0406	1.42

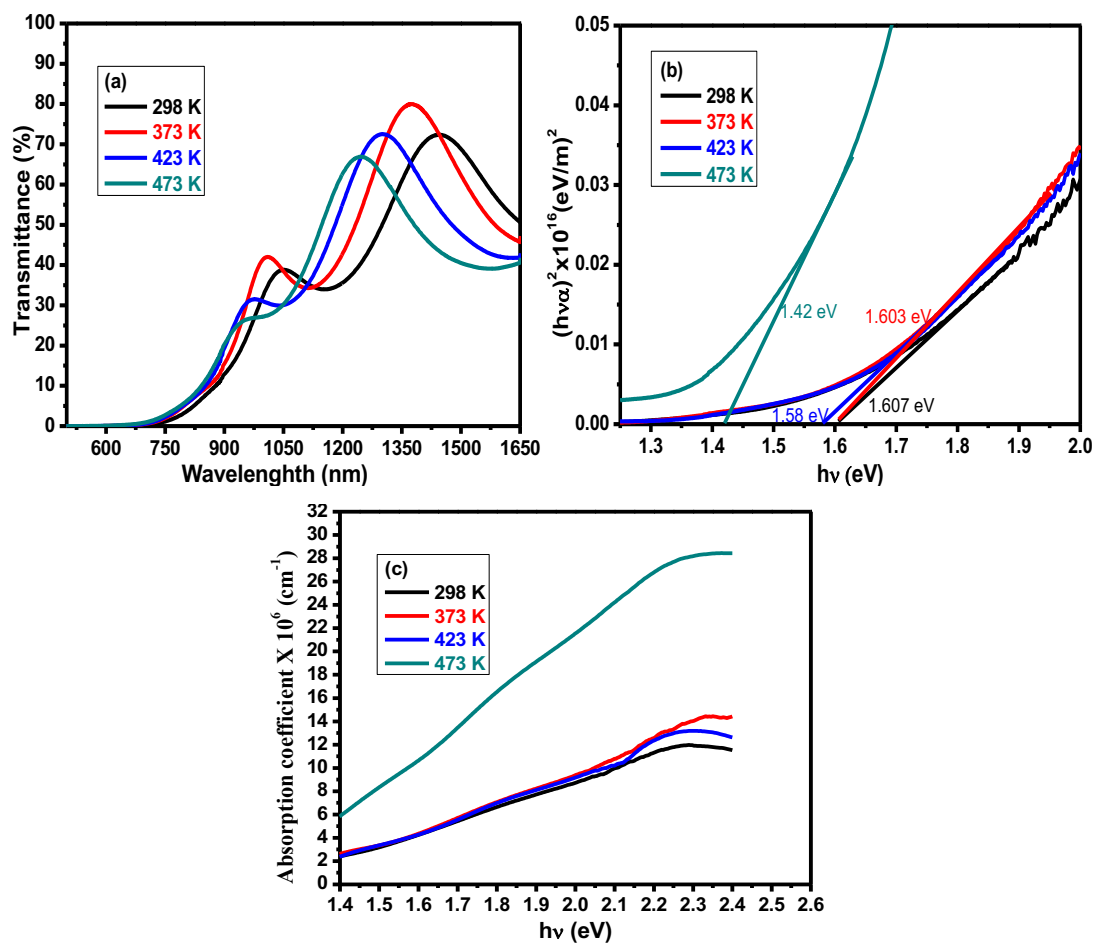


**Figure 3.15** (a). Transmittance as a function of wavelength (b). Tauc's plots and (c). Absorption coefficient as a function of energy for InTe thin films.

The optical band gap of the films is estimated by extrapolating the linear portion of  $(h\nu\alpha)^2$  curve to energy axis (table 3.6). As depicted in figure 3.15(b), the optical band gap of the films is found to be decreased from 1.6 eV to 1.42 eV with an increase in the substrate temperature from 298 K to 473 K. The optical band gap of stoichiometric and uniform films is found to 1.42 eV. The influence of substrate temperature on annealed films may cause changes in arrangement of clusters or grains due to variations in stoichiometries, resulting an alteration in inherent band gap of compound. Figure 3.15(c) represents the variation in absorption coefficient with photon energy of InTe films which is in the order of  $10^6 \text{ cm}^{-1}$  for all films.

## CHAPTER 4

### THERMOELECTRIC PROPERTIES OF INDIUM TELLURIDE THIN FILMS

*Overview:*

*This chapter deals with optimisation of growth conditions to enhance the thermoelectric properties of both  $\text{In}_2\text{Te}_3$  and  $\text{InTe}$  films by varying substrate temperature, annealing temperature and growth rate. The effect of doping (Bi,  $\text{Sb}_2\text{Te}_3$ , Al, Sb, Se and Te) on structural and thermoelectric properties of  $\text{In}_2\text{Te}_3$  films are reported. Additionally, a commercial thermoelectric material (p-type,)  $\text{Sb}_2\text{Te}_3$  is alloyed to  $\text{In}_2\text{Te}_3$  and results are compared.*

#### 4.1 Introduction

The thermoelectric materials have been paid attention in research due to its capability of direct conversion of thermal energy into the electric energy. The performance of a thermoelectric materials can be decided by dimensionless quantity called ‘figure of merit’,

$$ZT = \frac{S^2 \sigma T}{k}$$

where, S is seebeck coefficient or thermoelectric power,  $\sigma$  is electrical conductivity, T represents absolute temperature, and k indicates thermal conductivity (Jood et al. 2011).

The power factor ( $S^2\sigma$ ) is directly proportional to ZT and describes the electron transport properties of a materials which is useful to select a class of potential thermoelectric materials. Basically, the materials having higher electrical conductivity are suffering from low seebeck coefficient due to its symmetry in density of states (Markov et al. 2018). Hence improving the power factor is also a challenging criteria to enhance performance of a thermoelectric material. The power factor (PF) can be enhanced based on various strategies such as band engineering, defect engineering and exploitation of complex band structures (Zhou et al. 2018). As a part of complexing the

band structure, doped semiconductors are recommended for best thermoelectric performance due to its asymmetry between conduction and valence bands.

In<sub>2</sub>Te<sub>3</sub> has large density of intrinsic vacancies at cation sites which is  $\sim 5.5 \times 10^{21} \text{ cm}^{-3}$  due to the lattice mismatch between indium (In<sup>3+</sup>) and tellurium ions (Te<sup>2-</sup>) (Popov 1988; Rowe 2012). Hence, thermoelectric performance can be expected to be improved by phonon-vacancy scattering which plays a potential role in the reduction of thermal conductivity (Fu et al. 2010). Additionally, In<sub>2</sub>Te<sub>3</sub> has high radiation stability of electrical parameters even after fluency of ionization which was examined experimentally up to  $10^{18}$  fast neutrons per cm<sup>2</sup> (Volovichev et al. 1998). Hence this material can be used in thermoelectric power generators in the vicinities of nuclear reactors. Despite of its ample characteristics to exhibit good thermoelectric properties, research invested on In<sub>2</sub>Te<sub>3</sub> thin films is still meagre. Lakshminarayana et al. (2002) investigated the thermoelectric power of stoichiometric In<sub>2</sub>Te<sub>3</sub> thin films and observed that thermoelectric power is nearly independent of hot-end temperature (300-420 K) and dependent on thickness of the films which was predicted by the size effect theories (Lakshminarayana et al. 2002.). As well, Krisnasatry and Jayarama reddy investigated the thermoelectric properties of InTe thin films and reported that seebeck coefficient of InTe films increases with an increase in substrate temperature and weakly depends on the temperature (273-400 K) (Sastry and Reddy 1980).

It is interesting to investigate its thermoelectric properties of indium telluride films because of its basic properties as mentioned above. In the present work, the growth parameters such as substrate temperature, annealed temperature and deposition rate have been varied to enhance the thermoelectric power (seebeck coefficient). In addition, it has been doped by Bi, Sb<sub>2</sub>Te<sub>3</sub>, Al, Sb, Se and Te. A significant effect shown by the dopants on seebeck coefficient and power factor as well as marginal changes seen in electrical conductivity of indium telluride thin films are discussed in this chapter.

## 4.2 Thermoelectric properties of $\text{In}_2\text{Te}_3$ thin films

### 4.2.1 Growth conditions and optimisation

To investigate the thermoelectric properties,  $\text{In}_2\text{Te}_3$  films are thermally deposited on glass substrates. Prior to the deposition, the glass substrates were cleaned using chromic acid, liquid detergent and ultra-sonicated with acetone to remove the impurities present on the surface of the glass slides. An aluminium mask was used to maintain length to width ratio of the films at 5.5. The vacuum inside the deposition chamber was maintained at  $\sim 5 \times 10^{-6}$  torr. The distance between the substrate and source was fixed to 12 cm. A 200 A molybdenum boat was used to evaporate 99.999% pure  $\text{In}_2\text{Te}_3$  precursor material. The seebeck coefficient and electrical properties of prepared films are investigated in the temperature range from 298 K to 465 K. To enhance the seebeck coefficient, the deposition rate is changed from 4.2 nm/s to 11 nm/s and optimised to 11 nm/s. Figure 4.1 shows the higher thermo emf generation for the  $\text{In}_2\text{Te}_3$  films deposited at 11 nm/s rate compared with stoichiometric films (annealed at 573 K for 1h) and films deposited at lower rates. The substrate temperature and thickness of the films were varied from 298 K to 473 K and 50 nm to 500 nm ( $\pm 10$  nm), respectively.

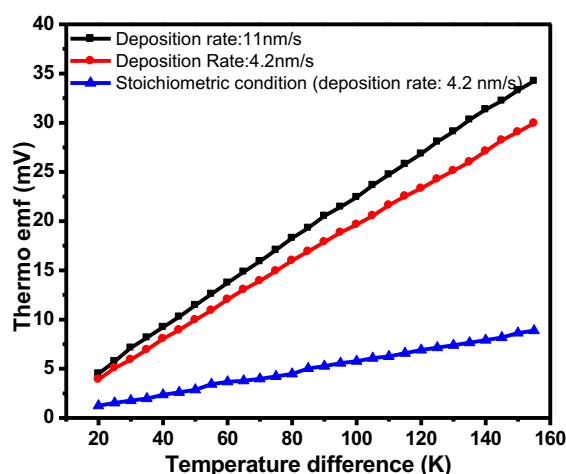


**Figure 4.1** Plot of thermo emf as a function of temperature difference of  $\text{In}_2\text{Te}_3$  films grown at different conditions.

## 4.2.2 Structural and thermoelectric properties of $\text{In}_2\text{Te}_3$ films

Structural properties and composition:

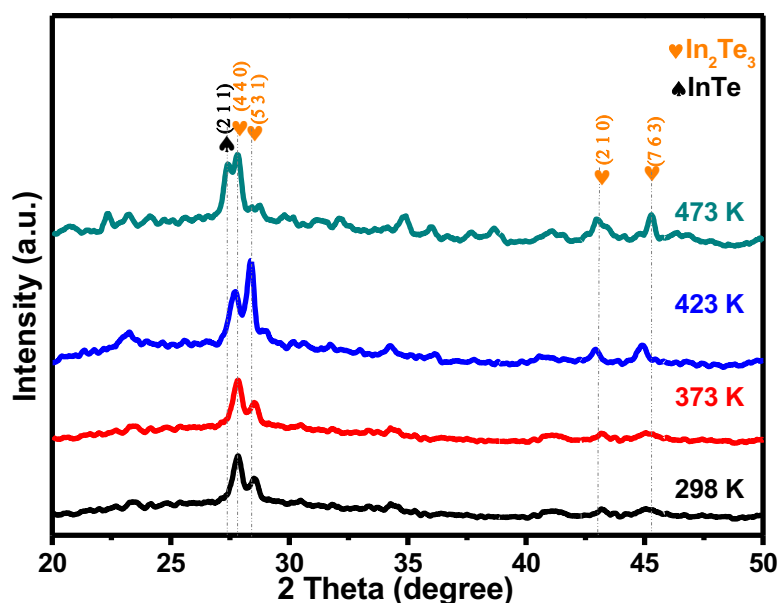


**Figure 4.2** XRD patterns of  $\text{In}_2\text{Te}_3$  thin films grown at different substrate temperatures.

Figure 4.2 shows the XRD patterns of  $\text{In}_2\text{Te}_3$  thin films deposited at different substrate temperatures ranging from 298 K to 473 K. The XRD patterns reveal the polycrystalline nature of prepared films. In the as-grown  $\text{In}_2\text{Te}_3$  films deposited at substrate temperature till 423 K (i.e., 298, 373 and 423 K), four peaks are observed which are corresponding to (4 4 0), (5 3 1), (2 1 0) and (7 6 3) planes of cubic phased  $\text{In}_2\text{Te}_3$  (JCPDS Card No. 33-1488). Further increase in the substrate temperature to 473 K resulted in the minor contribution of tetragonal  $\text{InTe}$  phase (JCPDS Card No. 00-007-0112). The (5 3 1) plane corresponding to  $\text{In}_2\text{Te}_3$  phase was diminished, while  $\text{InTe}$  (2 1 1) plane appeared in the as-grown films. The formation of  $\text{InTe}$  phase is reasonable because, according to phase diagram of indium telluride compound,  $\text{InTe}$  phase is next stable phase after  $\text{In}_2\text{Te}_3$  at relatively elevated temperatures. Therefore, films deposited at substrate temperature up to 423 K are pure and mono-phased, whereas films

deposited at 473 K are exhibiting mixed phase of  $\text{In}_2\text{Te}_3$  and  $\text{InTe}$ . The cubic lattice constant of  $\text{In}_2\text{Te}_3$  films is estimated from (4 4 0) peak which is  $\sim 18.503 \text{ \AA}$ .

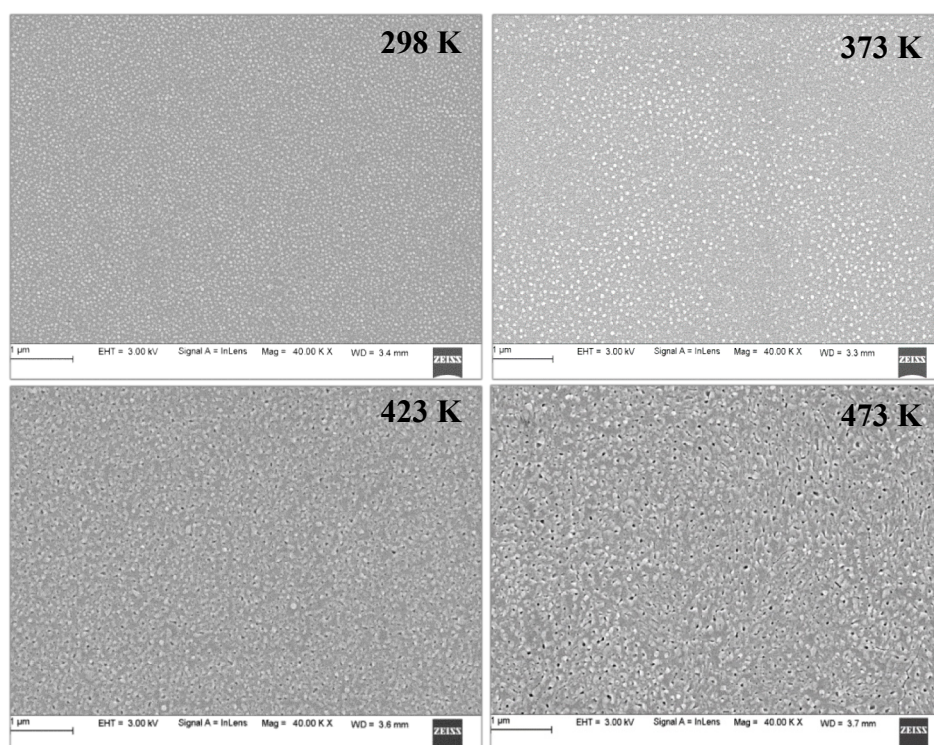


**Figure 4.3** Surface micrographs of indium telluride films prepared at different substrate temperatures.

The FESEM images of the as-deposited films at different substrate temperatures reveal that the surface of the films is granular (Figure 4.3). For the films deposited at 423 K and 473 K substrate temperatures, the inter-grain gaps are found to be originated. The average diameter of inter-grain gaps is 30 nm in 423 K deposited films, and 45 nm in 473 K deposited films. These inter-grain gaps do not affect the continuity of the films since films are thick enough to contain several layers.

The composition of  $\text{In}_2\text{Te}_3$  films are summarized in table 4.1 which reveals that the indium content in the films decreases with an increase in the substrate temperature. Generally, the energy required to create an indium vacancy is less than that of the tellurium vacancy. Hence, the indium atoms are knocked out of the lattice which

increases with an increase in substrate temperature. To investigate the sole effect of substrate temperature on the generation of thermo emf, the thickness of the films is maintained constant around 350 nm.

**Table 4.1** Variation in the composition of as-deposited films at different substrate temperatures

Substrate temperature (K)	Composition of elements (at.%)	
	In	Te
298	54.5	45.5
373	54.1	45.9
423	53.4	46.6
473	52.1	47.9

Thermoelectric properties:

Figure 4.4(a). shows the variation in thermo emf generation with temperature difference. The films grown at 423 K substrate temperature are generating higher thermo emf which can be attributed to the above mentioned changes in composition and structure of the as-prepared films. The thermoelectric power of  $\text{In}_2\text{Te}_3$  films is independent of hot end temperature (Figure 4.4b), hence the power factor of these films depends only on the electrical conductivity. The positive thermoelectric power values of the films reveal that  $\text{In}_2\text{Te}_3$  films are p-type.

The variation in electrical conductivity with inverse temperature for the as-grown films at different substrate temperatures is presented in figure 4.4(c). The exponential decrease of the conductivity with inverse temperature represents the semiconducting nature of the samples. The electrical conductivity of  $\text{In}_2\text{Te}_3$  films is found to decrease with an increase in the substrate temperature till 423 K due to the decrease of indium content. However, the conductivity of the films deposited at 473 K is higher than that of films deposited at 423 K which might be due to the existence of mixed phase of indium telluride. These observations revealed that, at higher deposition rates, the composition of the films is a dominating factor on properties of the films rather than substrate temperature.



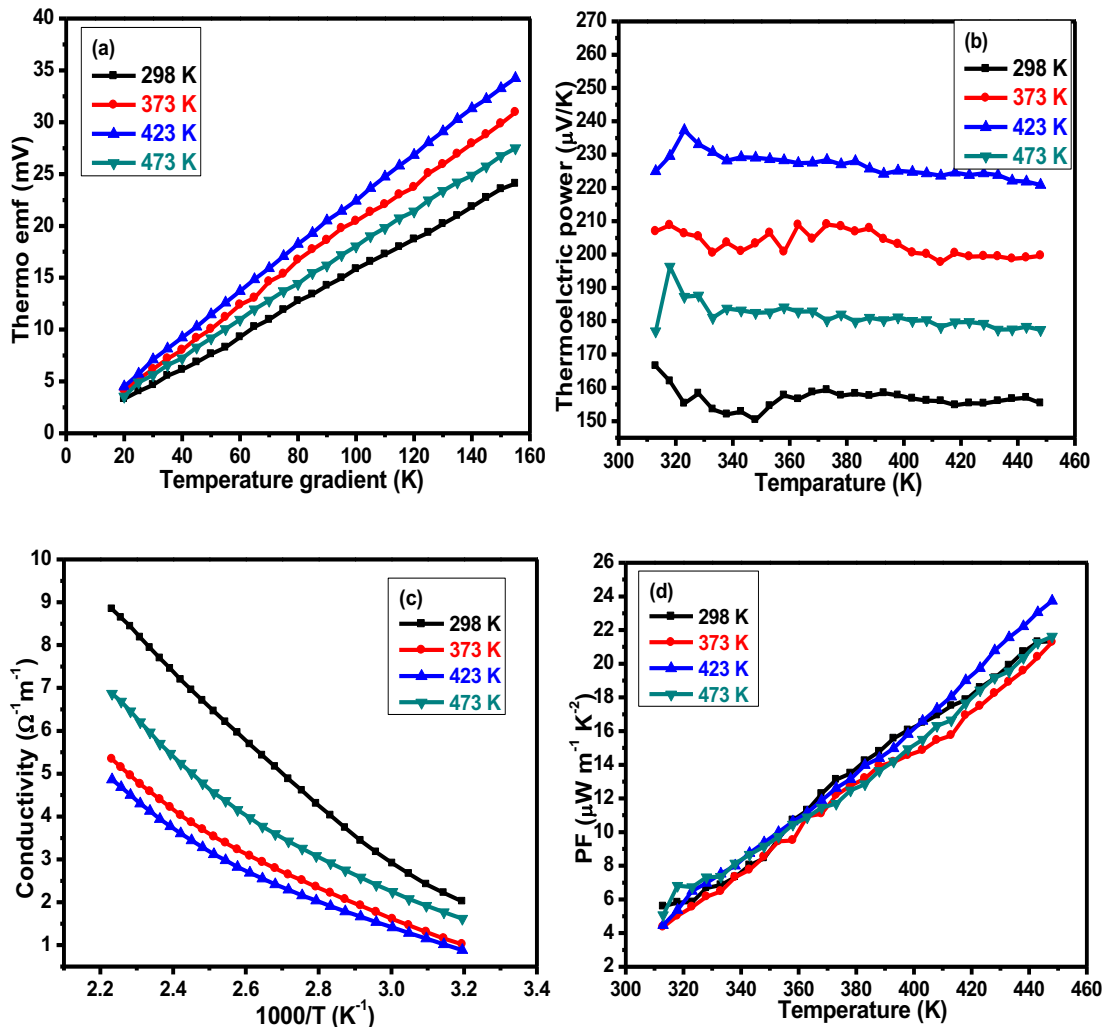


**Figure 4.4 (a).** Variation in thermo emf with temperature difference **(b).** Plot of thermoelectric power versus hot end temperature, **(c).** Variation in electrical conductivity with inverse temperature and **(d).** Variation of power factor with temperature, of  $\text{In}_2\text{Te}_3$  films deposited at different substrate temperature.

Figure 4.4(d) shows the variation in power factor as a function of temperature. The power factor of these films increases with temperature in the investigated range. The power factor of films is marginally altered by the substrate temperature and found maximum for films deposited 423 K which is  $24 \mu\text{W m}^{-1}\text{K}^{-2}$  at 450 K. To study the effect of the film thickness on thermoelectric power generation of  $\text{In}_2\text{Te}_3$  films, the substrate temperature is kept constant at 423 K since these films have ascendant thermoelectric power as well as power factor.

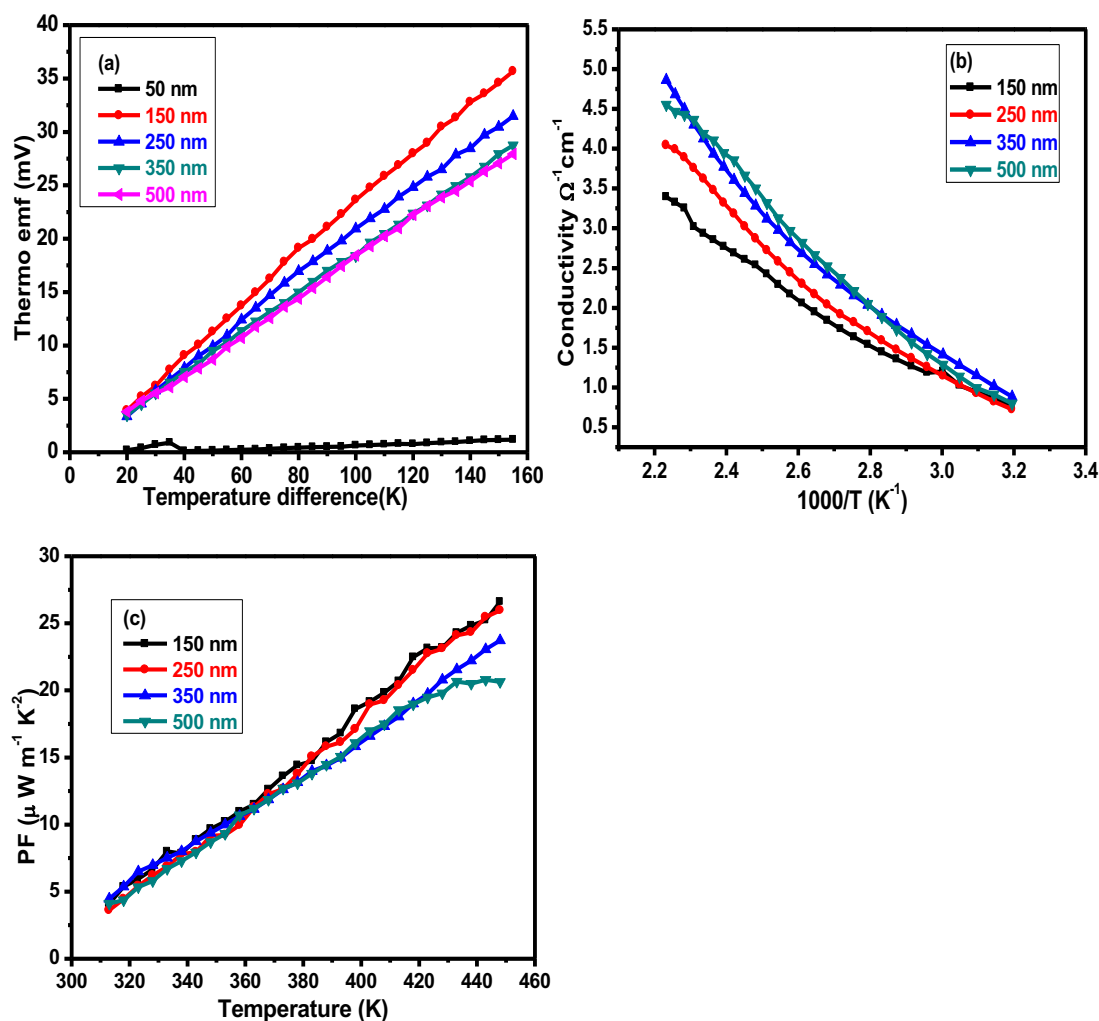


**Figure 4.5 (a).** Plot of thermo emf versus temperature difference, **(b).** Temperature dependent electrical conductivity for different thickness films and **(c).** Power factor of different thickness  $\text{In}_2\text{Te}_3$  films as function of temperature.

The generation of thermo emf is found to decrease marginally with an increase in the film thickness (Figure 4.5a). All films follow the same increasing trend with rise in the temperature. Thickness of samples make a contribution to change in the band structure and fermi energy in nano regime, thus the value of thermoelectric power is higher for the thin films. The films with 150 nm thickness have ascendant thermo emf value than that of other films. Films with lower thickness (50 nm) showed an abrupt fall in thermo emf compared with the films of thickness 150 nm and this is mainly due to the inter-grain gaps (Figure 4.3b) that causes discontinuity in films at lower thicknesses.

The electrical conductivity of samples showed an increasing trend with an increase in the film thickness (Figure 4.5b). As the thickness increases, the diminution of crystallite boundaries can be responsible for the increase in electrical conductivity of the films. The power factor as a function of temperature for the films having different thicknesses is shown in figure 4.5(c). Due to increase in both thermoelectric power and electrical conductivity with the rise in the temperature, the power factor of the samples shows an increasing tendency with temperature. The thin films with 150 nm thickness shows higher power factor value than any other films which is  $27 \mu\text{Wm}^{-1}\text{K}^{-2}$  at 450 K.

### **4.3 Thermoelectric properties of doped $\text{In}_2\text{Te}_3$ thin films**

#### **4.3.1 Growth conditions of doped $\text{In}_2\text{Te}_3$ thin films**

In order to enhance the seebeck coefficient of  $\text{In}_2\text{Te}_3$  films, the materials, bismuth (Bi), antimony telluride ( $\text{Sb}_2\text{Te}_3$ ), aluminium (Al), antimony (Sb), selenium (Se) and tellurium (Te) were used as dopants. Glass slides were used as substrate material which were cleaned with chromic acid, liquid detergent and acetone. The substrate temperature of the films is varied from room temperature to 473 K and optimized based on two factors namely homogeneity and thermoelectric power shown by the films. It has been observed that un-doped  $\text{In}_2\text{Te}_3$  films deposited at 423 K are uniform with fine-grained structure (Figure 4.3c) and show high thermoelectric power. Beyond this substrate temperature, the thermoelectric power is observed to decrease due to the formation of an additional InTe phase. The thickness of the films is maintained at  $\sim 350$  nm. The precursors of both source material (99.999 % pure  $\text{In}_2\text{Te}_3$ ) and dopants (Bi-99.5 %,  $\text{Sb}_2\text{Te}_3$ -99.999 %, Al-99.9995%, Sb-99.9 %, Se-99.999 % and Te-99.99%) are used in pellet form and evaporated using a molybdenum boat. For evaporation, the current supplied to boat is gradually increased and maintained constant thereafter. The seebeck coefficient and electrical conductivity of the films was investigated in the temperature range from 298 K to 465 K.

### 4.3.2 Bi doped $\text{In}_2\text{Te}_3$ thin films

Structural properties and composition:

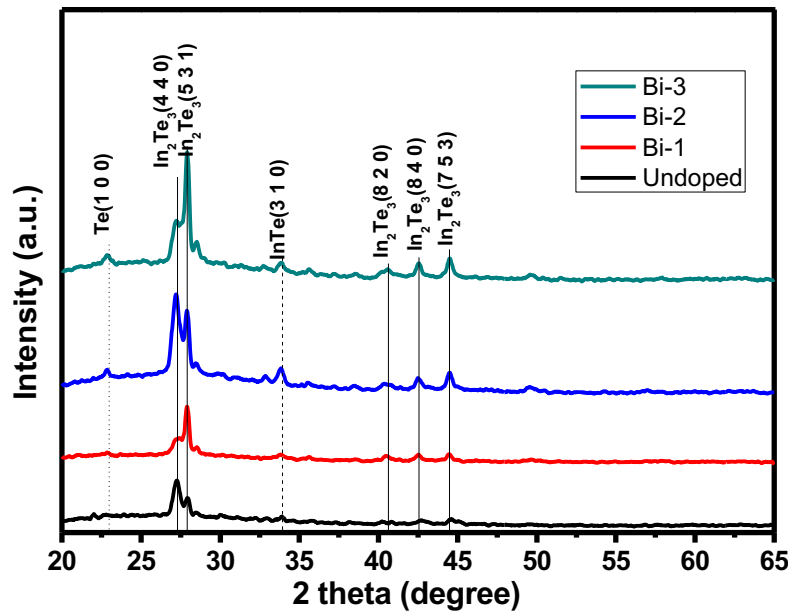


**Figure 4.6** XRD patterns of Bi doped  $\text{In}_2\text{Te}_3$  thin films deposited at 423 K.

Figure 4.6 shows the XRD patterns of Bi doped  $\text{In}_2\text{Te}_3$  thin films. All Bi doped  $\text{In}_2\text{Te}_3$  films are polycrystalline in nature with multiple peaks corresponding to cubic  $\text{In}_2\text{Te}_3$  phase along with minor contribution of hexagonal Te and tetragonal InTe phases. In Fig 4.6, (4 4 0), (5 3 1), (8 2 0), (8 4 0), (7 5 3) peaks corresponding to  $\text{In}_2\text{Te}_3$  phase, (3 1 0) peak belongs to InTe and (1 0 0) peak corresponding to Te phases are appearing. Bi-1 and Bi-3 films are predominantly orientated along  $\text{In}_2\text{Te}_3$  (5 3 1) plane whereas, Bi-2 are dominantly orientated along (4 4 0) plane of  $\text{In}_2\text{Te}_3$  phase. The lattice parameter of these films is calculated using equation 2.5 along  $\text{In}_2\text{Te}_3$  (5 3 1) plane which is 18.503 Å. FESEM micrographs of Bi-doped  $\text{In}_2\text{Te}_3$  are given in figure 4.7. The surface of the  $\text{In}_2\text{Te}_3$  films is basically granular and grain size increases with increasing Bi doping percentage. There are few inter-grain gaps on films surface which reduces with an increase in Bi concentration. The inter-grain gaps are more pronounced in Bi-1 films and does not affect the films continuity due to enough thickness (~350 nm).

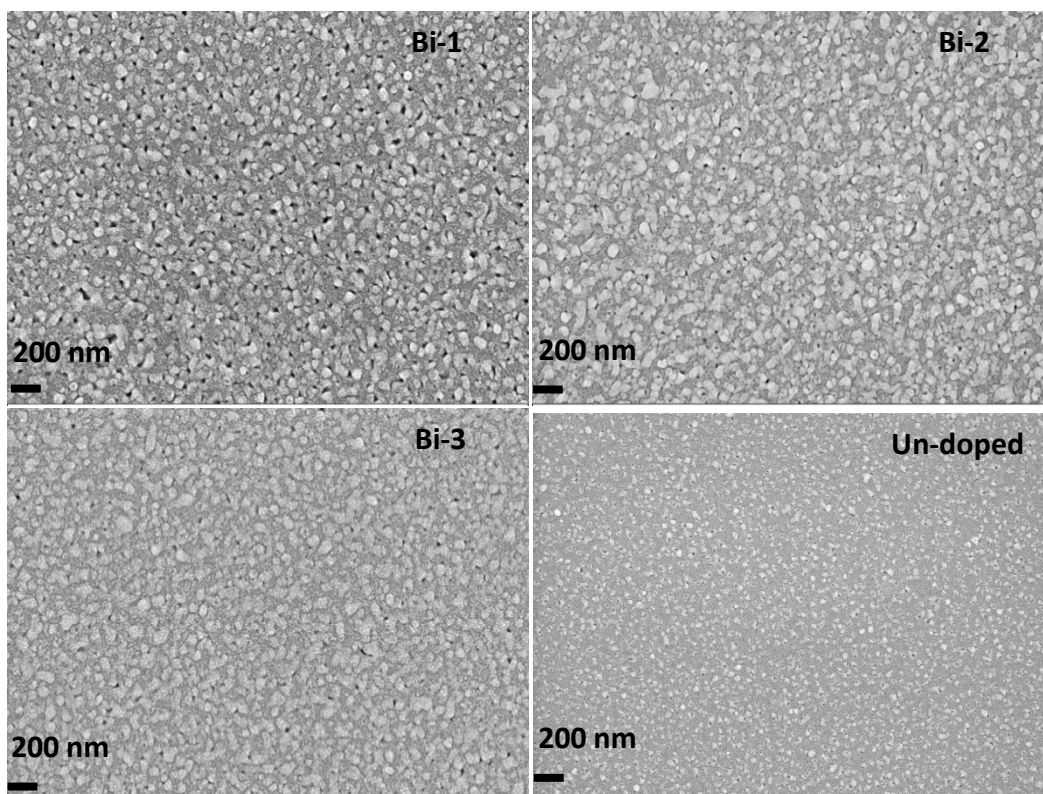


**Figure 4.7** FESEM micrographs of Bi doped  $\text{In}_2\text{Te}_3$  thin films.

**Table 4.2** Composition of Bi doped  $\text{In}_2\text{Te}_3$  thin films

Sample names	Dopant conc. (%) in source	Film Composition ( at%.)		
		Bi	In	Te
<b>Bi-1</b>	<b>1%</b>	0.9	52.4	46.7
<b>Bi-2</b>	<b>3%</b>	2.3	52.1	45.6
<b>Bi-3</b>	<b>5%</b>	3.0	52.3	44.7

The Compositional analysis of Bi doped  $\text{In}_2\text{Te}_3$  films revealed that Bi doping percentage in the prepared films is less than the precursor Bi percentage which might be due to the difference in vapour pressures of dopant and source material ( $\text{Te} > \text{Bi} > \text{In}$ ). The elemental atomic percentage of the constituents is given in table 4.2. Figure 4.8 is

an EDAX spectrum showing the presence of Bi in prepared films. Similarly, all the prepared films show the presence of corresponding amount of dopant added in bulk precursor material.

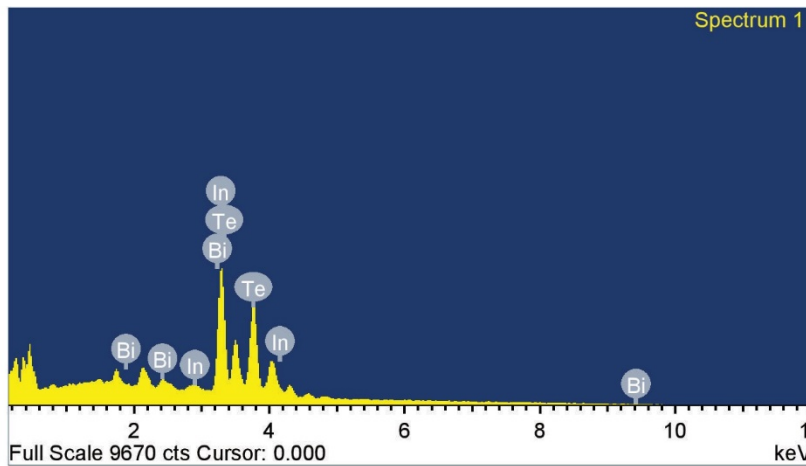


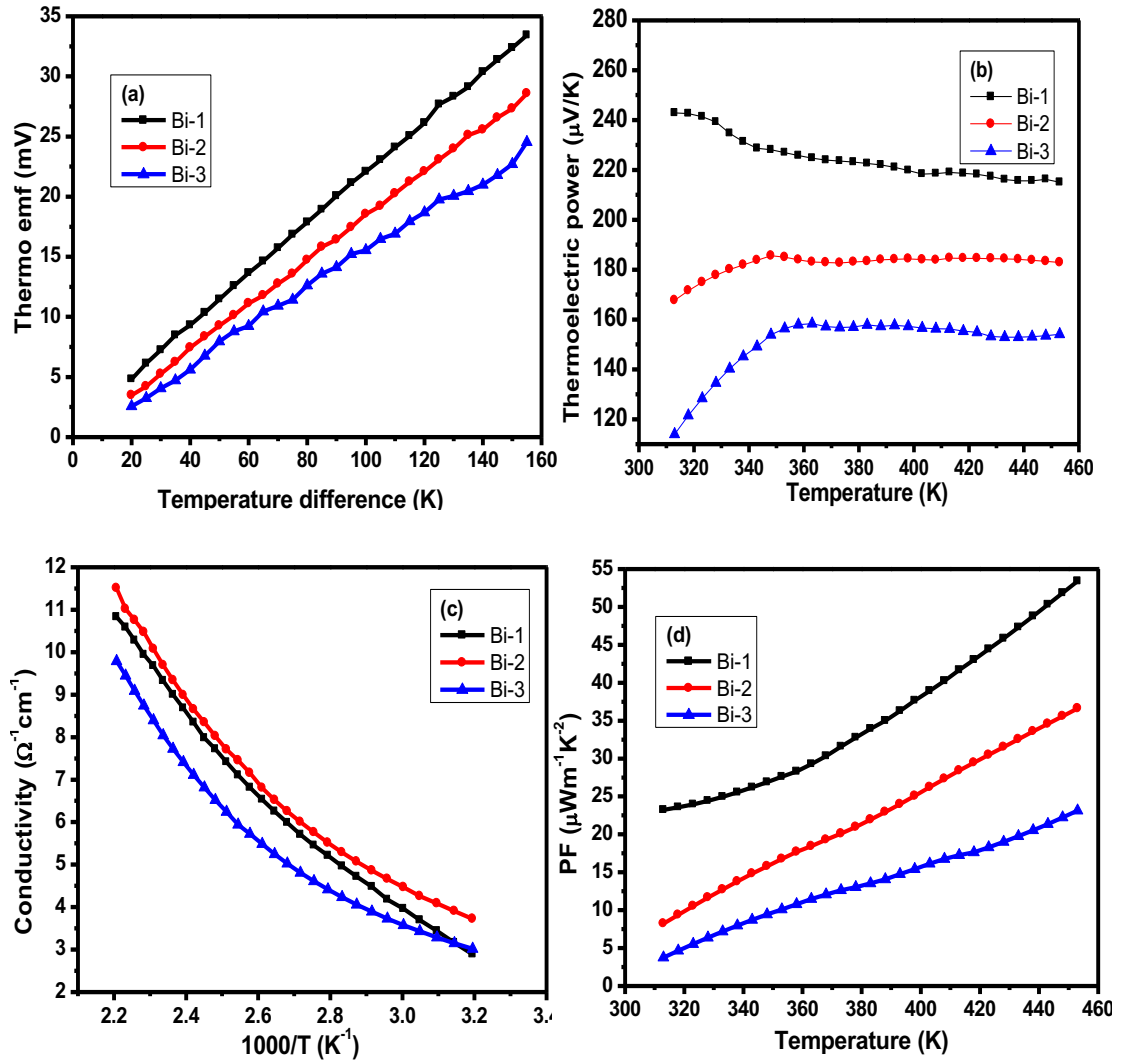
**Figure 4.8** EDAX spectra of doped  $\text{In}_2\text{Te}_3$  films (Bi-1).

Thermoelectric properties:

To investigate thermoelectric properties of Bi doped  $\text{In}_2\text{Te}_3$  films, silver contacts (Ohmic) are thermally deposited on the films using thermal evaporation method. Figure 4.9 (a) represents the variation in thermo emf with temperature difference. The thermo emf of the Bi doped  $\text{In}_2\text{Te}_3$  films is proportionally increasing with an increase in temperature but decreasing with an increase in Bi doping concentration. The positive slope of figure 4.9 (a) indicates the p-type conductivity of the films. The seebeck coefficient of these films decreases with an increase in Bi doping concentration (Figure 4.9b). The seebeck coefficient is maximum for Bi-1 films which is  $288 \mu\text{V K}^{-1}$  at 320 K.

The electrical conductivity of  $\text{In}_2\text{Te}_3$  films is marginally affected with Bi doping which can be seen in figure 4.9(c). The exponential decrease of electrical conductivity with inverse temperature indicates the semiconducting behaviour of the prepared films (Figure 4.9c). However, Bi-2 films are showing maximum electrical conductivity which might be due to involvement of InTe (which have higher conductivity than

$\text{In}_2\text{Te}_3$ ) phase and reduction in inter-grain gaps. The electrical conductivity of Bi-2 films is around  $3.72 \Omega^{-1} \text{cm}^{-1}$  at 320 K.



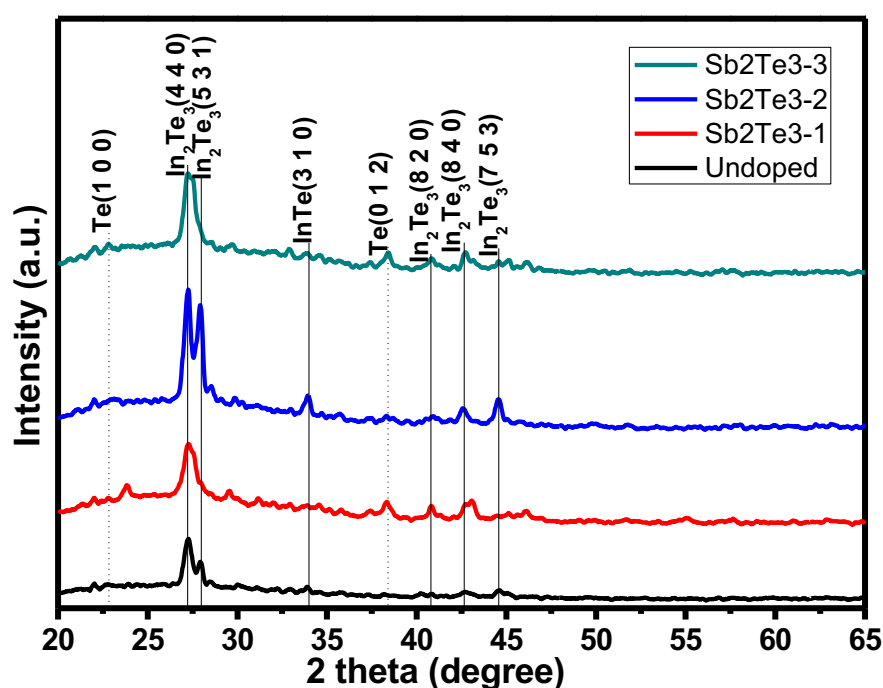
**Figure 4.9** (a). Variation in thermo emf with temperature difference, (b). Plot of thermoelectric power versus hot end temperature, (c). Electrical conductivity as function of inverse temperature and (d). Variation of power factor with temperature, of Bi doped  $\text{In}_2\text{Te}_3$  films.

Figure 4.9 (d) shows the power factor of Bi doped  $\text{In}_2\text{Te}_3$  films as a function of temperature which is showing an increasing trend with an increase in temperature. As Bi doping percentage increases, the power factor of the films found to be decreased. Since the power factor ( $S^2\sigma$ ) depends on both electrical conductivity and seebeck co-

efficient, Bi-1 films have shown higher power factor of  $\sim 23.89 \mu\text{W m}^{-1} \text{K}^{-2}$  (at 320 K) which is enhanced by 4.8 times than that of un-doped  $\text{In}_2\text{Te}_3$  films.

#### 4.3.3 (a) $\text{Sb}_2\text{Te}_3$ doped $\text{In}_2\text{Te}_3$ thin films

Structural properties and composition:



**Figure 4.10** XRD patterns of  $\text{Sb}_2\text{Te}_3$  doped  $\text{In}_2\text{Te}_3$  films deposited at 423 K.

Figure 4.10 shows the XRD patterns of un-doped and  $\text{Sb}_2\text{Te}_3$  doped  $\text{In}_2\text{Te}_3$  thin films which are showing the polycrystalline nature. The diffraction patterns of un-doped films are showing (4 4 0) and (5 3 1) peaks which are matching with standard cubic  $\text{In}_2\text{Te}_3$  data and dominant (4 4 0) reflection. The intensity of  $\text{In}_2\text{Te}_3$  (4 4 0) peak gradually increases with an increase in  $\text{Sb}_2\text{Te}_3$  doping concentration. No peaks corresponding to  $\text{Sb}_2\text{Te}_3$  phase are found in XRD patterns. The lattice constant of doped films has been estimated along  $\text{In}_2\text{Te}_3$  (4 4 0) plane which is predominant peak in pure  $\text{In}_2\text{Te}_3$  diffraction pattern. From the XRD data, the estimated lattice constant is 18.503 Å for  $\text{Sb}_2\text{Te}_3$  doped  $\text{In}_2\text{Te}_3$  films which is matching well with un-doped  $\text{In}_2\text{Te}_3$  films.



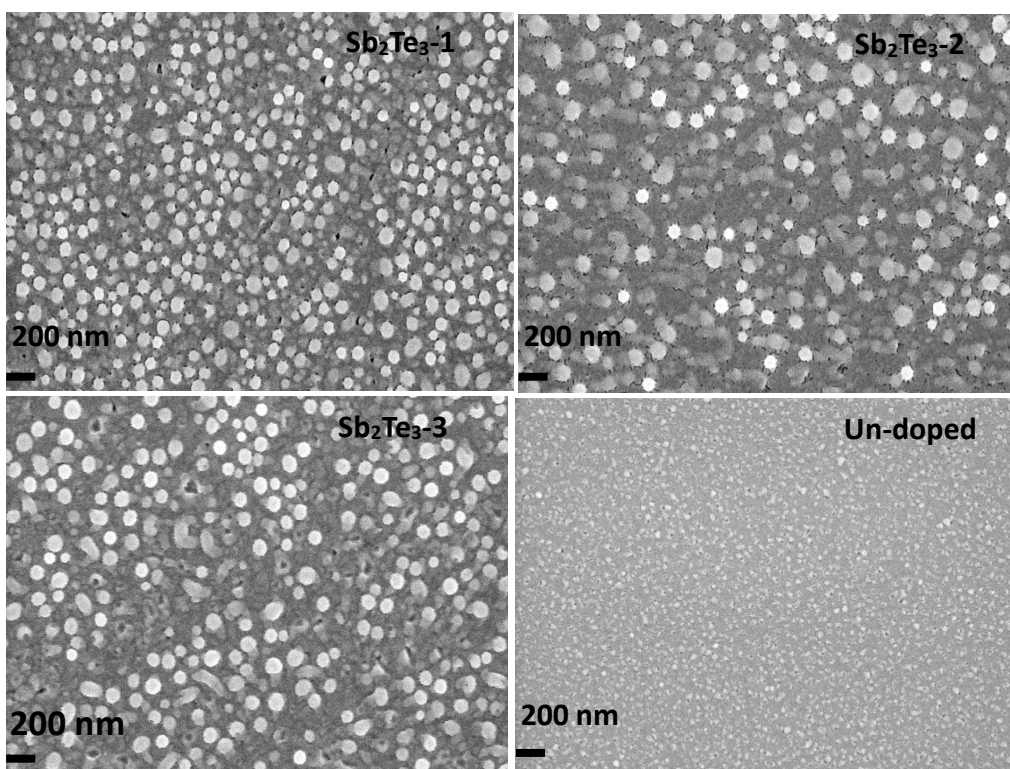


**Figure 4.11** FESEM micrographs of  $\text{Sb}_2\text{Te}_3$  doped  $\text{In}_2\text{Te}_3$  thin films deposited at 423 K substrate temperature.

**Table 4.3** Composition of  $\text{Sb}_2\text{Te}_3$  doped  $\text{In}_2\text{Te}_3$  thin films

Sample names	Dopant conc. (%) in source	Film Composition ( at%.)		
		Sb	In	Te
$\text{Sb}_2\text{Te}_3\text{-1}$	1%	0.4	46.0	53.6
$\text{Sb}_2\text{Te}_3\text{-2}$	3%	1.2	47.7	51.1
$\text{Sb}_2\text{Te}_3\text{-3}$	5%	2.1	50.0	47.9

Figure 4.11 shows the surface morphology of un-doped and  $\text{Sb}_2\text{Te}_3$  doped films. A significant modification can be observed from the FESEM micrographs. The grain area

of the  $\text{In}_2\text{Te}_3$  films is significantly increased with  $\text{Sb}_2\text{Te}_3$  doping. Due to an increase in grain area, grain boundaries also increased. Table 4.3 summarises the elemental concentration of  $\text{Sb}_2\text{Te}_3$  doped films. The composition of the films reveals that the films are indium rich, whereas antimony is following its stoichiometry with respect to added percentage.

Thermoelectric properties:

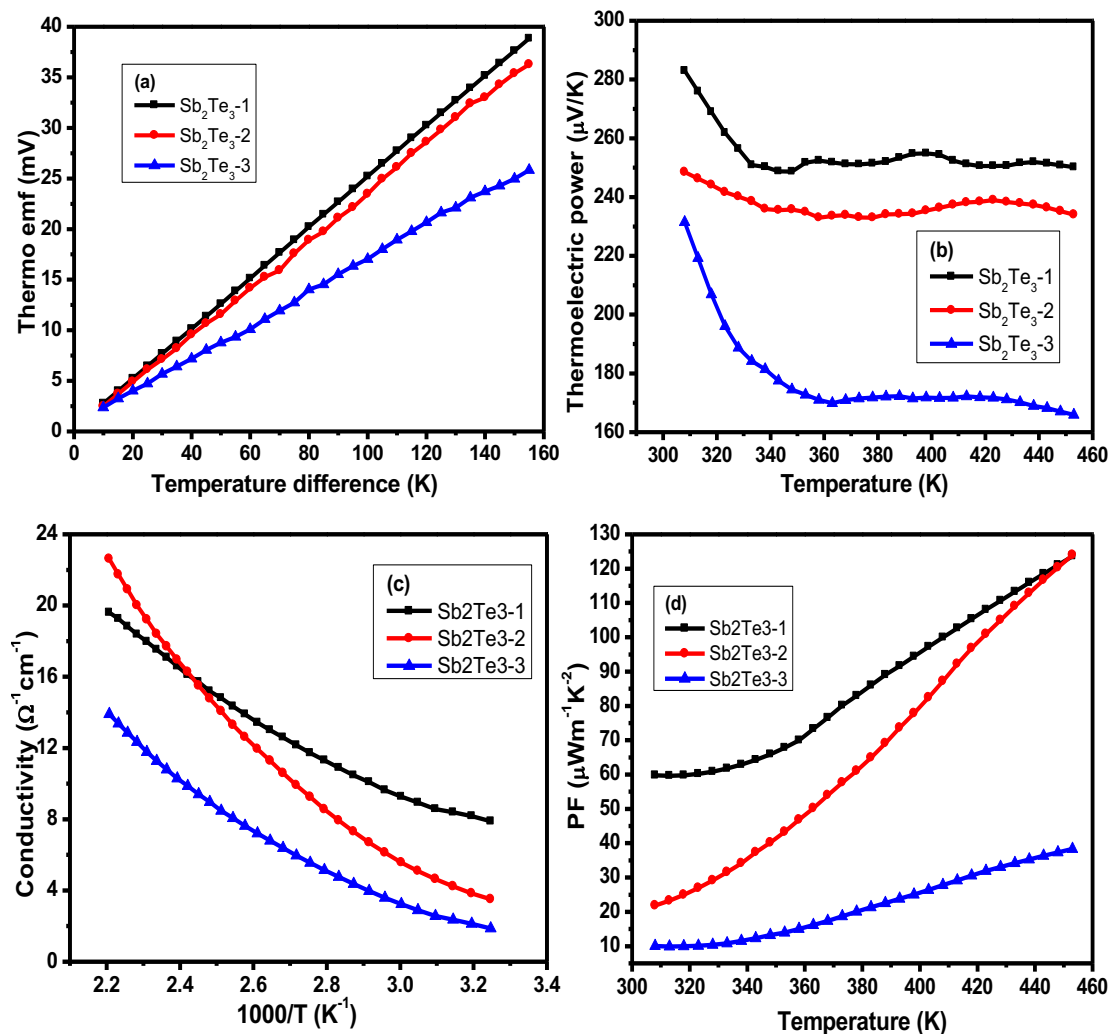


**Figure 4.12** (a). Variation in thermo emf with temperature difference, (b). Plot of thermoelectric power versus hot end temperature, (c). Electrical conductivity as function of inverse temperature and (d). Variation of power factor with temperature, of  $\text{Sb}_2\text{Te}_3$  doped  $\text{In}_2\text{Te}_3$  films.

The thermo emf of  $\text{Sb}_2\text{Te}_3$  doped films is proportionally increasing with temperature as depicted in figure 4.12(a). The positive slope of figure 4.12(a) is an indication of p-type conductivity of  $\text{Sb}_2\text{Te}_3$  doped  $\text{In}_2\text{Te}_3$  films. Figure 4.12(c) shows the typical plot of variation in thermoelectric power with temperature. Thermoelectric power of all films is decreased drastically at lower temperatures and reached saturation after 330 K. The maximum thermoelectric power is found in  $\text{Sb}_2\text{Te}_3$ -1 films ( $\sim 266 \mu\text{VK}^{-1}$  at room temperature) and further decreased with an increase in doping percentage. An increase in thermoelectric power at lower doping concentration is an indication of asymmetric phase formation in the films structure. At relatively higher doping concentration, the films are intended to be more symmetric leading to a decrease in thermoelectric power.

The electrical conductivity of the films marginally decreased with an increase in doping concentration and is maximum for  $\text{Sb}_2\text{Te}_3$ -1 films. At 320 K, the electrical conductivity of  $\text{Sb}_2\text{Te}_3$ -1 films is around  $8.47 \Omega^{-1}\text{cm}^{-1}$ . The thermoelectric power factor of  $\text{Sb}_2\text{Te}_3$  films increased significantly compared with un-doped films. As doping concentration increases, the power factor of the films decreases and found to be maximum for  $\text{Sb}_2\text{Te}_3$ -1 films which is  $60.04 \mu\text{Wm}^{-1}\text{K}^{-2}$  at 320 K. Moreover, the power factor of  $\text{Sb}_2\text{Te}_3$ -1 films is enhanced by 12.2 times of un-doped  $\text{In}_2\text{Te}_3$  films.

#### 4.3.3 (b). $\text{Sb}_2\text{Te}_3$ alloyed $\text{In}_2\text{Te}_3$ thin films:

Structural properties and composition:

Figure 4.13 shows the typical XRD patterns of  $\text{Sb}_2\text{Te}_3$  alloyed  $\text{In}_2\text{Te}_3$  films. The films are showing polycrystalline nature and intensity of  $\text{In}_2\text{Te}_3$  peaks gradually reduced when  $\text{Sb}_2\text{Te}_3$  peaks are raised with an increase in  $\text{Sb}_2\text{Te}_3$  percentage. The XRD pattern of pure  $\text{Sb}_2\text{Te}_3$  films deposited at same growth conditions is also given in figure 4.13 for comparison purpose. In all alloyed films, (0 1 5), (1 0 10) and (0 1 11) planes corresponding to  $\text{Sb}_2\text{Te}_3$  phase are appearing. The peak corresponding to Sb (1 0 4) is appearing in both 50 % and 75 %  $\text{Sb}_2\text{Te}_3$  mixed  $\text{In}_2\text{Te}_3$  films. As  $\text{Sb}_2\text{Te}_3$  percentage increases, the peak at  $2\theta$  of  $27.24^\circ$  corresponding to  $\text{In}_2\text{Te}_3$  phase disappeared and gradually shifted to higher angle of  $28.24^\circ$  belonging to  $\text{Sb}_2\text{Te}_3$  phase which might be

due to replacement of  $\text{In}^{3+}$  with  $\text{Sb}^{3+}$  (effective ionic radius:  $\text{In}^{3+} \sim 80$  pm and  $\text{Sb}^{3+} \sim 76$  pm).

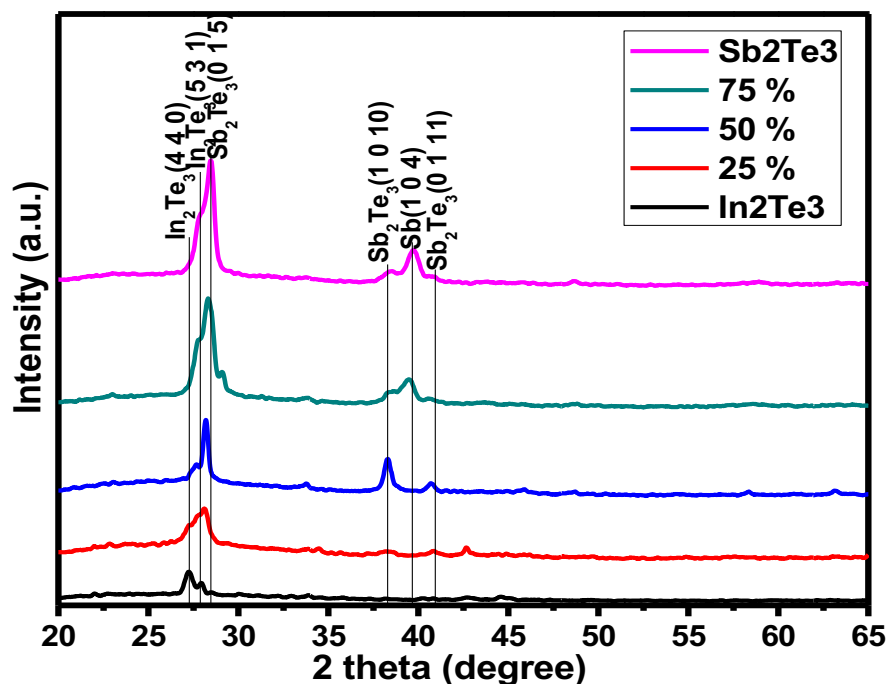


**Figure 4.13** XRD patterns of  $\text{Sb}_2\text{Te}_3$  alloyed  $\text{In}_2\text{Te}_3$  films deposited at 423 K substrate temperature.

Figure 4.14 shows the FESEM images of  $\text{Sb}_2\text{Te}_3$  alloyed  $\text{In}_2\text{Te}_3$  films. The surface structure is gradually converting from  $\text{In}_2\text{Te}_3$  grain orientation to  $\text{Sb}_2\text{Te}_3$  grain orientation which is also evidenced in XRD patterns in the form of phase transformation from  $\text{In}_2\text{Te}_3$  to  $\text{Sb}_2\text{Te}_3$ . The EDAX analysis revealed that In composition gradually decreases with an increase in  $\text{Sb}_2\text{Te}_3$  percentage. The elemental composition of  $\text{Sb}_2\text{Te}_3$  alloyed  $\text{In}_2\text{Te}_3$  films is summarized in table 4.4. The composition of pure  $\text{Sb}_2\text{Te}_3$  films deposited at same growth condition are also given in table 4.4 which indicates that these films are Sb rich (Stoichiometric ratio Sb/Te: 2/3). The structural properties together with composition analysis revealed the replacement of  $\text{In}^{3+}$  by  $\text{Sb}^{3+}$  ions.

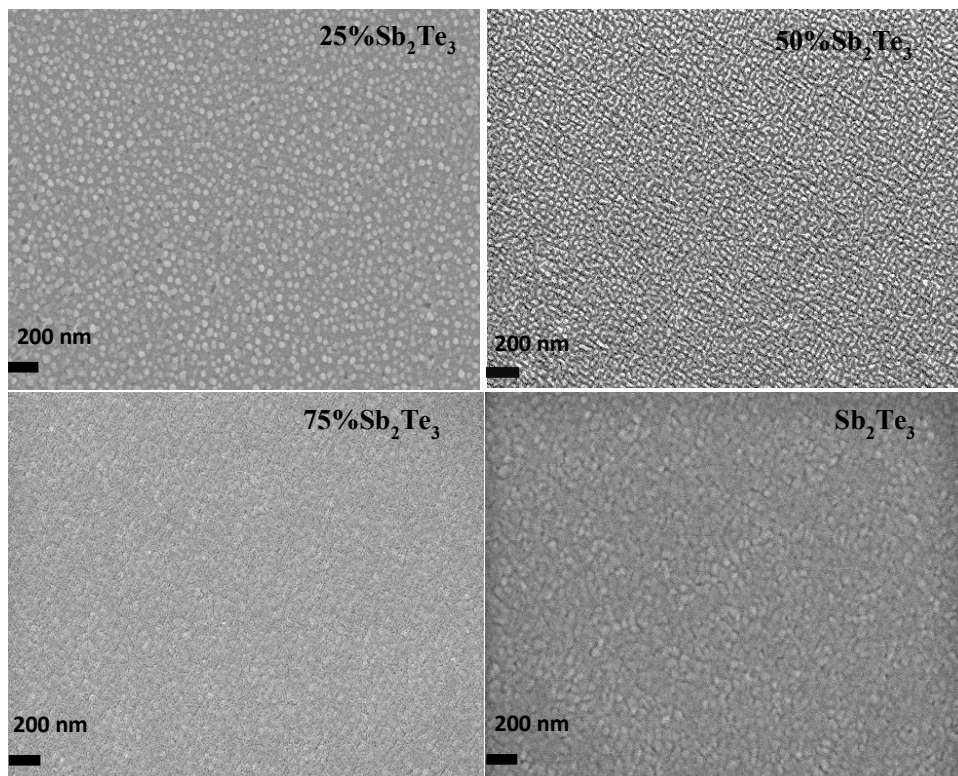
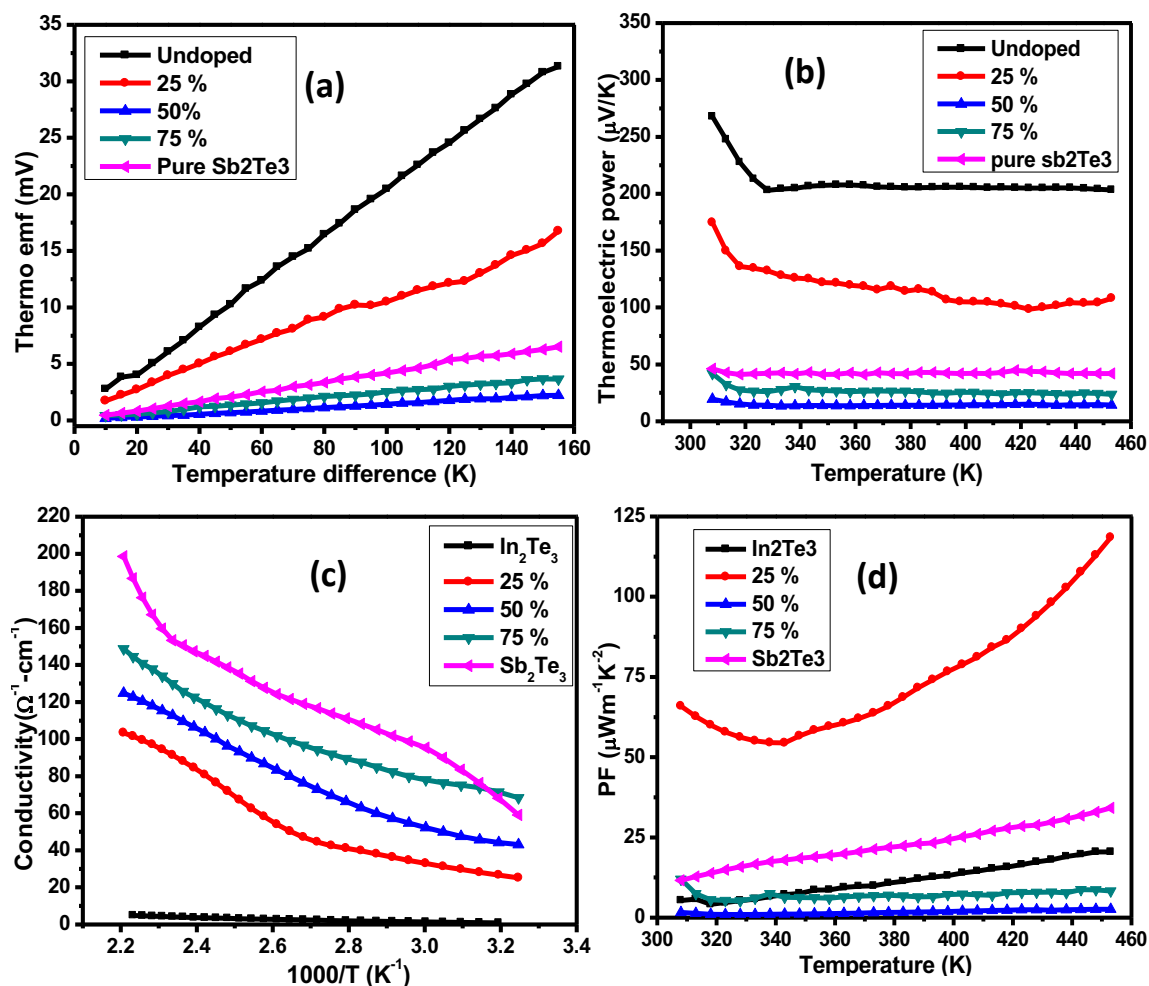


**Figure 4.14** FESEM micrographs of  $\text{Sb}_2\text{Te}_3$  alloyed  $\text{In}_2\text{Te}_3$  thin films.

**Table 4.4** Composition of  $\text{Sb}_2\text{Te}_3$  alloyed  $\text{In}_2\text{Te}_3$  thin films

Sample names	Dopant conc. (%) in source	Film Composition ( at%.)		
		Sb	In	Te
25% $\text{Sb}_2\text{Te}_3$	25%	7.0	37.4	55.6
50% $\text{Sb}_2\text{Te}_3$	50%	18.6	24.6	56.8
75% $\text{Sb}_2\text{Te}_3$	75%	32.9	11.9	55.2
$\text{Sb}_2\text{Te}_3$	pure	46.3	-	53.7

Thermoelectric properties:



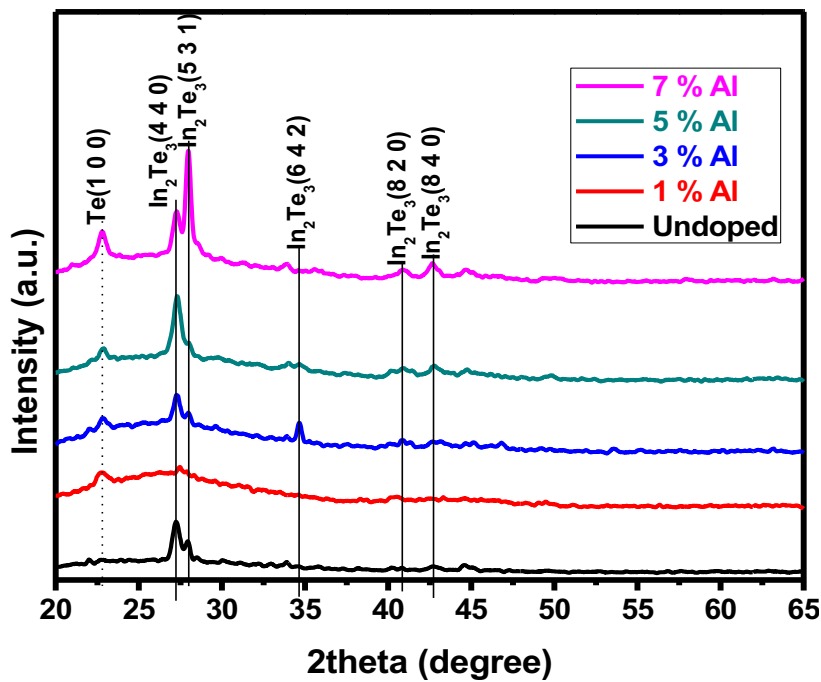
**Figure 4.15 (a).** Variation in thermo emf with temperature difference, **(b).** Plot of thermoelectric power versus hot end temperature, **(c).** Variation in electrical conductivity with inverse temperature and **(d).** Power factor as a function of temperature, of  $\text{Sb}_2\text{Te}_3$  alloyed  $\text{In}_2\text{Te}_3$  films.

Figure 4.15 (c) shows the electrical conductivity of  $\text{Sb}_2\text{Te}_3$  alloyed  $\text{In}_2\text{Te}_3$  films. The electrical conductivity of  $\text{Sb}_2\text{Te}_3$  films is greater than  $\text{In}_2\text{Te}_3$  films, hence the conductivity of  $\text{In}_2\text{Te}_3$  films is gradually increased with an increase in  $\text{Sb}_2\text{Te}_3$  percentage. The 75 %  $\text{Sb}_2\text{Te}_3$  alloyed  $\text{In}_2\text{Te}_3$  films showed maximum electrical conductivity of about  $71.46 \Omega^{-1}\cdot\text{cm}^{-1}$  (At 320 K). The variation in power factor with temperature of prepared films is depicted in figure 4.15 (d). The power factor of films

is increasing with an increase in temperature. Since the power factor is a function of seebeck coefficient and electrical conductivity ( $S^2\sigma$ ), the maximum power factor is showed by 25%  $\text{Sb}_2\text{Te}_3$ - $\text{In}_2\text{Te}_3$  films which is  $\sim 58.57 \mu\text{Wm}^{-1}\text{K}^{-2}$ . Moreover, the power factor of 25%  $\text{Sb}_2\text{Te}_3$  alloyed  $\text{In}_2\text{Te}_3$  films is enhanced by 11.9 times of un-doped  $\text{In}_2\text{Te}_3$  films and 4 times of pure  $\text{Sb}_2\text{Te}_3$  films.

#### 4.3.4 Al doped $\text{In}_2\text{Te}_3$ thin films

Structural properties and composition:



**Figure 4.16** XRD patterns of Al doped  $\text{In}_2\text{Te}_3$  films deposited at 423 K.

Figure 4.16(a) is a typical XRD pattern of Al doped  $\text{In}_2\text{Te}_3$  thin films deposited at 423 K substrate temperature. Irrespective of doping concentration, all films exhibit mixed phase of  $\text{In}_2\text{Te}_3$  and Te. It is observed that when dopant concentration increases the crystallinity of the films improves marginally with an improvement in the intensity of (4 4 0) peak corresponding to  $\text{In}_2\text{Te}_3$ . Furthermore, an increase in the presence of free tellurium is reflected in the XRD as well as in the electron micrographs (Figure 4.16). No peaks corresponding to reflections from other phases of indium telluride and free dopant materials were observed. In order to understand the effect of doping on lattice



of  $\text{In}_2\text{Te}_3$  films, the lattice constant of films was measured along (4 4 0) which is a prominent peak for source material. The estimated lattice constant of the films is 18.503 Å which matches with the reported data.

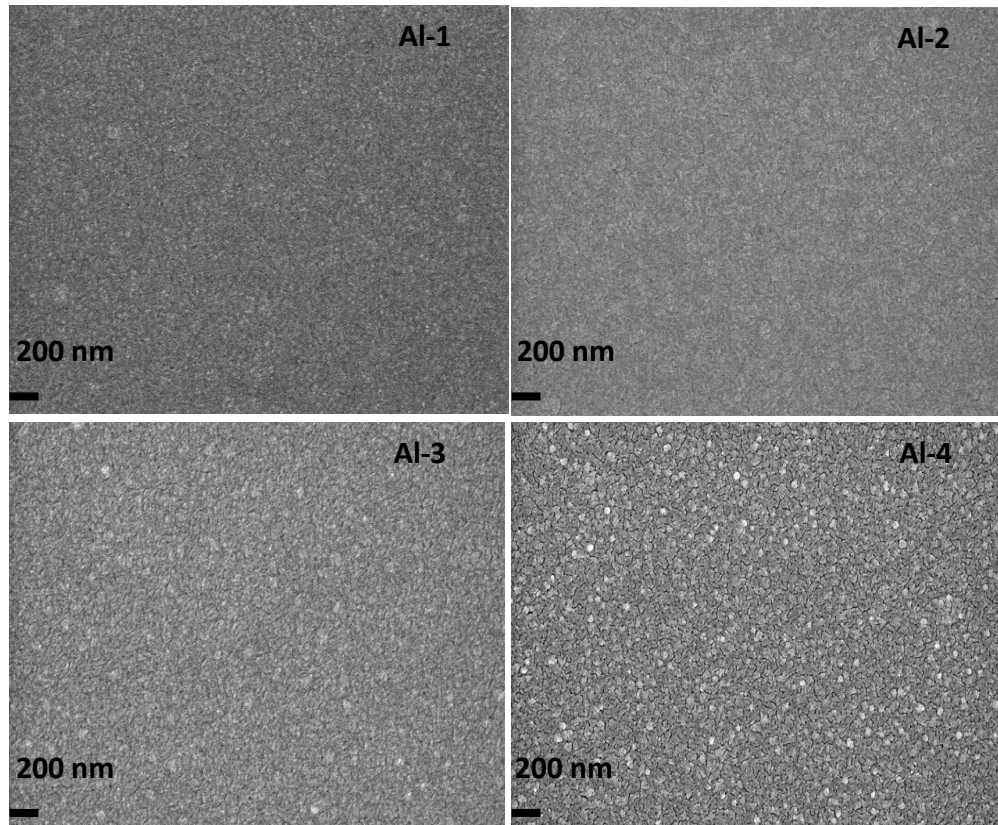


**Figure 4.16** FESEM micrographs of Al doped  $\text{In}_2\text{Te}_3$  thin films.

The FESEM images are depicted in figure 4.16. Al doping has shown a notable influence on the morphology of the films. The grain size of Al-1 films is reduced when compared with un-doped  $\text{In}_2\text{Te}_3$  films. Further increase in Al percentage shown gradual formation of grains with un-clear grain boundaries. The dopant concentration in the starting material and the final films is tabulated in table 4.5. The films are showing less doping percentage when compared with added doping percentage which is due to the difference in vapour pressures of the constituent elements ( $\text{Te} > \text{In} > \text{Al}$ ).



**Table 4.5** Elemental composition of Al doped  $\text{In}_2\text{Te}_3$  thin films

Sample names	Dopant conc. (%) in source	Film Composition ( at%.)		
		Al	In	Te
Al-1	1%	1.1	46.4	52.5
Al-2	3%	2.1	44.2	53.7
Al-3	5%	3.2	42.9	53.9
Al-4	7%	4.2	42.3	53.5

Thermoelectric properties:

Figure 4.17(a) shows the variation in thermo emf generation of aluminium doped  $\text{In}_2\text{Te}_3$  films with temperature difference. The positive slope of these graphs indicates the p-type conductivity of Al doped  $\text{In}_2\text{Te}_3$  films. Since the compound  $\text{In}_2\text{Te}_3$  is p-type and exhibits the ionic nature, the donors ( $\text{Te}^{2-}$ ) are mainly self-compensated by ionic defects while acceptors ( $\text{In}^{3+}$ ) are significantly compensated by holes. The Al dopant can produce ions isovalent to In and can produce substitutional defects. The p-type conductivity remains same in Al doped  $\text{In}_2\text{Te}_3$  films. The thermo emf of Al doped films are linearly increasing with temperature difference. Notably, the thermo emf shows increasing trend up to Al-2 and further decreases with an increase in dopant concentration. The increase in thermo emf at low dopant concentrations indicates that the dopant in the film forms a disordered phase leading to an increase in the electrical resistivity. At higher concentration of dopant, the films are relatively more ordered leading to a decrease in the electrical resistivity.

Figure 4.17(b) represents variation in seebeck coefficient with temperature of Al doped  $\text{In}_2\text{Te}_3$  thin films which in turn indicates that the rate of thermo emf is significantly higher at lower temperatures and gradually decreases to reach saturation level in the investigated temperature range. Higher seebeck coefficient has been seen for Al-2 doped  $\text{In}_2\text{Te}_3$  films which is  $\sim 384 \mu\text{VK}^{-1}$  at 320 K.

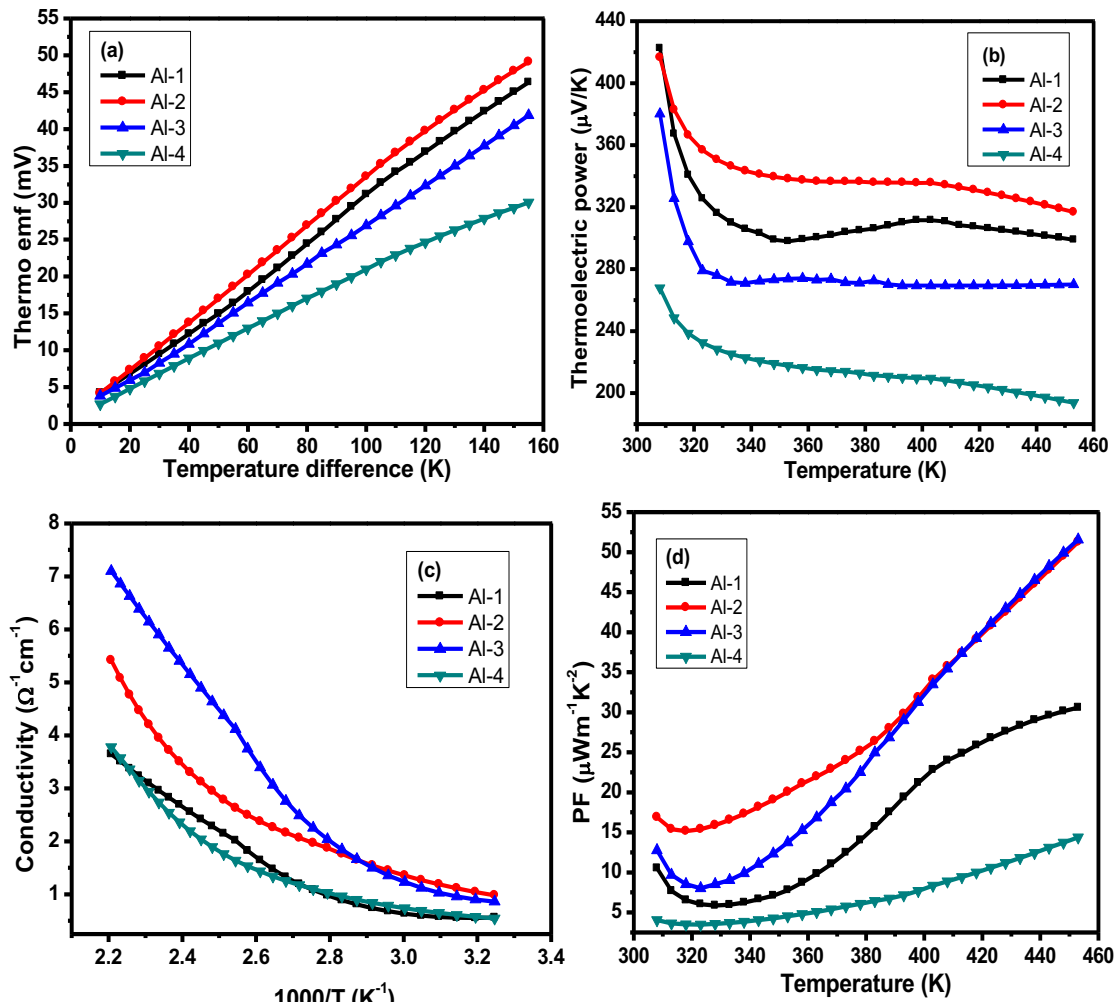


**Figure 4.17 (a).** Variation in thermo emf with temperature difference, **(b).** Plot of thermoelectric power versus hot end temperature, **(c).** Electrical conductivity as function of inverse temperature and **(d).** Variation of power factor with temperature, of Al doped  $\text{In}_2\text{Te}_3$  films.

The temperature dependent electrical conductivity ( $\sigma$ ) of Al doped films are shown in Figure 4.17(c). Doping can affect the conductivity due to the following reasons. The dopant impurity atoms can reduce the grain size and increase the grain boundaries which results in decrease of electrical conductivity. On the contrary, it may provide additional carriers to increase the conductivity. Hence, electrical conductivity will be a resultant of two effects and a strong function of the dopant concentration. The changes in the electrical conductivity of the films will have a direct influence on the thermoelectric power factor as can be seen from figure 4.17(d). However, the highest power factor of the films is showed by Al-2 films at room temperature whereas, the

power factor values of Al-2 films are merging with Al-3 films at higher temperatures than 390 K. The power factor of Al-2 films is  $\sim 15.41 \mu\text{Wm}^{-1}\text{K}^{-2}$  (at 320 K) which is enhanced by 3.1 times of un-doped  $\text{In}_2\text{Te}_3$  thin films.

#### 4.3.5 Sb doped $\text{In}_2\text{Te}_3$ thin films

Structural properties composition:

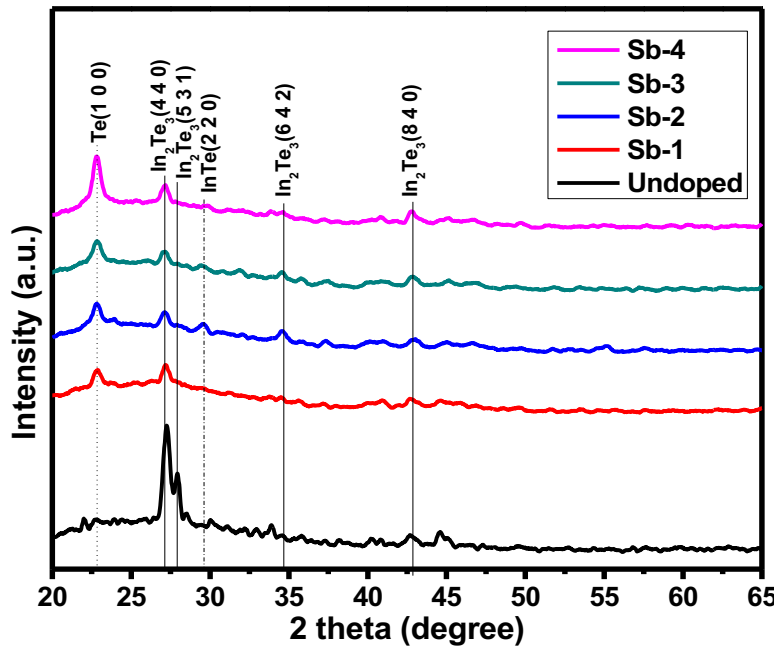


**Figure 4.18** XRD patterns of Sb doped  $\text{In}_2\text{Te}_3$  thin films deposited at 423 K substrate temperature.

The XRD patterns of Sb doped  $\text{In}_2\text{Te}_3$  films are depicted in figure 4.18. Sb-1 films are exhibiting mixed phase of cubic  $\text{In}_2\text{Te}_3$  and hexagonal Te. Further increase in Sb doping percentage leads to formation of an additional phase of tetragonal InTe. The Sb doped  $\text{In}_2\text{Te}_3$  films show no improvement in crystallinity and in addition to this, an increase in intensity of free tellurium peak is reflected in XRD. The calculated lattice parameter along the commonly exhibited peak of  $\text{In}_2\text{Te}_3$  (4 4 0) is  $\sim 18.503 \text{ \AA}$ .

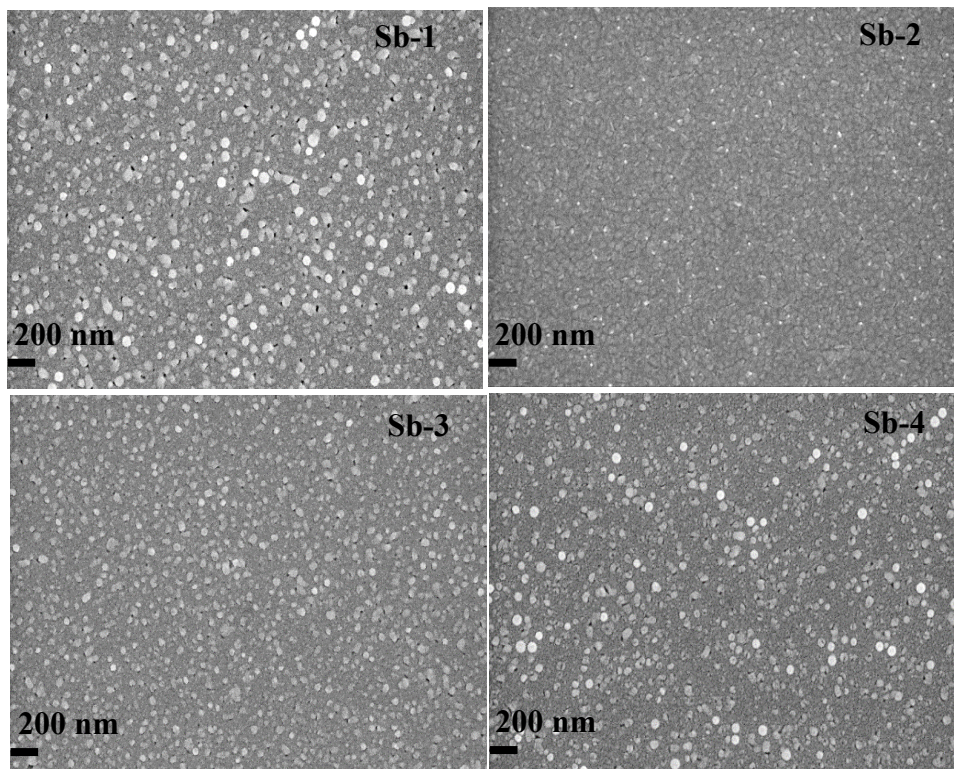


**Figure 4.19** FESEM micrographs of Sb doped  $\text{In}_2\text{Te}_3$  thin films.

Figure 4.19 shows the surface morphology of Sb doped  $\text{In}_2\text{Te}_3$  films. The FESEM images revealed that the grain size of Sb-1 films is increased compared with un-doped  $\text{In}_2\text{Te}_3$  films. For Sb-2 films, the re-orientation of grains can be seen which may be due to formation of additional  $\text{InTe}$  phase. Further, an increase in Sb doping percentage increases the grain size of  $\text{In}_2\text{Te}_3$  films. The EDAX analysis revealed that the presence of Sb doping percentage in samples are almost matching with an added percentage in source material. The In percentage found to be decreased with an increase in Sb concentration. The elemental composition of the Sb doped  $\text{In}_2\text{Te}_3$  films is given in table 4.6. The elemental mapping of Sb-1 films is given in figure 4.20 which indicates the uniform distribution of elements throughout the film surface. Similarly, elemental mapping of other dopant doped films is also showing uniform distribution at different concentrations at different dopants.

**Table 4.6.** Elemental composition of Sb doped In<sub>2</sub>Te<sub>3</sub> films

Sample names	Dopant conc. (%) in source	Film Composition ( at%.)		
		Sb	In	Te
Sb-1	1%	1.0	47.9	51.1
Sb-2	3%	3.0	45.5	51.5
Sb-3	5%	4.4	43.7	51.9
Sb-4	7%	7.0	42.5	50.5

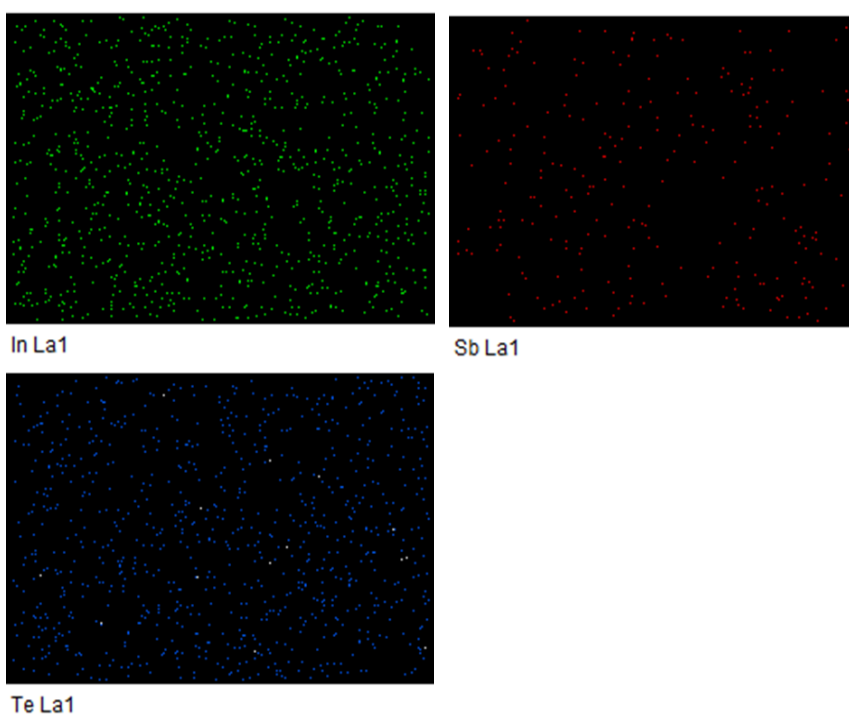


**Figure 4.20** Representative elemental mapping to uniform distribution of dopants (Sb-1 films).

Thermoelectric properties:

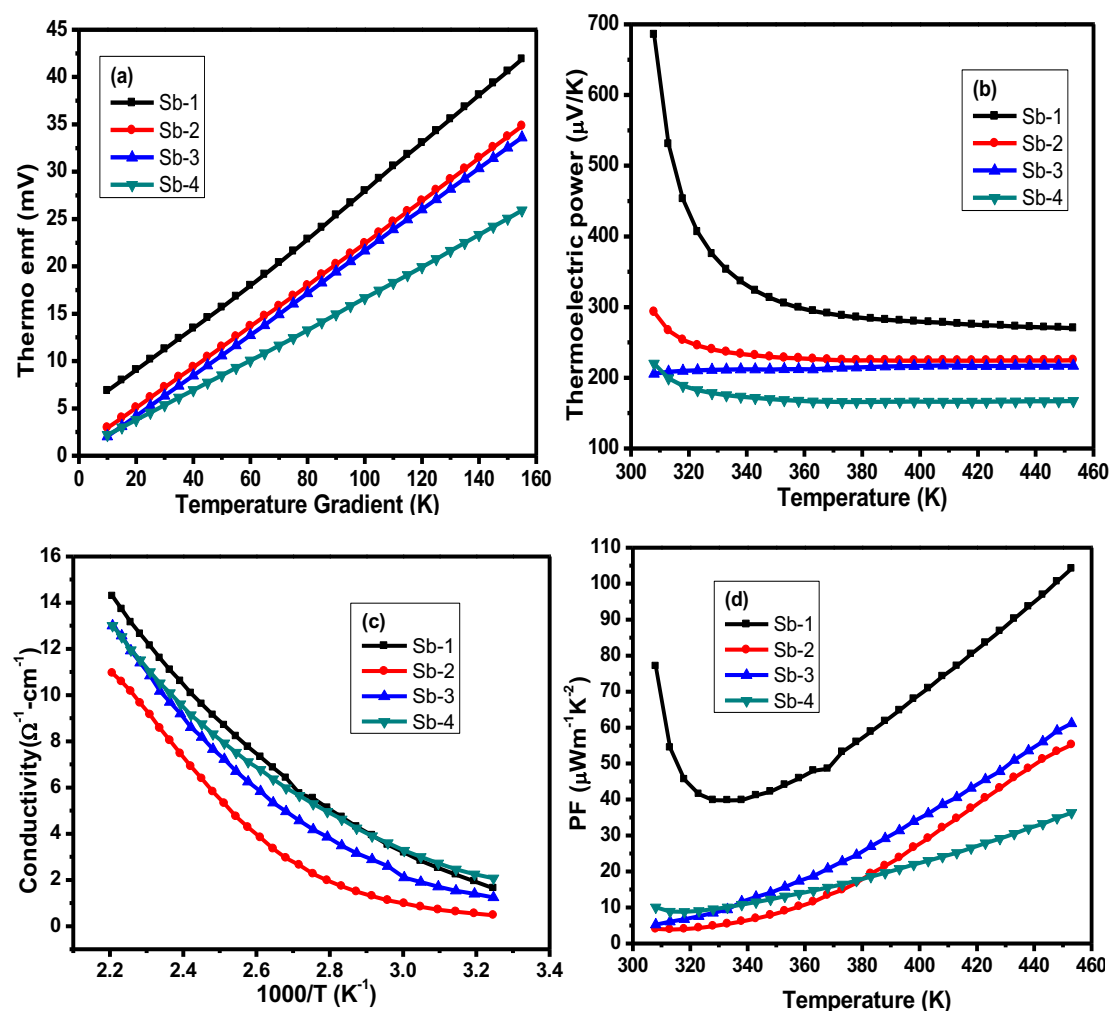


**Figure 4.21** (a). Thermo emf as a function of temperature difference, (b). Plot of thermoelectric power versus hot end temperature, (c). Electrical conductivity as function of inverse temperature and (d). Variation of power factor with temperature, of Sb doped  $\text{In}_2\text{Te}_3$  films.

Figure 4.21(a) represents the thermo emf generation of Sb doped  $\text{In}_2\text{Te}_3$  films with temperature difference. The thermo emf of the films is increasing with an increase in temperature difference. The positive values of thermo emf indicates the p-type conductivity of Sb doped  $\text{In}_2\text{Te}_3$  films. Figure 4.21(b) shows the variation in seebeck coefficient of Sb doped  $\text{In}_2\text{Te}_3$  films with temperature. Both thermo emf and seebeck coefficient are maximum for Sb-1 films and further increase in Sb doping percentage

results in a decrease of thermo emf and seebeck coefficient. As a part of structural changes, the formation of InTe phase and increase in free Te phase may be the cause for decrease in seebeck coefficient of Sb-2, Sb-3 and Sb-4 films. Similar type of observation was also seen in case of pure In<sub>2</sub>Te<sub>3</sub> films. However, the seebeck coefficient of Sb-1 films is  $\sim 477 \mu\text{VK}^{-1}$  (at 320 K). In this investigation, it is observed that seebeck coefficient of Sb-1 films is maximum compared with all doped and un-doped In<sub>2</sub>Te<sub>3</sub> films.

The variation in electrical conductivity with inverse temperature of Sb doped In<sub>2</sub>Te<sub>3</sub> films is depicted in figure 4.21(c). The electrical conductivity of Sb doped In<sub>2</sub>Te<sub>3</sub> films is found to be decreased up to Sb-2 films and further increase in Sb doping leads to an increase in electrical conductivity. The changes in conductivity with Sb doping percentage seems to be a cause of changes in grain orientation as seen in figure 4.19. However, the maximum electrical conductivity is showed by Sb-4 films which is  $\sim 2.24 \Omega^{-1}\text{cm}^{-1}$ . The maximum power factor is observed for Sb-1 films and further increase in doping percentage leads to decrease in power factor. Furthermore, the power factor of Sb-1 films is improved by 8.9 times compared to that of un-doped In<sub>2</sub>Te<sub>3</sub> films.

#### **4.3.5 Se doped In<sub>2</sub>Te<sub>3</sub> thin films**

Structural properties and composition:

The phase configurations and crystal structure of the films are confirmed using XRD patterns. The XRD patterns of Se doped In<sub>2</sub>Te<sub>3</sub> films are polycrystalline in nature which are shown in figure 4.22. Se doped In<sub>2</sub>Te<sub>3</sub> films are exhibiting a free Te phase in addition with In<sub>2</sub>Te<sub>3</sub> phase. All Se doped films are preferentially oriented along the In<sub>2</sub>Te<sub>3</sub> (4 4 0) plane. The peak intensity of In<sub>2</sub>Te<sub>3</sub> (5 3 1) is gradually decreased and Te peak (1 0 0) is identified at  $2\theta \approx 23.2^\circ$ . Peaks corresponding to Se phase are absent in XRD patterns. The lattice parameters of Se doped In<sub>2</sub>Te<sub>3</sub> films are estimated using In<sub>2</sub>Te<sub>3</sub> (4 4 0) peak which is a commonly presented peak in all films. There is no peak shift in Se doped films and the estimated lattice parameter is 18.503 Å which matches well with that of un-doped In<sub>2</sub>Te<sub>3</sub> films.



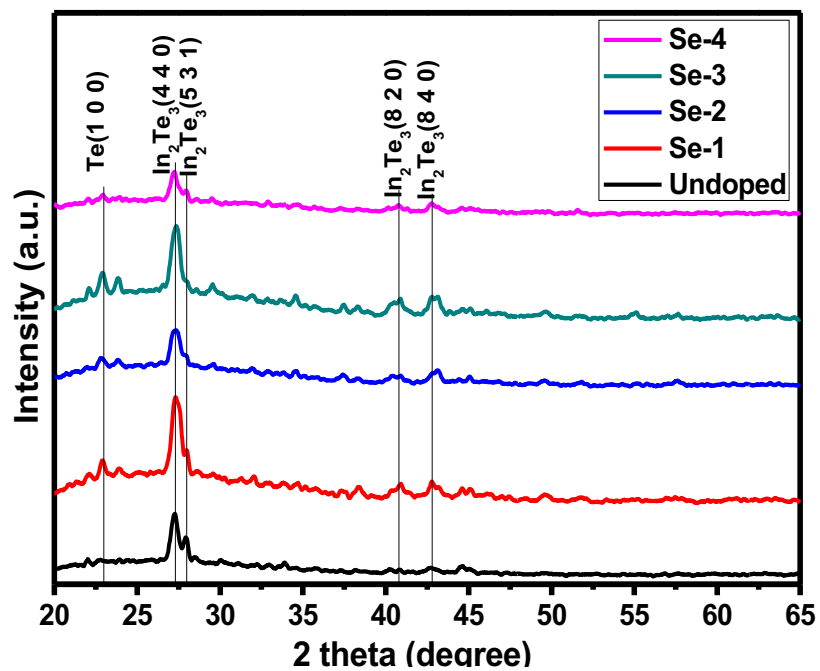


**Figure 4.22** XRD patterns of Se doped In<sub>2</sub>Te<sub>3</sub> thin films deposited at 423 K substrate temperature.

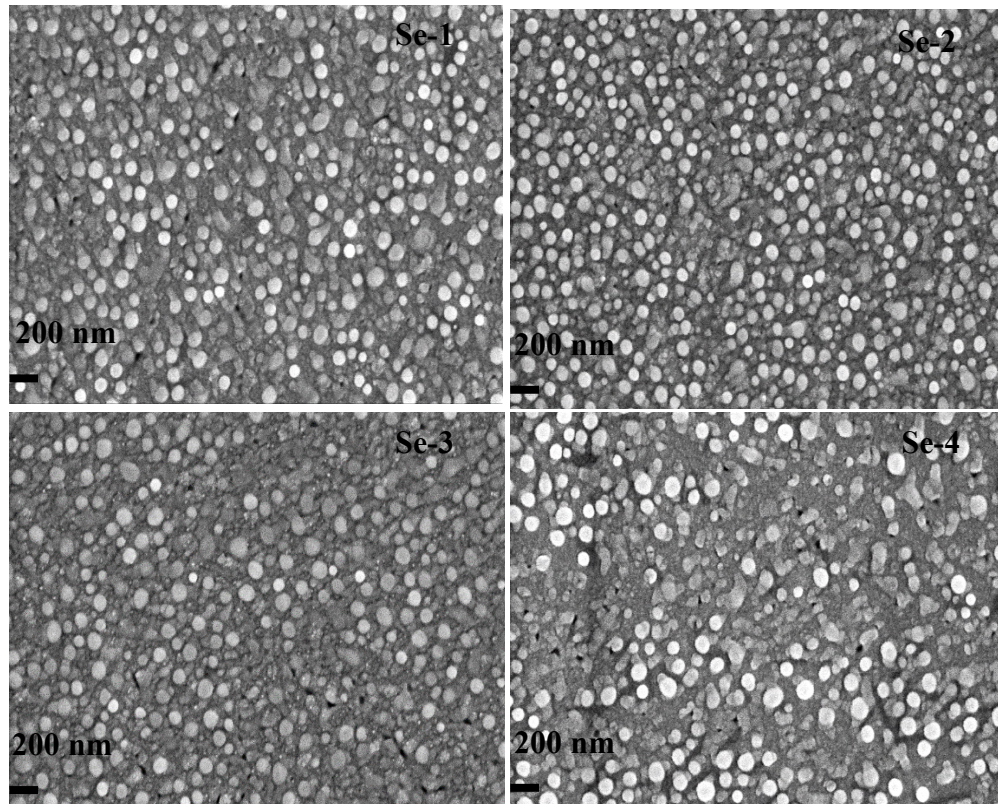


**Figure 4.23** FESEM micrographs of Se doped In<sub>2</sub>Te<sub>3</sub> thin films.



Figure 4.23 shows the FESEM micrographs of Se doped  $\text{In}_2\text{Te}_3$  thin films. The surface morphology of Se doped  $\text{In}_2\text{Te}_3$  is granular and grains are uniformly distributed in Se-1 and Se-2 films, further increase in Se percentage resulted in the non-uniform distribution of grains and deterioration of film quality. To determine the elemental composition of the films, Se doped  $\text{In}_2\text{Te}_3$  films are subjected to EDAX analysis. Table 4.7 reveals the elemental composition of Se doped  $\text{In}_2\text{Te}_3$  films. The amount of Se present in the film is relatively less than that of taken percentage for deposition. This might be due to the higher vapor pressure of Se than that of both Te and In ( $\text{Se} > \text{Te} > \text{In}$ ). Hence Se might be re-evaporated from the substrate.

**Table 4.7** Elemental composition of Se doped  $\text{In}_2\text{Te}_3$  thin films

Sample names	Dopant conc. (%) in source	Film Composition ( at%.)		
		Se	In	Te
Se-1	1%	0.2	48.0	51.8
Se-2	3%	0.4	46.7	52.9
Se-3	5%	0.5	46.6	52.9
Se-4	7%	1.4	45.0	53.6

Thermoelectric properties:

Figure 4.24 (a) shows the generation of thermo emf with respect to temperature difference of Se doped  $\text{In}_2\text{Te}_3$  thin films. The thermo emf is linearly increasing with temperature difference. The positive slope of figure 4.24 is an indication of p-type conductivity of Se doped  $\text{In}_2\text{Te}_3$  films. Thermo emf has shown an increasing trend with Se doping up to Se-2 and further increase in Se percentage resulted a marginal decrease in thermo emf which might be due to the diminished quality of films as mentioned in morphological studies.

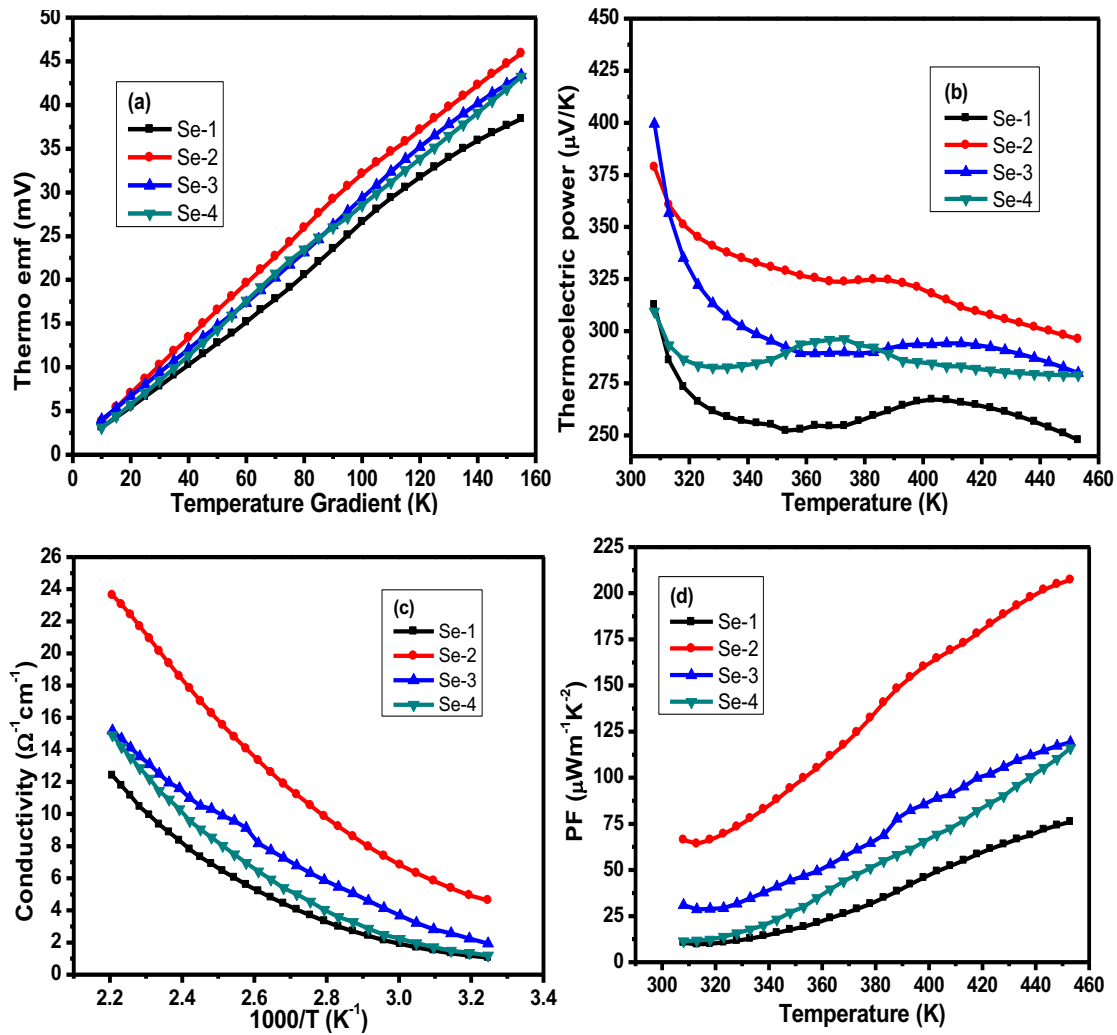


**Figure 4.24** (a). Thermo emf as a function of temperature difference and (b). Plot of thermoelectric power versus hot end temperature, (c). variation in electrical conductivity with of inverse temperature and (d). Power factor versus temperature plot, of Se doped  $\text{In}_2\text{Te}_3$  films.

Figure 4.24 (c) shows the temperature dependence of thermoelectric power for Se doped  $\text{In}_2\text{Te}_3$  films. The rate of change of thermoelectric power with respect to temperature is drastically decreased below 320 K and further reached the saturation in the investigated range of temperature. The maximum thermoelectric power is observed in Se-2 which shows  $\sim 350 \mu\text{V}/\text{K}$  at 320 K. Figure 4. 24 (c) shows the variation in electrical conductivity with temperature of Se doped  $\text{In}_2\text{Te}_3$  thin films. The exponential decrease of the conductivity with an inverse temperature is an indication of semiconductor behaviour. The electrical conductivity of Se doped  $\text{In}_2\text{Te}_3$  films is

increased with an increase in Se percentage up to Se-2, further increase in Se percentage resulted a marginal decrease in electrical conductivity which might be due to electrons scattering at the defects of Se-3 and Se-4 films (Figure 4.23). The power factor as a function of temperature for Se doped  $\text{In}_2\text{Te}_3$  films is depicted in figure 4.24 (d) which shows the linear increase of power factor with respect to the temperature. Since the power factor depends on thermoelectric power and electrical conductivity, the maximum power factor is attained by Se-2 films. The maximum power factor of Se doped films is  $68.8 \mu\text{Wm}^{-1}\text{K}^{-2}$  at 320 K for Se-2 sample. Impressively, in this investigation it is observed that the power factor of Se-2 films is enhanced by 14 times of un-doped  $\text{In}_2\text{Te}_3$  films which is maximum compared with any other dopants used in this study.

#### 4.3.6 Te doped $\text{In}_2\text{Te}_3$ thin films

Structural properties composition:

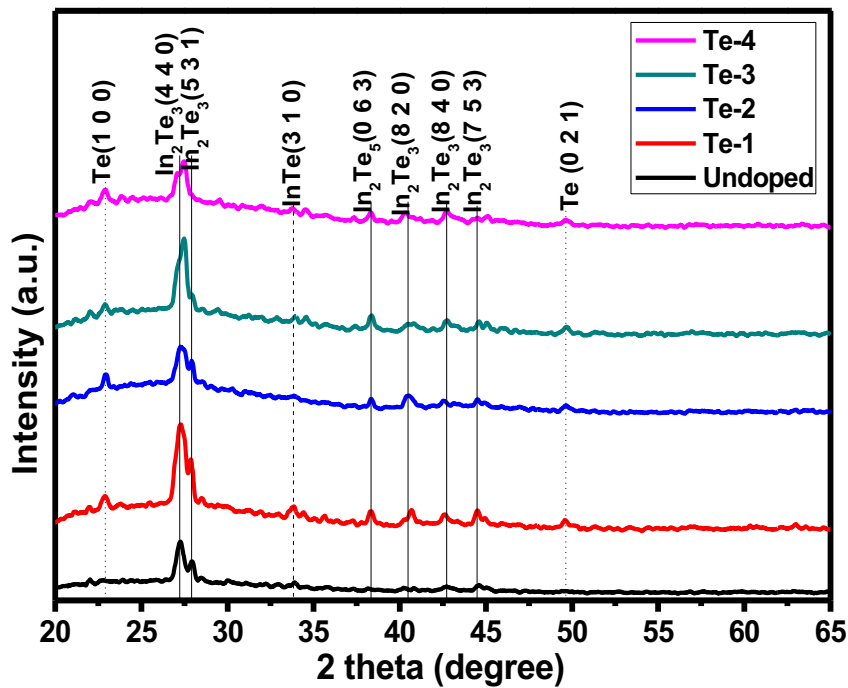
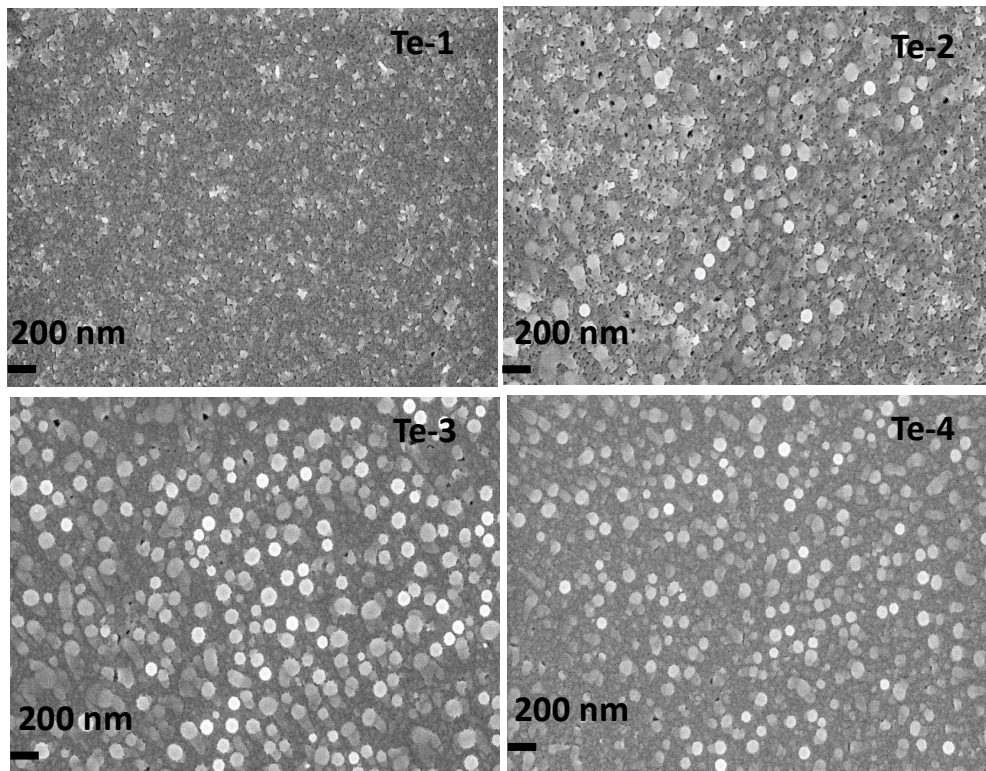


Figure 4.25 XRD patterns of Te doped  $\text{In}_2\text{Te}_3$  thin films deposited at 423 K.

XRD patterns are employed in order to confirm the phase contribution of Te doped  $\text{In}_2\text{Te}_3$  films shown in figure 4.25. XRD patterns revealed that the Te doped  $\text{In}_2\text{Te}_3$  films have an additional Te phase along and very minor contribution of InTe phase along with  $\text{In}_2\text{Te}_3$  phase. The films namely Te-1 and Te-2 are preferentially oriented along  $\text{In}_2\text{Te}_3$  (4 4 0) plane. Further increase in Te percentage results in peak shift of  $\text{In}_2\text{Te}_3$  (4 4 0) towards higher  $2\theta$  side which is an indication of distortion in the lattice. The peak intensity of  $\text{In}_2\text{Te}_3$  (5 3 1) is gradually reduced and disappeared in Te-3 and Te-4 diffraction patterns. The lattice constants of the films are estimated along  $\text{In}_2\text{Te}_3$  (4 4 0) peak and value is 18.503 Å for Te-1 and Te-2, whereas 18.3225 Å for both Te-3 and Te-4 films.



**Figure 4.26** FESEM micrographs of Te doped  $\text{In}_2\text{Te}_3$  thin films.

The FESEM images of Te doped  $\text{In}_2\text{Te}_3$  films are presented in figure 4.26. The Te doped  $\text{In}_2\text{Te}_3$  films have shown a distinct surface structure at different Te percentages. The Te-1 film depicts flake like structure and Te-2 is having the combination of both flakes and grains. Further increase in Te percentage changes the complete grain

morphology which can be seen in both Te-3 and Te-4 films FESEM images. The EDAX analysis has been used for composition confirmation and values are tabulated in table 4.8.

**Table 4.8** Elemental composition of Te doped  $\text{In}_2\text{Te}_3$  thin films

Sample names	Dopant conc. (%) in source	Film Composition ( at%.)	
		In	Te
Te-1	1%	45.3	54.7
Te-2	3%	44.7	55.3
Te-3	5%	43.7	56.3
Te-4	7%	42.4	57.6

Thermoelectric properties:

The variation in thermo emf of Te doped  $\text{In}_2\text{Te}_3$  films with temperature difference is plotted in figure 4.27(a). The positive thermo emf values indicate p-type conductivity of Te doped  $\text{In}_2\text{Te}_3$  films. The Te doped  $\text{In}_2\text{Te}_3$  films are showing same thermo emf generation with temperature difference having a marginal change of  $\pm 2$  mV. Figure 4.27(b) is a typical plot of thermoelectric power versus temperature of Te doped  $\text{In}_2\text{Te}_3$  films. The thermoelectric power of Te-1 and Te-2 films is almost independent of temperature whereas, Te-3 and Te-4 films are showing an increasing trend of thermoelectric power at lower temperature ( $<350$  K) and reached saturation at higher temperatures. The variation in thermoelectric power with temperature of Te-3 and Te-4 is contrary to the Te-1 and Te-2 which might be due to the peak shift as shown in XRD patterns (Figure 4.25). However, the maximum thermoelectric power of  $\sim 303$   $\mu\text{VK}^{-1}$  is shown by the Te-2 films at 320 K.

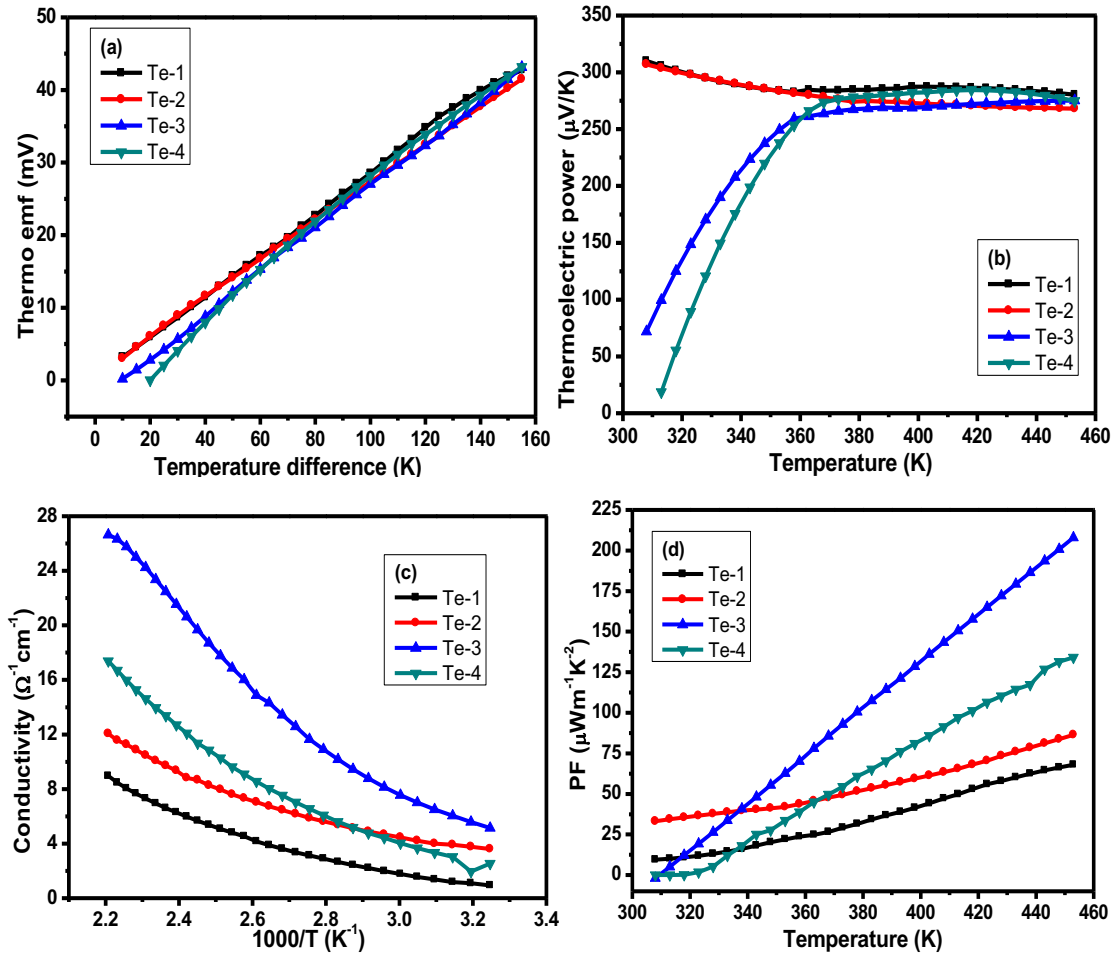


**Figure 4.27 (a).** The plot of thermo emf versus temperature difference, **(b).** Plot of thermoelectric power versus hot end temperature, **(c).** Electrical conductivity as function of inverse temperature and **(d).** Variation of power factor with temperature, of Te doped  $\text{In}_2\text{Te}_3$  films.

Figure 4.27 (c) represents the variation in electrical conductivity of Te doped  $\text{In}_2\text{Te}_3$  films with inverse temperature. The electrical conductivity of Te doped films is increased with an increase in Te percentage up to Te-3 and decreased for Te-4 films. This decrease might be due to the increased grain boundaries as seen in surface morphology of Te-4 films. Figure 4.27 (d) shows the power factor of Te doped  $\text{In}_2\text{Te}_3$  films as a function of temperature. The power factor versus temperature of Te-3 and Te-4 films are showing distinct variation compared with Te-1 and Te-2 plots which might be due to the peak shift caused by higher doping percentage. The Te doped films show the maximum power factor of  $207.8 \mu\text{Wm}^{-1} \text{K}^{-2}$  at 450 K for Te-3 sample.

However, Te-2 films show the maximum power factor of  $38.89 \mu\text{Wm}^{-1}\text{K}^{-2}$  at 320 K. Moreover, the power factor of Te-2 films is improved by 7.4 times of un-doped  $\text{In}_2\text{Te}_3$  films.

#### **4.4 Thermoelectric properties of InTe thin films**

##### **4.4.1 Growth conditions and optimisation**

The thermoelectric properties of InTe films are verified by depositing them at different substrate temperatures ranging from 298 K to 473 K on soda lime glass substrates using thermal evaporation method. Prior to the deposition, the glass substrates were cleaned using chromic acid, liquid detergent and ultra-sonicated with acetone which removes the impurities on the surface of glass slides. An aluminium foil was used as a mask to maintain length to width ratio of the film at 5.5. The distance between the substrate to source was fixed to 11 cm. A 100 A molybdenum boat was used to evaporate the 99.999% pure InTe precursor material. The vacuum inside the deposition chamber was maintained at  $\sim 5 \times 10^{-5}$  torr. The seebeck coefficient of as-deposited InTe films was measured in the temperature range from 298 K to 465 K, but these films are not showing thermoelectric behaviour. Hence, as-deposited films were subjected to annealing treatment at 523 K for 1h and investigated thermoelectric properties. The electrical properties of prepared films are investigated in the temperature range from 298 K to 465 K.

##### **4.4.2 Structural and thermoelectric properties of InTe films**

Structural properties and composition:

The InTe films deposited at 298 K, 373 K, 423 K and 473 K are annealed at 523 K for 1 h. Aforementioned in chapter 3, the InTe films annealed at 523 K for 1h are mono-phased, polycrystalline and are exhibiting tetragonal InTe phase irrespective of applied substrate temperature (Figure 3.12). All these annealed films are preferentially oriented along InTe (2 0 2) plane. The estimated lattice parameters of annealed films are  $a=b=8.4363 \text{ \AA}$  and  $c=7.1129 \text{ \AA}$  which matches well with standard data. The FESEM

images (Figure 3.13) of these films show different morphology at different substrate temperatures. The InTe deposited at 298 K are showing flake like morphology with porous top layer, 373 K deposited films represents the annihilation of flakes portions and further increase in substrate temperature resulted in the grain formation with unclear grain boundaries. Whereas InTe films deposited at 473 K shows uniform distribution of grains throughout the surface. The EDAX analysis of these films revealed that the films are nearly stoichiometric with In of  $49.60 \pm 0.40$  at % and Te of  $50.50 \pm 0.45$  at % (Table 3.5).

Thermoelectric properties:

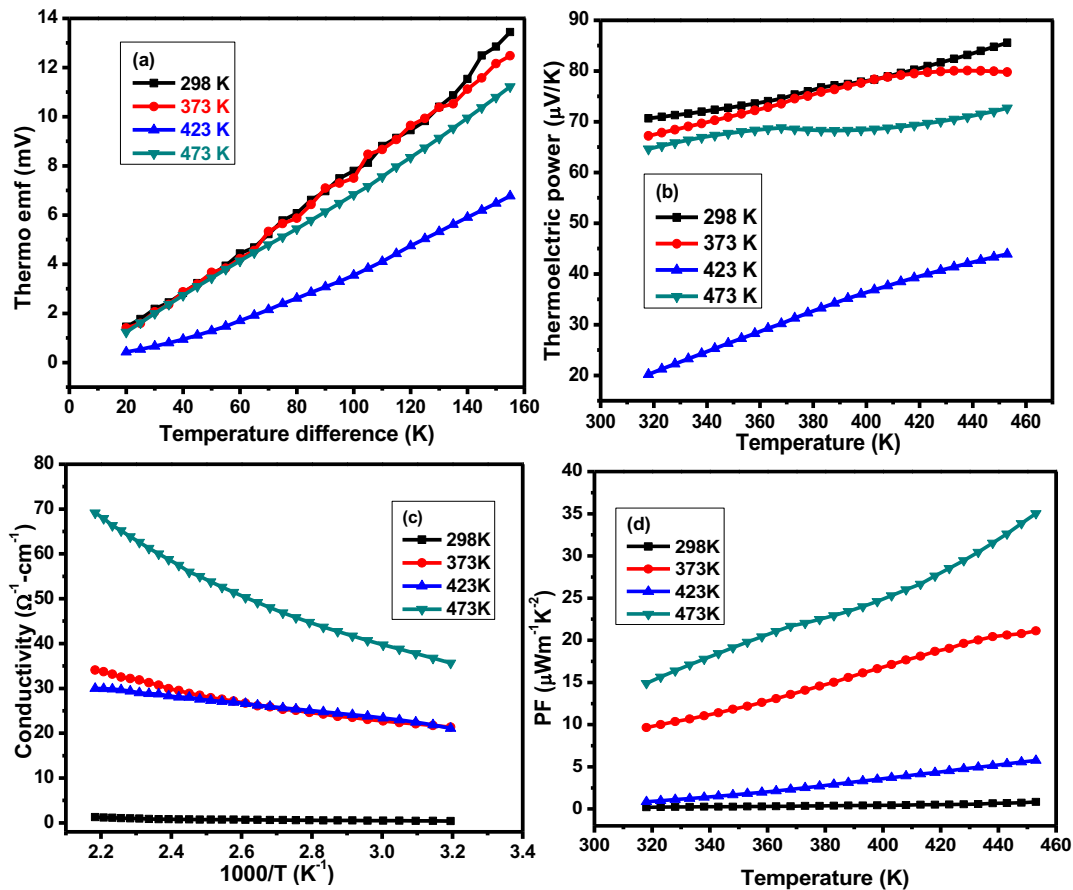


**Figure 4.28** (a). Thermo emf as a function of temperature difference, (b). Variation in thermoelectric power with temperature, (c). Temperature dependent conductivity and (d). Power factor as a function of temperature of InTe films deposited at different substrate temperature and annealed at 523 K for 1 h.



Figure 4.28(a) shows the variation in thermo emf of InTe films with temperature difference. The thermo emf of InTe films is linearly increased with an increase in temperature difference. The positive values of thermo emf indicate the p-type conductivity of annealed InTe films. The thermo emf values of InTe films deposited at 298 K and 373 K are almost same. Further, increase in substrate temperature leads in decrease of thermo emf generation up to 423 K deposited films and increased for 473 K deposited InTe films. Figure 4.28 (b) shows the thermoelectric power as a function of temperature. The thermoelectric power of InTe films is decreasing with an increase in substrate temperature up to 423 K and increased for 473 K deposited InTe films. These changes in thermo emf and thermoelectric power of InTe films may be due to the changes in structure as discussed based on FESEM images. However, the InTe films deposited at 298 K are showing higher thermoelectric power of  $70.71 \mu\text{VK}^{-1}$  at 320 K. The electrical conductivity as a function of inverse temperature of InTe films is depicted in figure 4.28 (c). As substrate temperature increases, the electrical conductivity of InTe films found to be decreased whereas, conductivity plots of InTe films deposited at 373 K and 423 K substrate temperature are merging at temperatures below 400 K and deviated at higher temperatures. Figure 4.28 (d) shows the variation in power factor as a function of temperature. Since the power factor is strong function of thermoelectric power and electrical conductivity, the InTe films deposited at 273 K and annealed at 523 K for 1 h are showing higher power factor which is around  $15.25 \mu\text{Wm}^{-1}\text{K}^{-2}$  at 320 K. Films deposited at substrate and annealing temperatures above 523 K were not studied in detailed as the characteristics did not lead of an improvement in the thermoelectric behavior of the films.

The effect of doping indium telluride films with various materials has been investigated in detail. Dopant atoms replace either of the elements in the compound depending on the valance of the dopant, the size of the ions interacting and the energies of such a replacement. This will lead to changes in the elemental, structural and thermoelectric properties of the films. Doping also results in the modification of the grain structure which in turn seriously affect the electrical conductivity of the films. Addition of dopant atoms may lead to an increase in electrical conductivity if the process results in the contribution of additional electrons or by way of changing the total grain boundary area.

Alternatively, the effect of the dopant may lead to addition of imperfections which might lead to a decrease in conductivity of the films. It is a considerable effect to analysis the effect in detail with the help of relevant experimental procedure to study the microstructure, conductivity, structure etc in detail.

Comprehensively, the doping of Bi, Sb<sub>2</sub>Te<sub>3</sub>, Al, Sb, Se and Te to In<sub>2</sub>Te<sub>3</sub> films resulted in the structural modifications such as involvement of additional phases, change in preferred orientation, peak shift, increase in grain area and grain size and change in grain orientation. These structural changes caused by dopants significantly affected the seebeck coefficient (or thermoelectric power) whereas marginally influenced the electrical conductivity of In<sub>2</sub>Te<sub>3</sub> films. However, among all dopants, Sb<sub>2</sub>Te<sub>3</sub> has shown more improvement in electrical conductivity (0.88 Ω<sup>-1</sup>cm<sup>-1</sup> to 8.47 Ω<sup>-1</sup>cm<sup>-1</sup>) whereas Sb doping significantly enhanced the seebeck coefficient of un-doped In<sub>2</sub>Te<sub>3</sub> films from 237 μVK<sup>-1</sup> to 477 μVK<sup>-1</sup> for 0.99 % of Sb doped In<sub>2</sub>Te<sub>3</sub> films (Sb-1) at 320 K. Finally, the product of seebeck coefficient and electrical conductivity is more for Se doped films (Se-2) which enhances the power factor of un-doped In<sub>2</sub>Te<sub>3</sub> films by 14 times.

## CHAPTER 5

### Si-In<sub>2</sub>Te<sub>3</sub> AND Si-InTe THIN FILM HETEROJUNCTIONS

*Overview:*

*This chapters describes a brief and conceptual importance of device building blocks, fabrication and temperature dependent I-V characteristics of both Si-In<sub>2</sub>Te<sub>3</sub> and Si-InTe heterojunction thin films. To define the performance of indium telluride heterojunction with Si, the interface properties such as rectification ratio, ideality factor and barrier height are estimated and reported.*

#### 5.1 Introduction

To implement any semiconductor in to a device, the interface properties has to be understood. There are four types of interfaces namely metal-semiconductor, metal oxide semiconductor, homo-junctions and heterojunction which in turn called as building blocks of solid-state devices. Metal-semiconductor interface is a familiar type which can be a rectifying contact or as ohmic contact. The rectifying contact controls the electric current flow in one direction whereas, the ohmic contact passes the current in either direction with negligible voltage drop across the interface. The metal oxide semiconductor structure is a combination of a metal-oxide and oxide-semiconductor interface. This structure is largely used as the gate in MOSFET which is a potential device for advanced integrated circuits. The homo-junction is an interface between two similar semiconductors with same band gap and having different doping profiles. In most of the practical applications, the homo-junction is made between p-type (acceptor doped) and n-type (donor doped) semiconductors such as Si. These homo junctions are widely used in p-n-p bipolar transistors and p-n-p-n switching devices like thyristor. The final type of interface is heterojunction, which is an interface formed between two dissimilar semiconductors. Heterojunctions are more efficient to pump carriers, hence they became key components for high-speed and photonic devices.

In order to utilize indium telluride in any solid-state devices, the electrical properties of interface have to be understood which can ensure the device performance. Aforementioned in literature survey, Dawar et al. (1982) are first to study the silver-sapphire-In<sub>2</sub>Te<sub>3</sub> thin films (Metal oxide semiconductor) and investigated the field effect transistor (FET) properties. Rousina and Shivakumar (1988 and 1989) investigated the interface properties of Al/Al<sub>2</sub>O<sub>3</sub>/n-InTe/Bi sandwich structures (metal-insulator-semiconductor) and Ni/p-InTe (metal-semiconductor) thin films. Desai et al. (2011) reported the interface properties of Al/p-In<sub>2</sub>Te<sub>3</sub> (metal-semiconductors) thin films. Most of the authors reported either metal-semiconductor or metal oxide semiconductor properties of indium telluride films. Since the heterojunctions are playing an efficient role in high speed solid state device applications which includes solar cells, transistors and semiconductor lasers, it is interesting to investigate the interface electrical properties of indium telluride heterojunction with other semiconductors. Hence to ensure the performance of indium telluride in interfaces of solid state devices, this chapter reports the interface properties such as ideality factor, barrier height and rectification ratio of n-Si/p-In<sub>2</sub>Te<sub>3</sub> and n-Si/p-InTe junctions using the temperature dependent I-V characteristic curves.

## **5.2 Si-In<sub>2</sub>Te<sub>3</sub> heterojunction**

### **5.2.1 Optimisation of growth conditions**

The p-type In<sub>2</sub>Te<sub>3</sub> thin films were thermally deposited on n-type Si (1 0 0) (Cubic crystalline with a  $\sim 5.4037 \text{ \AA}$ , and  $\rho \sim 10^{-1} \text{ \Omega cm}$ ) substrates using vacuum coating system. Prior to deposition, the Si wafers were thoroughly cleaned using diluted HF (1% concentration) which removes the oxide layer on the surface. The dimension of Si substrate was 0.05 cm x 1.5 cm x 1 cm (thickness x length x width), whereas the dimension of In<sub>2</sub>Te<sub>3</sub> thin film on Si was maintained to  $350 \times 10^{-7} \text{ cm} \times 0.5 \text{ cm} \times 0.5 \text{ cm}$ . The distance between evaporation source to substrate was maintained at 12 cm and deposition was carried out under the base pressure  $\sim 5 \times 10^{-6}$  torr. A molybdenum boat (200 A) was used to evaporate 99.999 % pure In<sub>2</sub>Te<sub>3</sub> pellets. The substrate temperature

and annealing temperature of the films were varied from 298 K to 473 K and 373 K to 573 K, respectively. To make the electrical contacts to Si-In<sub>2</sub>Te<sub>3</sub> heterojunction Ag (99.999 % pure) and Al (99.9995 % pure) were deposited on the heterojunction using thermal evaporation method. A computer-interfaced Keithley source meter (model-2400) was used for I-V measurements. The I-V characteristics of these heterojunction were measured in voltage range of +5V to -5V at different temperatures ranging from 303 K to 373 K. The pattern of the fabricated heterojunction is illustrated in figure 5.1.

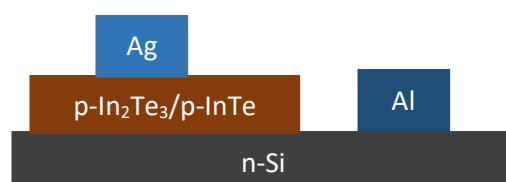


**Figure 5.1** Illustration of fabricated Si-In<sub>2</sub>Te<sub>3</sub> or Si-InTe heterojunction structure.

### 5.2.2 I-V-T characteristics of Si-In<sub>2</sub>Te<sub>3</sub> heterojunction

To study the interface properties of n-Si/p-In<sub>2</sub>Te<sub>3</sub> thin films, the films grown at 423 K and annealed films at 423 K for 1h were used. The substrate and annealing temperature of the films were optimised based on the quality and adhesion of the films on Si substrates. Beyond 423 K substrate temperature or 423 K annealing treatment, the films were found to be peeling off from the substrates due to large difference in lattice parameters (for In<sub>2</sub>Te<sub>3</sub> films a ~ 18.4860 Å and for Si a ~ 5.4037 Å).

**Table 5.1** Compositional analysis of In<sub>2</sub>Te<sub>3</sub> thin films on Si wafer

Sample conditions	Elemental composition (at %)	
	In	Te
As-deposited films at 423 K	45.0	55.0
Deposited at 423 K and annealed at 423 K for 1h	44.8	55.2

The interface properties of a material mainly depend on composition and structure. Hence, the prepared samples are subjected to both EDAX and XRD analysis. The EDAX revealed that the elemental composition of both as-deposited at 423 K and annealed at 423 K films are indium rich when compared with stoichiometric condition (In/Te: 2/3). The composition of both as-deposited and annealed films are summarised in table 5.1.

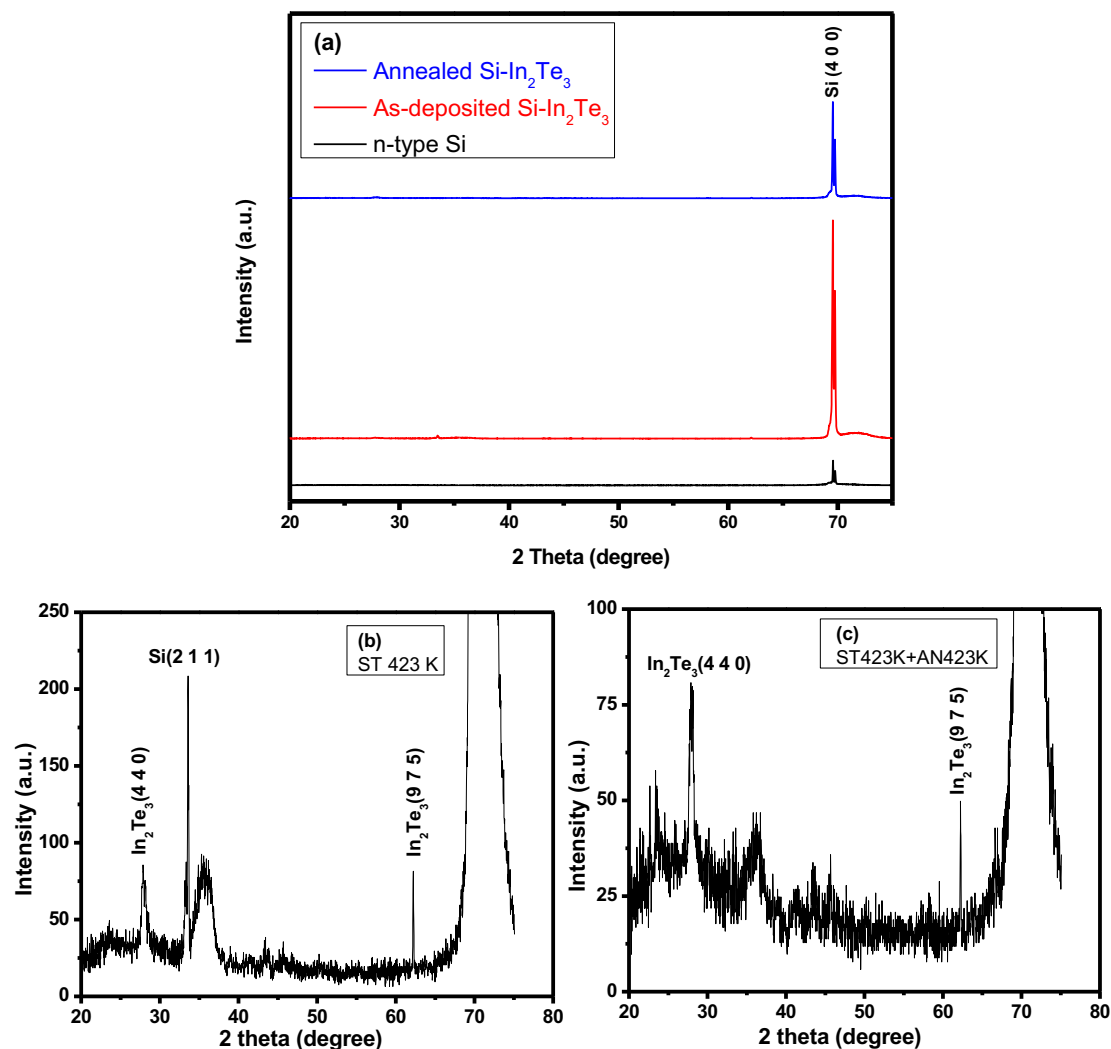
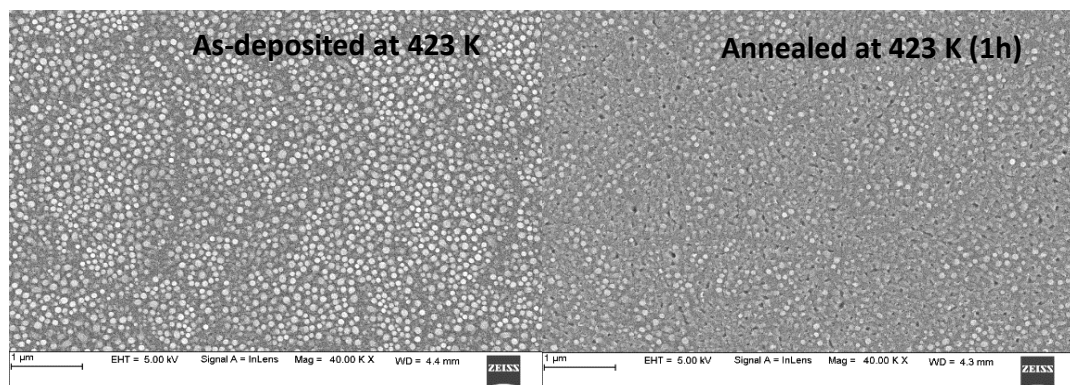


Figure 5.2. XRD patterns of n-Si/p-In<sub>2</sub>Te<sub>3</sub> thin films.

Figure 5.2 shows the XRD patterns of n-Si/p-In<sub>2</sub>Te<sub>3</sub> thin films. The XRD patterns of prepared junctions reveal the polycrystalline nature with prominent peak of Si (4 0 0). The peaks belong to cubic In<sub>2</sub>Te<sub>3</sub> are low in intensity compared with Si peaks which are indicated in figure 5.2 (b) and figure 5.2 (c). The XRD pattern of both as-deposited films at 423 K and post-annealed films at 423 K for 1 h are showing two peaks (4 4 0) and (9 7 5) corresponding to In<sub>2</sub>Te<sub>3</sub> material. The diffraction patterns of the films are indexed using cubic In<sub>2</sub>Te<sub>3</sub> (JCPDS No. 00-033-1488) and Si (JCPDS No. 00-005-0565) standard data. A peak shift is observed at  $2\theta$  of 27.28° to 27.70° in XRD patterns of both as-deposited and annealed films which might be due to the large difference in substrate to film lattice constants. The estimated lattice parameter of In<sub>2</sub>Te<sub>3</sub> films is calculated using equation 2.5 and found to be 18.2150 Å.



**Figure 5.3** FESEM images of n-Si/p-In<sub>2</sub>Te<sub>3</sub> thin film.

Figure 5.3 show the surface morphology of the Si/In<sub>2</sub>Te<sub>3</sub> thin films. The FESEM images show the granular arrangement of In<sub>2</sub>Te<sub>3</sub> on Si substrate. The grains are non-uniformly distributed in as-deposited films whereas, almost uniformly distributed in annealed films. The inter-grain gaps are originated among the grains of annealed films which were limited to top layer of the surface. Hence the continuity of films does not affect because of enough thickness (~ 350 nm) of the In<sub>2</sub>Te<sub>3</sub> films which contains many atomic layers.

There are many techniques proposed by many researchers to estimate the interface properties such as ideality factor ( $\eta$ ), rectification ratio (RR), barrier height ( $\phi_B$ ). Among those the temperature dependent I-V characteristics is a simple and efficient

method. The I-V characteristics of both as-deposited and annealed samples are taken at temperature varying from 303 K to 373 K. The temperature dependent I-V curves of n-Si/p-In<sub>2</sub>Te<sub>3</sub> junctions are depicted in figure 5.4 which are representing the typical rectification nature. Rectification ratio is the ratio between forward and reverse bias current at particular voltage which determines the efficiency of p-n junction to direct the current in one direction. The rectification ratio of Si/In<sub>2</sub>Te<sub>3</sub> diodes are determined at different voltages ( $\pm 0.5$ ,  $\pm 1$ ,  $\pm 2$ ,  $\pm 3$ ,  $\pm 4$  and  $\pm 5$  at room temperature) and the values are tabulated in table 5.2. The as-deposited Si/In<sub>2</sub>Te<sub>3</sub> diode is showing higher rectification ratio compared with annealed films. The higher RR of as-deposited Si/In<sub>2</sub>Te<sub>3</sub> diode is 61.2 at  $\pm 5$  V. The series resistance of the Si/In<sub>2</sub>Te<sub>3</sub> diodes are calculated from the linear portion of forward bias in higher voltage region which is found in the order of K $\Omega$  (0.82 – 0.75 K $\Omega$  for as-deposited films and 0.50 – 0.55 K $\Omega$  for annealed films).

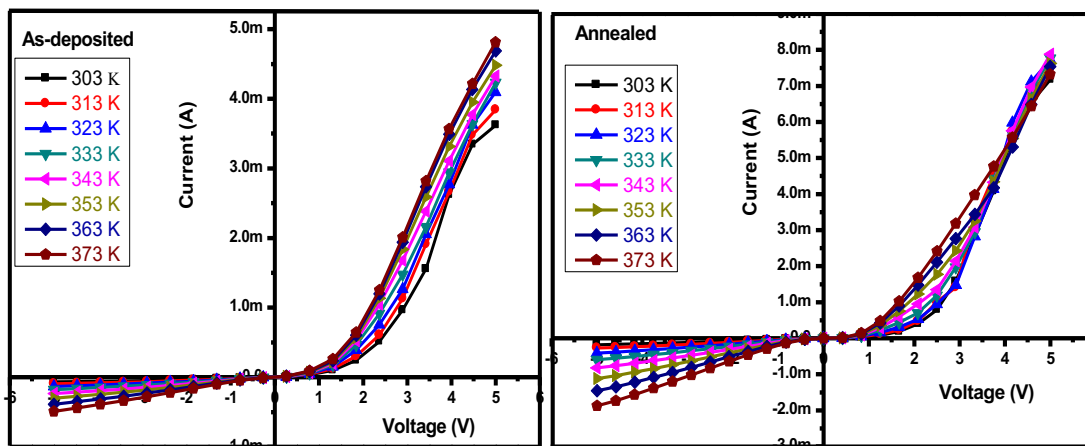


**Figure 5.4** I-V-T curve of n-Si/p-In<sub>2</sub>Te<sub>3</sub> thin films.

**Table 5.2** Rectification ratio of as-deposited and annealed Si/In<sub>2</sub>Te<sub>3</sub> heterojunction

Sample condition ↓	Rectification ratio					
	± 0.5	± 1	± 2	± 3	± 4	± 5
As-deposited at 423 K	1.11	1.65	11.35	25.27	46.46	61.20
Annealed at 423 K for 1 h	1.00	1.38	7.43	13.69	29.33	39.09



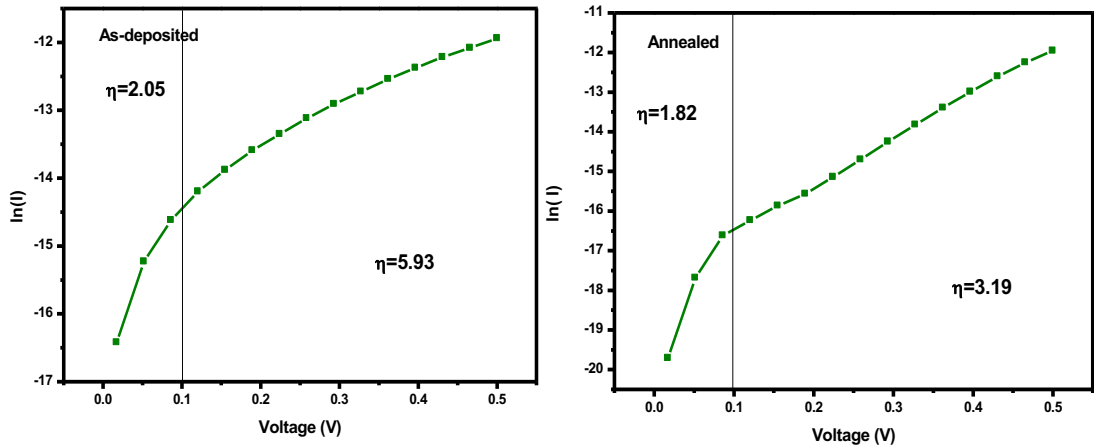


**Figure 5.5**  $\ln(I)$  versus voltage curve in forward bias at room temperature.

Ideality factor is an important parameter to define the uniformity of the diode in terms of deviation from unity (for ideal diode ideality factor  $\eta = 1$ ). To calculate the  $\eta$ ,  $\ln(I)$  as a function of voltage is depicted based on the equation (2.8) which is shown in figure 5.5. In both as-deposited and annealed diodes, two distinct slopes can be observed, below 0.1 V and beyond 0.1 V. For as-deposited films, below 0.1 V, the ideality factor  $\eta \approx 2$  indicating that the dominant conduction is due to trap-assisted generation-recombination current in the depletion region. Beyond 0.1 V, the  $\eta > 2$  represents the conduction due to high injection or inhomogeneities induced current. Whereas in annealed diodes,  $\eta \approx 2$  at voltage range below 0.1 V and  $\eta > 2$  which is combination of different conduction mechanisms as mentioned above. However, decrease in the ideality factor from as-deposited to annealed films is indicating that the annealing treatment is useful to reduce the voltage drop across the junction. In addition to this the presence of two different slopes in  $\ln(I)$  versus V plots indicates the possibility of other mechanisms in addition to thermionic conduction. Hence, I versus  $V^2$  graph is plotted to check the scope of space charge limited conduction (SCLC) mechanism ( $I = (AV^2N_c \mu \epsilon_0 \epsilon_r / 8L^3N_t) \exp(-E_t/kT)$ , hence,  $I \propto V^2$ ). Figure 5.6 shows the representative plots of current versus  $V^2$  at room temperature. The linear nature of these plots confirm the SCLC mechanism involved in the interface of Si and  $\text{In}_2\text{Te}_3$  junction.

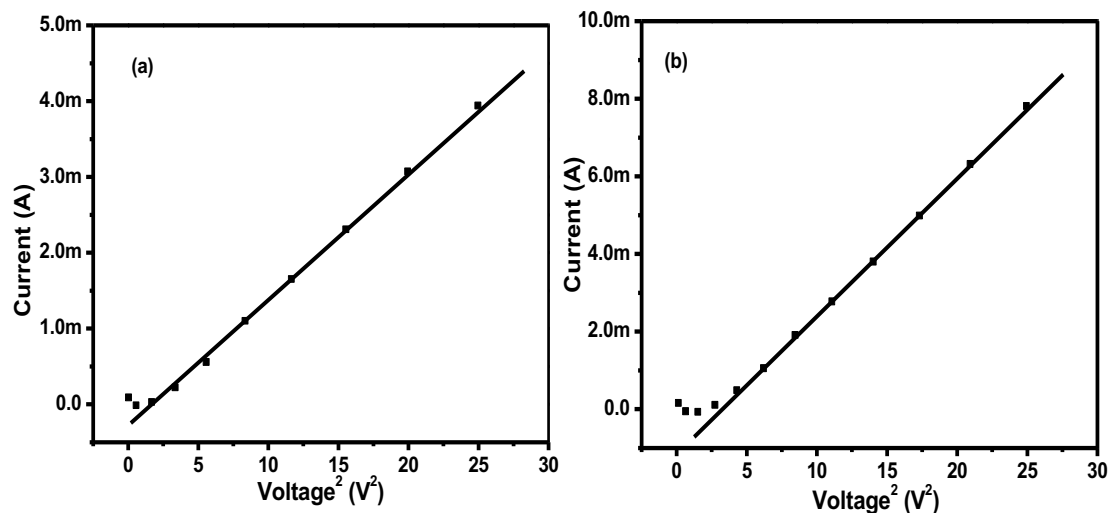


**Figure 5.6** The plots of current versus square of voltage at room temperature for (a). as-deposited and (b). annealed Si/In<sub>2</sub>Te<sub>3</sub> thin film diodes.

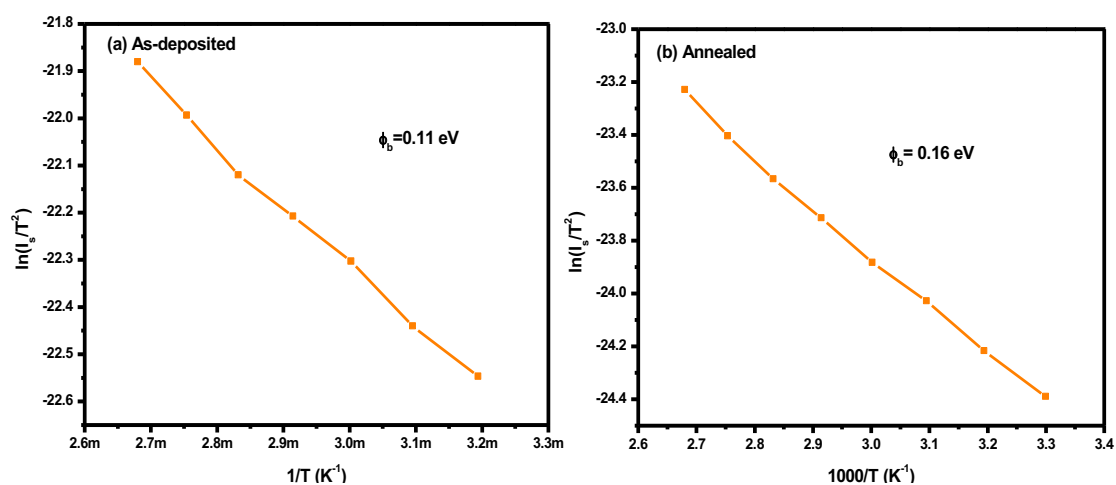


**Figure 5.7** Richardson plot of Si-In<sub>2</sub>Te<sub>3</sub> junction.

Figure 5.7 shows the Richardson plots of Si-In<sub>2</sub>Te<sub>3</sub> junction for both as-deposited and annealed samples. The reverse saturation current ( $I_s$ ) is estimated from the temperature dependent I-V plots and those values are used in Richardson plots. The barrier height offered by n-Si/p-In<sub>2</sub>Te<sub>3</sub> junction are determined from the slopes of figure 5.7 using equation 2.9. The barrier height of junction is found to be marginally increased by annealing treatment. The estimated barrier height of as-deposited films is 0.11 eV

whereas, 0.16 eV for annealed films at 423 K for 1h. However, the low values of (0.11 and 0.16 eV) barrier heights of both as-deposited and annealed Si/In<sub>2</sub>Te<sub>3</sub> allow for easy carrier transport across the barrier.

### **5.3 Si-InTe heterojunction**

#### **5.3.1 Optimisation of growth conditions**

The p-type InTe thin films were deposited on n-type Si (1 0 0) (Cubic crystalline with  $a \sim 5.4037 \text{ \AA}$ , and  $\rho \sim 10^{-1} \text{ \Omega cm}$ ) substrates using thermal evaporation method. The distance between evaporation source to substrate was fixed to 11 cm and deposition was carried out under the vacuum  $\sim 5 \times 10^{-5}$  torr. The pre-deposited Si substrates were cleaned with diluted HF (1% concentration) to remove the oxide layer on the surface. The Si substrate were used in the dimension of 0.05 cm x 1.5 cm x 1 cm (thickness x length x width), whereas the InTe thin film coated on Si in the dimension of  $300 \times 10^{-7}$  cm x 0.5 cm x 0.5 cm. A molybdenum boat (100 A) was used for evaporation and 52 A of current was passed through the boat to evaporate 99.999 % pure InTe pellets. The substrate temperature and annealing temperature of the films were varied from 298 K to 473 K and 373 K to 573 K, respectively. The electrical contacts, Ag (99.999 % pure) and Al (99.9995 % pure) were thermally deposited on Si/InTe heterojunction using thermal evaporation method. A computer interfaced Keithley source meter (model-2400) was used for I-V measurements. The I-V characteristics of these heterojunction were measured in voltage range of +5V to -5V at different temperatures ranging from 303 K to 373 K.

#### **5.3.2 I-V-T characteristics of Si-InTe heterojunction**

In order to grow InTe films on Si wafers, different substrate temperatures are applied ranging from 298 K to 523 K. It is observed that the films are peeling off from the substrate beyond 473 K. Hence the InTe films deposited at 473 K and annealed at 473 K for 1 h are used to study the junction properties.

The EDAX analysis revealed that indium composition decreases with annealing treatment. As-deposited InTe films on Si substrate are indium rich whereas, annealed films are nearly stoichiometric compared with stoichiometric ratio (In/Te =1). The composition of both as-deposited and annealed films are given in table 5.3.

**Table 5.3** Compositional analysis of InTe thin films on Si wafer

Sample conditions	Elemental composition (at %)	
	In	Te
As-deposited films at 473 K	54.8	45.2
Deposited at 473 K and annealed at 473 K for 1h	51.1	48.9

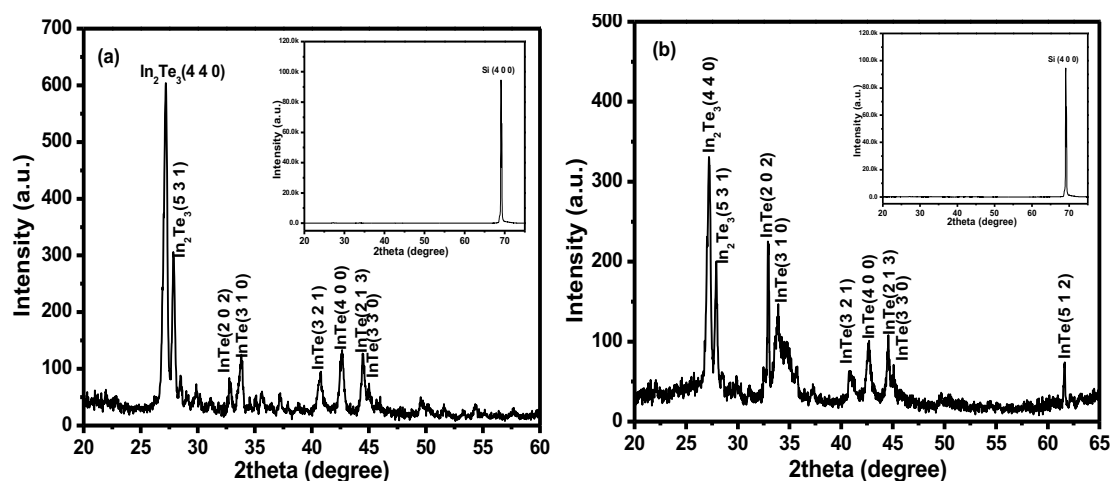


**Figure 5.8.** XRD patterns of (a). As-deposited at 473 K and (b). Annealed at 473 K for 1 h, n-Si/p-InTe thin films.

To verify the phase composition of Si/InTe films, the prepared films are subjected to XRD analysis. Figure 5.8 show the XRD patterns of both as-deposited (at 473 K) and annealed Si/InTe films. Both as-deposited and annealed films are polycrystalline in nature and predominantly oriented along Si (4 0 0) direction which can be seen in inserted figures in figure 5.8 (a) and (b). The peaks regarding cubic  $\text{In}_2\text{Te}_3$  and tetragonal InTe are found at lower intensities. Both as-deposited and annealed films are exhibiting the mixed phase of  $\text{In}_2\text{Te}_3$  and InTe with (4 4 0), (5 3 1) planes from  $\text{In}_2\text{Te}_3$

and (2 0 2), (3 1 0), (3 2 1), (4 0 0), (2 1 3), (3 3 0) planes from InTe. The peak intensity of InTe phase is increased in annealed films when compared with as-deposited films.

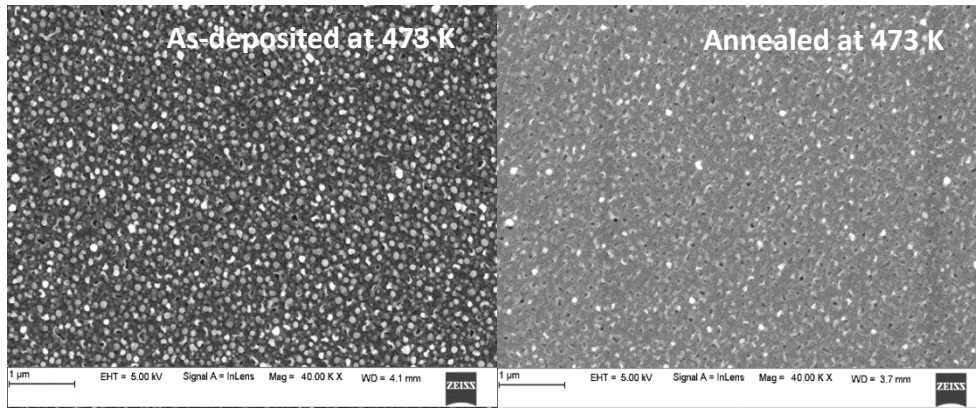


**Figure 5.9** FESEM images of n-Si/p-InTe thin film.

Figure 5.9 show the FESEM micrographs of as-deposited and annealed Si/InTe heterojunctions. Both as-deposited and annealed samples are showing granular structure and grains are uniformly distributed throughout the surface. In annealed samples few inter-grain gaps are appearing which might be due to annealing treatment. Since the InTe film thickness is  $\sim 350$  nm, the inter-grain gaps are not affecting the film continuity.

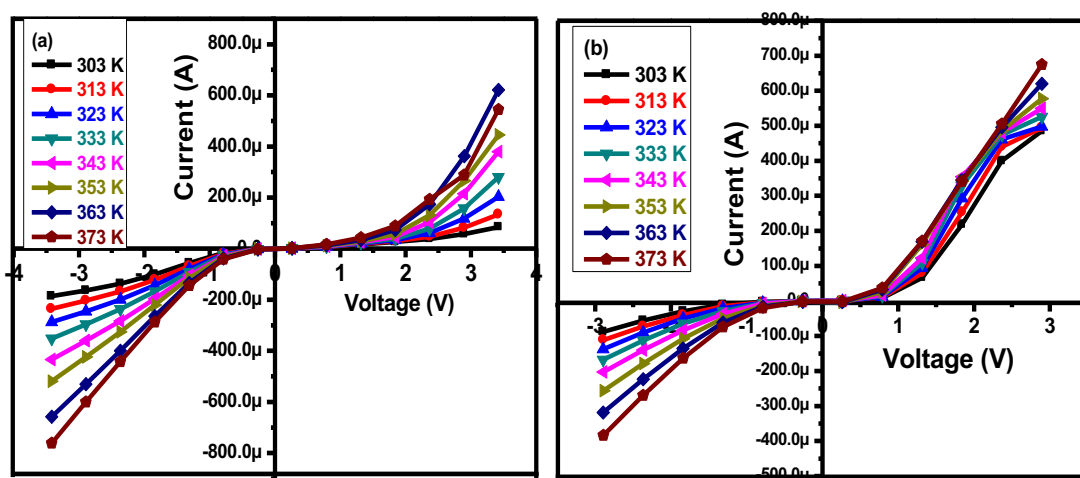


**Figure 5.10** Temperature dependent I-V curve of (a). as-deposited and (b). annealed n-Si/p-InTe thin films.

Figure 5.10 show the I-V characteristic curves of both as deposited and annealed Si/InTe heterojunction. The rectification behaviour of Si/InTe heterojunction can be seen in figure 5.10. The rectification ratio of Si/InTe diodes are determined at different voltages ranging from  $\pm 0.5$  V to  $\pm 3$  V and values are tabulated in table 5.4. The Si/InTe heterojunction prepared at 473 K substrate temperature and annealed at 473 K for 1 h shown higher rectification ratio of 3.85 at  $\pm 3$  V, compared with as-deposited Si/InTe junction prepared at 473 K substrate temperature. The series resistance of the heterojunctions is estimated from the linear portion of forward bias I-V curves and found to be in 72-22 K $\Omega$  for both as-deposited and annealed samples.

**Table 5.4** Rectification ratio of as-deposited and annealed Si/InTe heterojunction

Sample condition ↓	Rectification ratio			
	± 0.5	± 1	± 2	± 3
As-deposited at 473 K	0.09	0.25	0.29	0.37
Annealed at 473 K for 1 h	1.6	3.11	6.28	3.85

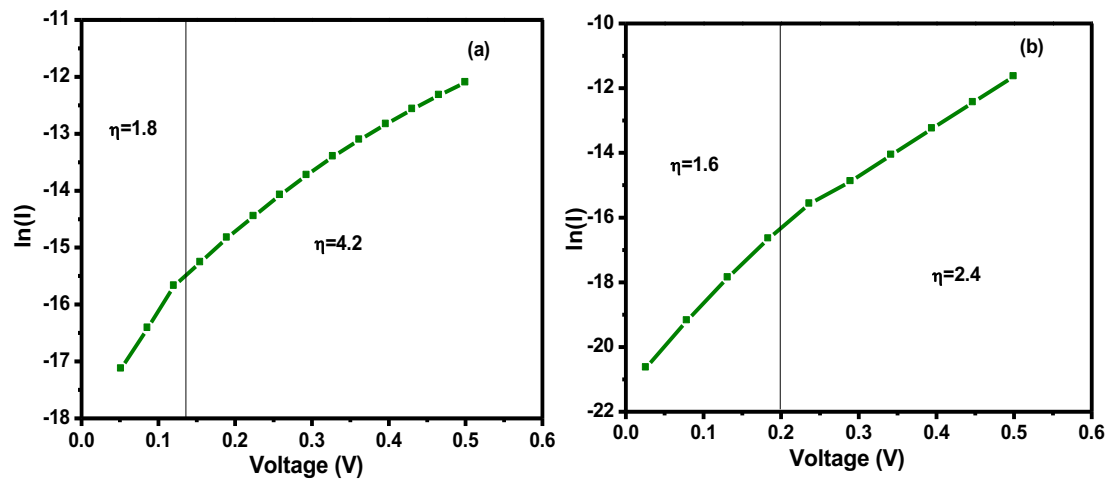


**Figure 5.11**  $\ln(I)$  versus voltage curve of (a). as-deposited at 473 K and (b). annealed at 473 K for 1 h in forward bias at room temperature.

To analyse the conduction mechanism involved in the Si/InTe heterojunction,  $\ln(I)$  versus voltage plot is depicted as shown in figure 5.11. The ideality factor can be estimate from the slope of figure 5.11 using equation 2.8. The junction prepared at 473 K substrate temperature is showing two different slopes. Aforementioned,  $\eta \approx 1$  is an

indication of ideal diode nature and  $\eta$  changes from 1 to 2 if the density of recombination increases.  $\eta \approx 2$  is an indication of trap-assisted recombination and  $\eta > 2$  represents the high injection current. The Si/InTe junction prepared at 473 K substrate temperature are showing  $\eta \approx 1.8$  at the voltage below 0.15 V and  $\eta \approx 4.2$  in the voltage range above 0.15 V, whereas the junction annealed at 473 K are showing  $\eta \approx 1.6$  below 0.2 V and  $\eta \approx 2.4$  above 0.2 V. In order to verify the presence of space charge limited conduction mechanism (SCLC), the current plotted as a function of square of voltage using the proportionality relation between I and  $V^2$  in SCLC. Figure 5.12 shows the current as a function of  $V^2$  in forward bias which is linear in nature and confirms the presence of SCLC in addition to thermionic emission.

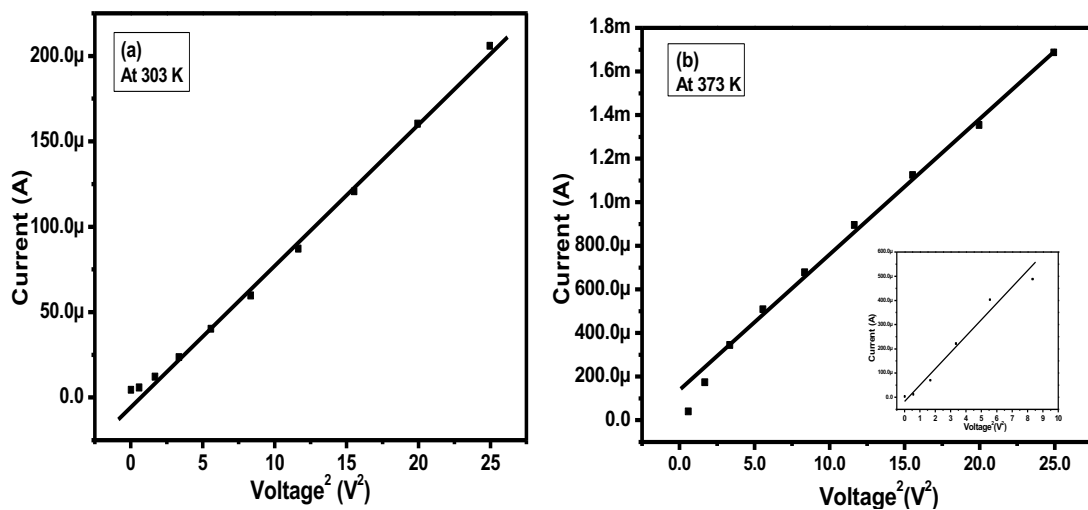


**Figure 5.12** Current as a function of square of voltage at (a) 303 K and (b) 373 K of (a). As-deposited and (b). annealed Si/InTe diodes.

Figure 5.13 show the Richardson plot of Si-InTe heterojunction for both as-deposited and annealed samples. The I-V plots are used to determine reverse saturation current ( $I_s$ ) and those values are used in Richardson plots. The barrier height of n-Si/p-InTe heterojunction are calculated from the slopes of figure 5.13 using equation 2.9. The barrier height of heterojunction was found to be marginally increased by annealing treatment. The barrier height of as-deposited Si/InTe junction is 0.10 eV whereas, 0.17 eV for annealed condition at 473 K for 1h. However, the Si/In<sub>2</sub>Te<sub>3</sub> heterojunction is

showing the better rectification behaviour when compared with Si/InTe heterojunctions.

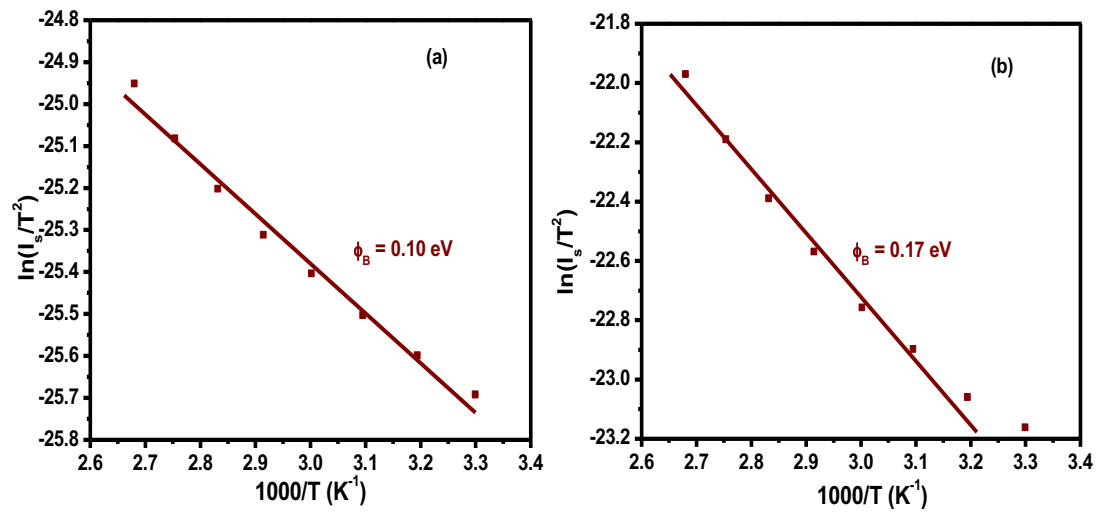


**Figure 5.13** Richardson plot of (a). as-deposited at 473 K and (b). annealed at 473 K for 1 h of Si-InTe junction.



## CHAPTER 6

### SUMMARY AND CONCLUSIONS

*Overview:*

*This chapter deals with the summary of work reported in thesis and conclusions drawn from results of investigations. Scope for the future work is also discussed.*

#### **6.1 Summary of the present work**

The research work presented in this thesis is broadly classified into six chapters with several sub-divisions in each chapter. The first chapter covers a brief introduction to various topics namely thin film technology, III-VI compound semiconductor and indium telluride thin films. The literature survey on indium telluride thin films, scope and objectives of the work have been reported. In second chapter, the details of experimental methods and characterisation techniques are mentioned. The third chapter deals with the detailed information about preparation of stoichiometric  $\text{In}_2\text{Te}_3$  and  $\text{InTe}$  thin films using thermal evaporation method and also discussed about structural, electrical and optical properties of these films. Fourth chapter describes about the thermoelectric properties of un-doped, doped  $\text{In}_2\text{Te}_3$  and  $\text{InTe}$  thin films and fifth chapter explains the junction properties of both n-Si/p- $\text{In}_2\text{Te}_3$  and n-Si/p- $\text{InTe}$  heterojunctions. Finally, the sixth chapter contains the summary of work reported in thesis and conclusions drawn from investigations.

#### **6.2 Conclusions**

##### **6.2.1 Stoichiometric and mono-phased indium telluride thin films**

$\text{In}_2\text{Te}_3$  thin films:

The optimized annealing temperature to obtain pure, mono-phased and stoichiometric  $\text{In}_2\text{Te}_3$  films was found to be 573 K for a duration of 1 h irrespective of applied substrate temperature.

1. All prepared films were polycrystalline with cubic  $\alpha$ - $\text{In}_2\text{Te}_3$  structure. The grain size of annealed films was found to increase with an increase in substrate temperature.
2. The electrical properties of the films revealed the p-type conductivity which is of the order of  $10^{-1} \Omega^{-1}\text{cm}^{-1}$  and thermal activation energy of the films was  $0.01 \pm 0.005$  eV irrespective of substrate temperature.
3. The optical band gap of the films was  $0.99 \pm 0.02$  eV irrespective of applied substrate temperature.  $\text{In}_2\text{Te}_3$  films have higher absorption coefficient of the order of  $10^5 \text{cm}^{-1}$ . The optical transmittance of the films was found to be 90% in IR region.

#### InTe thin films:

The InTe films deposited at 473 K and annealed at 523 K for 1h were found to be stoichiometric and mono-phased.

1. The annealing of as-deposited films resulted in the structural transformation from mixed phase of cubic  $\text{In}_2\text{Te}_3$  and tetragonal InTe to mono-phase of tetragonal InTe.
2. The InTe films have p-type conductivity which is of the order of  $10^1 \Omega^{-1} \text{cm}^{-1}$  and activation energy of these films was found to be  $0.05 \pm 0.03$  eV.
3. An optical band gap of the films was found to be decreased from 1.61 eV to 1.42 eV with an increase in the substrate temperature from 298 K to 473 K. The absorption co-efficient of all the films was found in the order of  $10^6 \text{cm}^{-1}$ .

The electrical properties accompanied with optical properties of  $\text{In}_2\text{Te}_3$  and InTe films makes them suitable for absorbent layer in photovoltaic cells.

### **6.2.2 Thermoelectric properties of indium telluride thin films**

#### Un-doped $\text{In}_2\text{Te}_3$ thin films:

The growth conditions to enhance the thermoelectric properties of  $\text{In}_2\text{Te}_3$  films were done based on the maximum seebeck coefficient. In this study, the thermoelectric properties of  $\text{In}_2\text{Te}_3$  films were investigated by tailoring the substrate temperature and film thickness.

1. At constant thickness of 350 nm, the thermoelectric power was maximum for films deposited at 423 K substrate temperature and corresponding power factor of these films was  $4.93 \mu\text{Wm}^{-1}\text{K}^{-1}$  at 320 K and  $24 \mu\text{Wm}^{-1}\text{K}^{-1}$  at 450 K.
2. At constant substrate temperature of 423 K, the power factor was found to decrease with an increase in film thickness and films with 150 nm thickness showed higher power factor of  $27 \mu\text{W m}^{-1} \text{K}^{-2}$  at 450 K.

#### Doped $\text{In}_2\text{Te}_3$ thin films:

The doping of  $\text{In}_2\text{Te}_3$  brought many changes in the structural properties of films which significantly affected the thermoelectric power and marginally influenced electrical conductivity of prepared films.

1. *Bi doped  $\text{In}_2\text{Te}_3$  films:* Bi-2 films are showing maximum electrical conductivity of  $3.72 \Omega^{-1} \text{cm}^{-1}$ . The thermoelectric power and power factor of the films were decreased with an increase in Bi percentage. Bi-1 films showed the maximum power factor of  $23.89 \mu\text{Wm}^{-1}\text{K}^{-2}$  which was improved by 4.8 times of un-doped  $\text{In}_2\text{Te}_3$  films.
2.  *$\text{Sb}_2\text{Te}_3$  doped  $\text{In}_2\text{Te}_3$  films:* The electrical conductivity of the films was marginally decreased with an increase in doping concentration and maximum for  $\text{Sb}_2\text{Te}_3$ -1 films which was  $8.47 \Omega^{-1}\text{cm}^{-1}$ . As doping concentration increases, the thermoelectric power and power factor of the films decreases. However,  $\text{Sb}_2\text{Te}_3$ -1 films showed maximum power factor of  $60.04 \mu\text{Wm}^{-1}\text{K}^{-2}$  which was enhanced by 12.2 times of un-doped  $\text{In}_2\text{Te}_3$  films.
3.  *$\text{Sb}_2\text{Te}_3$  alloyed  $\text{In}_2\text{Te}_3$  films:* The electrical conductivity of these films gradually increased with an increase in  $\text{Sb}_2\text{Te}_3$  percentage. The seebeck co-efficient and power factor were found maximum for 25% of  $\text{Sb}_2\text{Te}_3$  alloyed  $\text{In}_2\text{Te}_3$  films. The power factor of 25%  $\text{Sb}_2\text{Te}_3$  alloyed  $\text{In}_2\text{Te}_3$  films was  $58.57 \mu\text{Wm}^{-1}\text{K}^{-2}$  which was enhanced by 11.9 times of un-doped films.
4. *Al doped  $\text{In}_2\text{Te}_3$  films:* The electrical conductivity of Al doped films was found maximum for Al-2 films which was  $1.04 \Omega^{-1}\text{cm}^{-1}$ . Higher seebeck coefficient and power factor has been seen for Al-2 films. The power factor of Al-2 films was  $15.41 \mu\text{Wm}^{-1}\text{K}^{-2}$  which improved the power factor of  $\text{In}_2\text{Te}_3$  films by 3.1 times.

5. *Sb doped In<sub>2</sub>Te<sub>3</sub> films*: The maximum electrical conductivity of Sb doped In<sub>2</sub>Te<sub>3</sub> films was found maximum for Sb-4 which was 2.24  $\Omega^{-1}\text{cm}^{-1}$ . The thermoelectric power was more for Sb-1 films and further increase in Sb dopant percentage (Sb-2, Sb-3, and Sb-4) resulted in a decrease of thermoelectric power. The maximum thermoelectric power and power factor were observed for Sb-1 films. The power factor of Sb-1 films was 44  $\mu\text{Wm}^{-1}\text{K}^{-2}$  which was improved by 8.9 times than that of un-doped In<sub>2</sub>Te<sub>3</sub> films.
6. *Se doped In<sub>2</sub>Te<sub>3</sub> films*: The electrical conductivity of Se doped In<sub>2</sub>Te<sub>3</sub> films was maximum for Se-2 films which was 5.57  $\Omega^{-1}\text{cm}^{-1}$ . The maximum thermoelectric power was observed in Se-2 which showed  $\sim 350 \mu\text{VK}^{-1}$  at 320 K. Power factor of Se-2 films was 68.8  $\mu\text{Wm}^{-1}\text{K}^{-2}$  and enhanced by 14 times of un-doped In<sub>2</sub>Te<sub>3</sub> films.
7. *Te doped In<sub>2</sub>Te<sub>3</sub> films*: The electrical conductivity of Te doped films was maximum for Te-3 films which was 6.28  $\Omega^{-1}\text{cm}^{-1}$  at 320 K. The maximum thermoelectric power and power factor were shown by Te-2 films. The power factor of Te-2 films was 36.89  $\mu\text{Wm}^{-1}\text{K}^{-2}$  which was 7.5 times greater than that of un-doped In<sub>2</sub>Te<sub>3</sub> films.

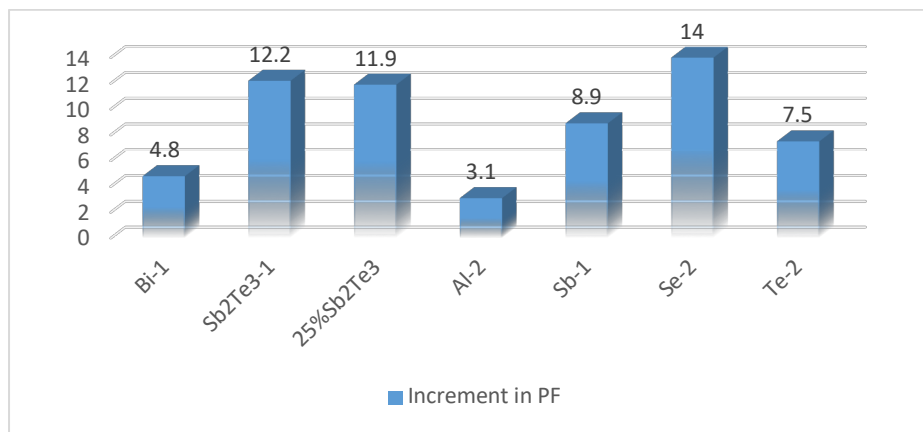


**Figure 6.1** Statistics of improvement in power factor of doped In<sub>2</sub>Te<sub>3</sub> films.

Among all dopants, Se doping enhanced the power factor of In<sub>2</sub>Te<sub>3</sub> films by 14 times which in turn was 4.7 times greater than Sb<sub>2</sub>Te<sub>3</sub> films (commercial thermoelectric material) prepared at same growth conditions.

#### Thermoelectric properties of InTe thin films:

1. The thermoelectric power of InTe films was found maximum for the films deposited at 298 K and annealed at 523 K for 1 h.
2. The electrical conductivity of InTe films increased with an increase substrate temperature.
3. The maximum power factor shown by the films deposited at 473 K and annealed at 523 K for 1 h was  $15.25 \mu\text{Wm}^{-1}\text{K}^{-2}$  at 320 K.

The  $\text{In}_2\text{Te}_3$  films are showing good thermoelectric properties when compared with InTe thin films.

#### **6.2.3 Junction properties of Si-Indium telluride interface**

##### n-Si/p- $\text{In}_2\text{Te}_3$ heterojunction:

1. Si/ $\text{In}_2\text{Te}_3$  heterojunction was polycrystalline in nature with cubic  $\text{In}_2\text{Te}_3$  peaks at lower intensity compared with Si peaks.
2. The as-deposited Si/ $\text{In}_2\text{Te}_3$  diode prepared at 423 K substrate temperature is showing higher rectification ratio of 61.2 at  $\pm 5$  V.
3. The series resistance of Si/ $\text{In}_2\text{Te}_3$  diodes was found in the order of  $\text{K}\Omega$ .
4. The barrier height of junction was found to be marginally increased by annealing treatment. The barrier height of as-deposited films at 423 K was 0.11 eV whereas, 0.16 eV for annealed films at 423 K for 1h.

##### n-Si/p-InTe heterojunction:

1. Si/InTe heterojunctions were polycrystalline in nature and exhibited the mixed phase of  $\text{In}_2\text{Te}_3$  and InTe.
2. The Si/InTe heterojunction prepared at 473 K substrate temperature and annealed at 473 K for 1 h showed higher rectification ratio of 3.85 at  $\pm 3$  V compared with as-deposited Si/InTe junction prepared at 473 K substrate temperature.
3. The series resistance of heterojunctions was found in the range of 72-22  $\text{K}\Omega$  for both as-deposited and annealed samples.

4. The barrier height of heterojunction was found to be marginally increased by annealing treatment. The barrier height of as-deposited Si/InTe junction was 0.10 eV whereas, 0.17 eV for annealed films at 473 K for 1h.

The Si/In<sub>2</sub>Te<sub>3</sub> films are showing good rectification behaviour and device quality compared with Si/InTe films.

### **6.3 Scope for future work**

In this investigation, we proposed the optimization and characterization of both In<sub>2</sub>Te<sub>3</sub> and InTe films up to the extent of device quality. Hence there is a scope to implement these materials in solar cells and can check efficiency of those devices.

To make use of un-doped and doped In<sub>2</sub>Te<sub>3</sub> films in thermoelectric applications, thermal conductivity is one of the impending factor along with power factor. Due to the presence of stoichiometric defects in indium telluride, the thermal conductivity of these films is expected to decrease in huge amount which in turn increase the figure of merit of device. Hence conversion efficiency of the device can be estimated using the derived values of power factor reported in this thesis as well as value of thermal conductivity. In this investigation, we used thermal evaporation method to enhance thermoelectric power. Other methods which can create more asymmetry in band structure can also be utilised to enhance the seebeck coefficient.

In this investigation, we reported heterojunction properties of indium telluride thin films with silicon which showed a moderate rectification ratio with low barrier heights. Hence, there is scope to fabricate more effective heterojunctions of indium telluride with other efficient n-type compound semiconductors.

## REFERENCES

- Afifi, M. A., Hegab, N. A., and Bekheet, A. E. (1996). "The switching phenomenon in amorphous  $\text{In}_2\text{Te}_3$  thin films." *Vacuum.*, 43(3), 265-269.
- Afifi, M.A., Abd El-Wahabb, E., Bekheet, A. E., and Atyia, H. E. (2000). "Effect of annealing on AC conductivity and the dielectric properties of  $\text{In}_2\text{Te}_3$  thin films, *Acta Phys. Pol. A.*, 98(4), 401-409.
- Aly, K. A., Dahshan, A., Abbady, G., and Saddeek, Y. (2016). "Electrical and thermoelectric properties of different compositions of Ge-Se-In thin films." *Phys. B Condens. Matter.*, 497, 1-7.
- Anwar, S., Gowthamaraju, S., Mishra, B. K., Singh, S. K., and Anwar, S. (2015). "Spray pyrolysis deposited tin selenide thin films for thermoelectric applications." *Mater. Chem. Phys.*, 153, 236-242.
- Arab, A., and Li, Q. (2015). "Anisotropic thermoelectric behavior in armchair and zigzag mono-and fewlayer  $\text{MoS}_2$  in thermoelectric generator applications." *Sci. Rep.*, 5, 13706.
- Balitskii, O. A., and Jaegermann, W. (2006). "XPS study of  $\text{InTe}$  and  $\text{GaTe}$  single crystals oxidation." *Mater. Chem. Phys.*, 97, 98-101.
- Boschker, J. E., Boniardi, M., Redaelli, A., Riechert, H., and Calarco, R. (2015). "Electrical performance of phase change memory cells with  $\text{Ge}_3\text{Sb}_2\text{Te}_6$  deposited by molecular beam epitaxy." *Appl. Phys. Lett.*, 106, 023117.
- Budnik, A. V., Rogacheva, E. I., Pinegin, V. I., Sipatov, A. Y., and Fedorov, A. G. (2013). "Effect of initial bulk material composition on thermoelectric properties of  $\text{Bi}_2\text{Te}_3$  thin films." *J. Electron. Mater.*, 42(7), 1324-1329.
- Bulman, G., Barletta, P., Lewis, J., Baldasaro, N., Manno, M., Bar-Cohen, A., and Yang, B. (2016). "Superlattice-based thin-film thermoelectric modules with high cooling fluxes." *Nat. Commun.*, 7, 10302.
- Cao, X.-H., Zhou, W.-X., Chen, C.-Y., Tang, L.-M., Long, M., and Chen, K.-Q. (2017).

“Excellent thermoelectric properties induced by different contact geometries in phenalenyl-based single-molecule devices.” *Sci. Rep.*, 7(1), 10842.

Chen, Z. G., Hana, G., Yanga, L., Cheng, L., and Zou, J. (2012). “Nanostructured thermoelectric materials: Current research and future challenge.” *Prog. Nat. Sci. Mater. Int.*, 22(6), 535–549.

Cui, J. L., Xue, H. F., Xiu, W. J., Mao, L. D., Ying, P. Z., and Jiang, L. (2008). “Crystal structure analysis and thermoelectric properties of p-type pseudo-binary  $(\text{Al}_2\text{Te}_3)_x(\text{Bi}_{0.5}\text{Sb}_{1.5}\text{Te}_3)_{1-x}$  ( $x = 0\sim 0.2$ ) alloys prepared by spark plasma sintering.” *J. Alloys Compd.*, 460(1–2), 426–431.

Dawar, A. L., Kumae, A., Taneja, O. P., Kumar, P., and Mathur, P. C. (1982). “Field effect studies in  $\text{In}_2\text{Te}_3$  metal-insulator-semiconductor structure.” *Phys. Stat. Sol.*, 74, 403-409.

Desai, R. R., Lakshminarayana, D., Patel, P. B., and Panchal, C. J. (2005a). “Indium sesquiterelluride ( $\text{In}_2\text{Te}_3$ ) thin film gas sensor for detection of carbon dioxide.” *Sensors Actuators B*, 107, 523–527.

Desai, R. R., Lakshminarayana, D., Patel, P. B., and Panchal, C. J. (2005b). “Indium sesquiterelluride ( $\text{In}_2\text{Te}_3$ ) thin film strain gauge.” *Sensors Actuators, A Phys.*, 121, 405-409.

Desai, R. R., Lakshminarayana, D., Patel, P. B., Patel, P. K., and Panchal, C. J. (2005c). “Growth and structural properties of indium sesquiterelluride ( $\text{In}_2\text{Te}_3$ ) thin films.” *Mater. Chem. Phys.*, 94, 308–314.

El-Sayed, K., Sedeek, K., Heiba, Z. K., and Hantour, H. H. (2013a). “Microstructures, magnetic and electric properties of diluted magnetic semiconductors  $\text{InTe}_{1-x}\text{Fe}_x(\text{Co}_x)$ .” *Mater. Res. Bull.*, 48(6), 2383–2389.

Emziane, M., Ade, J. C. B., Ouerfelli, J., Essaidi, H., and Barreau, A. (1999). “A novel method for preparing  $\alpha\text{-In}_2\text{Te}_3$  polycrystalline thin films.” *Mater. Phys. Chem.*, 61, 229-236.

Faita, F. L., Ersching, K., Ac Na, J. J. S., Campos, C. E. M., and Pizani, P. S. (2011).



- “Structure and microstructure of  $\text{In}_4\text{Te}_3$  nanopowders prepared by solid state reaction.” *Mater. Chem. Phys.*, 130, 1361–1365.
- Fu, H., Ying, P. Z., Cui, J. L., Yan, Y. M., and Zhang, X. J. (2010). “Vacancy phonon scattering and thermoelectric properties in  $\text{In}_2\text{Te}_3$ – $\text{SnTe}$  Compounds.” *Mater. Sci. Forum*, 650, 126–131.
- Golding, T. D., Boyd, P. R., Martinka, M., Amirtharaj, P. M., Dinan, J. H., Qadri, S. B., Zahn, D. R. T., and Whitehouse, C. R. (1989). “Molecular-beam-epitaxial growth and characterization of  $\text{In}_2\text{Te}_3$ .” *J. Appl. Phys.*, 65, 1936-1941.
- Grochowski, E. G., Mason, D. R., Schmitt, G. A., and Smith, P. H. (1964). “The phase diagram for the binary system indium-tellurium and electrical properties of  $\text{In}_3\text{Te}_5$ .” *J. Phys. Chem. Solids*, 25(6), 551–558.
- Guettari, N., Amory, C., Morsli, M., Bernede, J. C., and Khelil, A. (2003). “ $\text{In}_x\text{Te}_y$  semiconductor thin films obtained by co-evaporation.” *Thin Solid Films*, 431-432, 497-501.
- Gui, Y. Q., Zheng, Y. S., Liu, F. S., Zhang, S. L., Ao, W. Q., Li, Y., and Li, J. Q. (2016). “Effect of Na and Ba co-doping on the structure and thermoelectric performance of  $\text{PbTe}_{0.5}\text{Se}_{0.5}$ .” *Scr. Mater.*, 120, 9-13.
- Han, C., Sun, Q., Li, Z., and Dou, S. X. (2016). “Thermoelectric enhancement of different kinds of metal chalcogenides.” *Adv. Energy Mater.*, 1600498, 1-36.
- Haras, M., Lacatena, V., Monfray, S., Robillard, J. F., Skotnicki, T., and Dubois, E. (2014). “Unconventional thin-film thermoelectric converters: Structure, simulation, and comparative study.” *J. Electron. Mater.*, 43(6), 2109–2114.
- Hatsuta, N., Takemori, D., and Takashiri, M. (2016). “Effect of thermal annealing on the structural and thermoelectric properties of electrodeposited antimony telluride thin films.” *J. Alloys Compd.*, 685, 147-152.
- Hegab, N. A., Afifi, M. A., El-shaz Ly, A. E., and Bekheet, A. E. (1998a). “Effect of annealing on the structural and electrical properties of  $\text{In}_2\text{Te}_3$ .” *J. Mater. Sci.*, 33, 2441–2445.

- Hegab, N. A., Bekheet, A. E., Afifi, M. A., and El-Shazly, A. A. (1998b). "Effect of annealing on the optical properties of  $\text{In}_2\text{Te}_3$  thin films." *Appl. Phys A. Mater. Sci. Process.*, 66, 235–240.
- Hossain, M. S., Islam, R., Shahjahan, M., and Khan, K. A. (2008). "Studies on the thermoelectric effect in semiconducting ZnTe thin films." *J. Mater. Sci. Mater. Electron.*, 19, 1114-1121.
- Hromadko, L., Prikryl, J., Strizik, L., Kost Al, P., Benes, L., and Frumar, M. (2014). "Physico-chemical properties of Sb-rich (Sb, In)-Te thin films." *J. Alloys Compd.*, 617, 306–309.
- Hwang, I., Cho, Y. J., Lee, M. J., and Jo, M. H. (2015). "The role of contact resistance in GeTe and  $\text{Ge}_2\text{Sb}_2\text{Te}_5$  nanowire phase change memory reset switching current." *Appl. Phys. Lett.*, 106, 193106.
- Jantrasee, S., Moontragoon, P., and Pinitsoontorn, S. (2016). "Thermoelectric properties of Al-doped ZnO: Experiment and simulation." *J. Semicond.*, 37(9), 092002, 1-18.
- Jin, Z., Liao, Q., Fang, H., Liu, Z., Liu, W., Ding, Z., Luo, T., and Yang, N. (2015). "A Revisit to High Thermoelectric Performance of Single-layer  $\text{MoS}_2$ ." *Sci. Rep.*, 5, 18342.
- Jood, P., Mehta, R. J., Zhang, Y., Peleckis, G., Wang, X., Siegel, R. W., Borca-Tasciuc, T., Dou, S. X., and Ramanath, G. (2011). "Al-doped zinc oxide nanocomposites with enhanced thermoelectric properties." *Nano Lett*, 11(10), 4337–4342.
- Jung, C. S., Kim, H. S., Im, H. S., Seo, Y. S., Park, K., Back, S. H., Cho, Y. J., Kim, C. H., Park, J., and Ahn, J. P. (2013). "Polymorphism of GeSbTe superlattice nanowires." *Nano Lett.*, 13(2), 543-549.
- Kawakita, Y., Matsubara, R., Nakashima, H., and Takeda, S. (1998). "Structure of liquid In-Te mixtures." *J. Non. Cryst. Solids.*, 232-234, 483–489.
- Kim, J. H., Oh, S., Kim, Y. M., So, H. S., Lee, H., Rhyee, J. S., Park, S. D., and Kim, S. J. (2016). "Indium substitution effect on thermoelectric and optical properties of  $\text{Sn}_{1-x}\text{In}_x\text{Te}$  thin films." *J. Appl. Phys.*, 120, 045101.

$x\text{In}_x\text{Se}$  compounds.” *J. Alloys Compd.*, 682, 785–790.

Krishna Sastry, D. V., and Jayarama Reddy, P. (1983). “Optical absorption studies on InTe and InSe films.” *Solid State Commun.*, 45(2), 199–201.

Kumar, B. R., and Rao, T. S. (2011). “Studies on structural and optical properties of vacuum evaporated  $\text{In}_2\text{Te}_3$  thin films.” *Chalcogenide Lett.*, 8(2), 83–92.

Kumar, M., Vora-ud, A., Seetawan, T., and Han, J. G. (2018). “Thermoelectric power factor enhancement by pulsed plasma engineering in magnetron sputtering induced  $\text{Ge}_2\text{Sb}_2\text{Te}_5$  thin films.” *ACS Appl. Energy Mater.*, 1(8), 4025–4031.

Kunjomana, A. G., Chandrasekharan, K. A., and Teena, M. (2015a). “Physical properties of vapour grown indium monotelluride platelets.” *J. Cryst. Growth*, 411, 81–87.

Kusano, K., Yamamoto, A., Nakata, M., Suemasu, T., and Toko, K. (2018). “Thermoelectric inorganic SiGe film synthesized on flexible plastic substrate.” *ACS Appl. Energy Mater.*, 1(10), 5280–5285.

Lakshminarayana, D., Patel, P. B., Desai, R. R., and Panchal, C. J. (2002). “Investigation of thermoelectric power in indium sesquitelluride( $\text{In}_2\text{Te}_3$ ) thin films.” *J. Mater. Sci.: Mater. Electron.*, 13, 27–30.

Lee, B. S., Shelby, R. M., Raoux, S., Retter, C. T., Burr, G. W., Bogle, S. N., Darmawikarta, K., Bishop, S. G., and Abelson, J. R. (2014). “Nanoscale nuclei in phase change materials: Origin of different crystallization mechanisms of  $\text{Ge}_2\text{Sb}_2\text{Te}_5$  and  $\text{AgInSbTe}$ .” *J. Appl. Phys.*, 115, 063506.

Lee, M.-J., Ahn, J.-H., Sung, J. H., Heo, H., Jeon, S. G., Lee, W., Song, J. Y., Hong, K.-H., Choi, B., Lee, S.-H., and Jo, M.-H. (n.d.). “Thermoelectric materials by using two-dimensional materials with negative correlation between electrical and thermal conductivity.” *Nat. Commun.*, 7, 12011.

Lee, Y. M., Park, Y., Sun, C. W., Lee, J. Y., Shin, H. J., Kim, Y. T., and Jung, M. C. (2010a). “High-resolution X-ray photoelectron spectroscopy study of InTe thin film in structural phase transition from amorphous to crystalline phase.” *Thin Solid Films*,

518(15), 4442–4445.

Lee, Y. M., Park, Y., Sun, C. W., Lee, J. Y., Shin, H. J., Kim, Y. T., and Jung, M. C. (2010b). “High-resolution X-ray photoelectron spectroscopy study of InTe thin film in structural phase transition from amorphous to crystalline phase.” *Thin Solid Films*, 518(15), 4442–4445.

Li, A. H., Shahbazi, M., Zhou, S. H., Wang, G. X., Zhang, C., Jood, P., Peleckis, G., Du, Y., Cheng, Z. X., Wang, X. L., and Kuo, Y. K. (2010). “Electronic structure and thermoelectric properties of Bi<sub>2</sub>Te<sub>3</sub> crystals and graphene-doped Bi<sub>2</sub>Te<sub>3</sub>.” *Thin Solid Films*, 518, e57–e60.

Li, L., Fang, L., Zhou, X. J., Liu, Z. Y., Zhao, L., and Jiang, S. (2009). “X-ray photoelectron spectroscopy study and thermoelectric properties of Al-doped ZnO thin films.” *J. Electron Spectros. Relat. Phenomena.*, 173, 7-11.

Li, T., Pickel, A. D., Yao, Y., Chen, Y., Zeng, Y., Lacey, S. D., Li, Y., Wang, Y., Dai, J., Wang, Y., Yang, B., Fuhrer, M. S., Marconnet, A., Dames, C., Drew, D. H., and Hu, L. (2018). “Thermoelectric properties and performance of flexible reduced graphene oxide films up to 3,000 K.” *Nat. Energy*, 3(2), 148–156.

Liu, D., Li, X., Castro Borlido, P. M. De, Botti, S., Schmechel, R., and Rettenmayr, M. (2017). “Anisotropic layered Bi<sub>2</sub>Te<sub>3</sub>-In<sub>2</sub>Te<sub>3</sub> composites: Control of interface density for tuning of thermoelectric properties.” *Sci. Rep.*, 7, 43611.

Liu, D., Stotzel, J., Seyring, M., Drue, M., Li, X., Schmechel, R., and Rettenmayr, M. (2016). “Anisotropic n-Type Bi<sub>2</sub>Te<sub>3</sub>-In<sub>2</sub>Te<sub>3</sub> thermoelectric material produced by seeding zone melting and solid state transformation.” *Cryst. Growth Des.*, 16(2), 617–624.

Lv, Y., Chen, J., Zheng, R.-K., Song, J., Zhang, T., Li, X., Shi, X., and Chen, L. (2015). “Photo-induced enhancement of the power factor of Cu<sub>2</sub>S thermoelectric films.” *Sci. Rep.*, 5, 16291.

M. Bohm, O. Madelung, G. Huber, A. MacKinnon, A. Scharmann, E.-G. S. (1985). *Physics of Ternary Compounds / Physik Der Ternären Verbindungen*. (O. Madelung, ed.), Springer Science & Business Media, 1985.

- Madelung, O., Rossler, U., and Schulz, M. (Eds.). (1998). "Indium telluride (InTe) electrical and thermal conductivity: Non-Tetrahedrally Bond. Elem. Bin. Compd. I," *Springer Berlin Heidelberg*, 1–3.
- Markov, M., Hu, X., Liu, H. C., Liu, N., Poon, S. J., Esfarjani, K., and Zebarjadi, M. (2018). "Semi-metals as potential thermoelectric materials." *Sci. Rep.*, 8(1), 9876, 1–10.
- Matheswaran, P., Abhirami, K. M., Gokul, B., Sathyamoorthy, R., Prakash, J., Asokan, K., and Kanjilal, D. (2012a). "130 MeV Au ion irradiation induced dewetting on In<sub>2</sub>Te<sub>3</sub> thin film." *Appl. Surf. Sci.*, 258, 8558–8563.
- Matheswaran, P., Gokul, B., Abhirami, K. M., and Sathyamoorthy, R. (2012b). "Thickness dependent structural and optical properties of In/Te bilayer thin films." *Mater. Sci. Semicond. Process.*, 15, 486-491.
- Matheswaran, P., Sathyamoorthy, R., and Asokan, K. (2013). "Effect of 130 MeV Au ion irradiation on CO<sub>2</sub> gas sensing properties of In<sub>2</sub>Te<sub>3</sub> thin films." *Sensors Actuators B*, 177, 8–13.
- Matheswaran, P., Sathyamoorthy, R., Saravanakumar, R., and Velumani, S. (2010). "AC and dielectric properties of vacuum evaporated InTe bilayer thin films." *Mater. Sci. Eng. B Solid-State Mater. Adv. Technol.*, 174, 269-272.
- Mehdizadeh Dehkordi, A., Zebarjadi, M., He, J., and Tritt, T. M. (2015). "Thermoelectric power factor: Enhancement mechanisms and strategies for higher performance thermoelectric materials." *Mater. Sci. Eng. R Reports*, 97, 1–22.
- Miao, N., Sa, B., Zhou, J., Sun, Z., Blomqvist, A., and Ahuja, R. (2010a). "First-principles investigation on the phase stability and chemical bonding of mInSb·nInTe phase-change random alloys." *Solid State Commun.*, 150(29–30), 1375–1377.
- Naghavi, S. S., He, J., Xia, Y., and Wolverton, C. (2018). "Pd<sub>2</sub>Se<sub>3</sub> monolayer: a promising two dimensional thermoelectric material with ultralow lattice thermal conductivity and high power factor." *Chem. Mater.*, 30, 5639–5647.
- Nukala, P., Agarwal, R., Qian, X., Jang, M. H., Dhara, S., Kumar, K., Johnson, A. T.

- C., Li, J., and Agarwal, R. (2014). "Direct observation of metal-insulator transition in single-crystalline Germanium telluride nanowire memory devices prior to amorphization." *Nano Lett.*, 14(4), 2201-2204.
- Ohuchi, F. S., and Olmstead, M. A. (1999). "III–VI Semiconductors." J. Webster. *Wiley Encyclopedia. Elec. Eltron. Engg.*, 147-158.
- Owens, A. (2016). "Compound semiconductor radiation detectors series in sensors," *Taylor & Francis.*, 567.
- P. N. Lebedeva Moskva. (1988). "Stoichiometry in crystal compounds and its influence on their physical properties." (I. M. Popov, ed.), *Nova Publishers.* 1-35.
- Pena, J. L. (2001). "Grown of InTe films by close spaced vapor transport." *superficies y vacio.*, 553(1), 69–71.
- Peranantham, P., Jeyachandran, Y. L., Viswanathan, C., Praveena, N. N., Chitra, P. C., Mangalaraj, D., and Narayandass, S. K. (2007a). "The effect of annealing on vacuum-evaporated copper selenide and indium telluride thin films." *Mater. Charact.*, 58, 756-764.
- Puneet, P., Podila, R., Karakaya, M., Zhu, S., He, J., Tritt, T. M., Dresselhaus, M. S., and Rao, A. M. (2013). "Preferential scattering by interfacial charged defects for enhanced thermoelectric performance in few-layered n-type Bi<sub>2</sub>Te<sub>3</sub>." *Sci. Rep.*, 3, 3212.
- Purkayastha, S. De, Mukherjee, J. K., and Bose, D. N. (1980). "The influence of the substrate temperature on the properties of thin film In<sub>2</sub>Te<sub>3</sub>." *Thin Solid Films*, 74, 219–222.
- Qin, D., Yan, P., Ding, G., Ge, X., Song, H., and Gao, G. (2018). "Monolayer PdSe<sub>2</sub>: A promising two-dimensional thermoelectric material." *Sci. Rep.*, 8(1), 2764.
- Reshmi, P. M., Kunjomana, A. G., Chandrasekharan, K. A., and Teena, M. (2014). "Vapour growth and characterization of beta indium sesquitelluride crystals." *J. Cryst. Growth.*, 394, 1-6.
- Rosenberg, A. J., and Strauss, A. J. (1961). "Solid solutions of In<sub>2</sub>Te<sub>3</sub> in Sb<sub>2</sub>Te<sub>3</sub> and Bi<sub>2</sub>Te<sub>3</sub>." *J. Phys. Chem. Solids.*, 9(1-2), 105-116.

- Rousina, R., and Yousefi, G. H. (1990). "Experimental study of optical absorption in  $\text{In}_2\text{Te}_3$  thin films ." *Mater. Latt.*, 9(7-8), 263-265.
- Rousina, R., and Shivakumar, G. K. (1988b). "Growth and characterization of indium telluride thin films." *Thin Solid Films*, 157, 345–350.
- Rousina, R., and Shivakumar, G. K. (1989). "Electron diffraction study of vacuum-deposited  $\text{In}_2\text{Te}_3$  thin films." *Surf. Coatings Technol.*, 38, 353-358.
- Rousina, R., Shivakumar, G. K., and Yousefi, G. H. (1990). "Optical absorption of as-deposited indium selenide thin films." *Vacuum.*, 41(4-6), 1451-1453.
- Rowe, D. M. (2012). "Modules, Systems, and Applications in Thermoelectrics. Thermoelectrics and Its Energy Harvesting", *CRC Press*.
- Roy, S., Banerjee, A., Mawkhlieng, B., Misra, A. K., Pattanayak, A., Harish, G. D., Singh, S. K., Ngachan, S. V., and Bansal, K. C. (2015). "Genetic diversity and population structure in aromatic and quality rice (*Oryza sativa* L.) landraces from North-eastern India." *PLoS One*, 10(6), 103357–103363.
- Sastry, D. V. K., and Reddy, P. J. (1980). "Electrical properties of flash evaporated thin films of  $\text{InTe}$ ." *Phys. Status Solidi*, 58(1), 213–218.
- Sathyamoorthy, R., Matheswaran, P., and Asokan, K. (2012). "Synthesis of  $\alpha\text{-In}_2\text{Te}_3$  thin films from  $\text{In/Te}$  bilayer by Si ion irradiation." *Radiat. Eff. Defects Solids*, 167(11), 799–806.
- Satyala, N., Tahmasbi Rad, A., Zamanipour, Z., Norouzzadeh, P., Krasinski, J. S., Tayebi, L., and Vashaee, D. (2014). "Reduction of thermal conductivity of bulk nanostructured bismuth telluride composites embedded with silicon nano-inclusions." *J. Appl. Phys.*, 115(4).
- Seyam, M. A. M. (2001). "Dielectric relaxation in polycrystalline thin films of  $\text{In}_2\text{Te}_3$ ." *Appl. Surf. Sci.*, 181, 128-138.
- Singh, M., Arora, J. S., Vijay, Y. K., and Sudharshan, M. (2006). "Optical, electrical and thermoelectric power studies of  $\text{Al-Sb}$  thin film bilayer structure." *Bull. Mater. Sci*, 29(1), 17–20.

Slack, G. A. (1995). “New materials and performance limits for thermoelectric cooling.” *Thermoelectr. Handb.*, 407-422.

Sowjanya, V., Bangera, K. V., and Shivakumar, G. K. (2017a). “Structural, electrical and optical properties of stoichiometric  $\text{In}_2\text{Te}_3$  thin films.” *Ceram. Int.*, 43, 3748-3751.

Sowjanya, V., Bangera, K. V., and Shivakumar, G. K. (2017c). “Effect of substrate temperature and film thickness on the thermoelectric properties of  $\text{In}_2\text{Te}_3$  thin films.” *J. Alloys Compd.*, 715, 224–229.

Sugiyama, Y., Chiba, R., Fujimori, S., and Funakoshi, N. (1990). “Crystallization process of InTe alloy films for optical recording.” *J. Non. Cryst. Solids*, 122(1), 83–89.

Tai, G, Miao, C., Wang, Y., Bai, Y., Zhang, H., and Guo, W. (2011). “Solvothermal synthesis and thermoelectric properties of indium telluride nanostring-cluster hierarchical structures.” *Nanoscale Res. Lett.*, 6, 329.

Tan, G., Zeier, W. G., Shi, F., Wang, P., Snyder, G. J., Dravid, V. P., and Kanatzidis, M. G. (2015). “High Thermoelectric Performance  $\text{SnTe-In}_2\text{Te}_3$  Solid Solutions Enabled by Resonant Levels and Strong Vacancy Phonon Scattering.” *Chem. Mater.*, 27(22), 7801-7811.

Tang, J., Gao, B., Lin, S., Wang, X., Zhang, X., Xiong, F., Li, W., Chen, Y., and Pei, Y. (2018). “Manipulation of Solubility and Interstitial Defects for Improving Thermoelectric  $\text{SnTe}$  Alloys.” *ACS Energy Lett.*, 3(8), 1969–1974.

Urmila, K. S., Namitha, T. A., Philip, R. R., and Pradeep, B. (2015). “Optical and low-temperature thermoelectric properties of phase-pure p-type  $\text{InSe}$  thin films.” *Appl. Phys. A Mater. Sci. Process.*, 120, 675-681.

Volovichev, I. N., Gurevich, Y. G., and Koshkin, V. M. (1998). “Reliable rectifiers and photovoltaic converters for high levels of ionizing irradiation.” *Microelectronics J.*, 29, 535–542.

Wang, X.-Y., Wang, H.-J., Xiang, B., Fu, L.-W., Zhu, H., Chai, D., Zhu, B., Yu, Y., Gao, N., Huang, Z.-Y., and Zu, F.-Q. (2018a). “Thermoelectric performance of  $\text{Sb}_2\text{Te}_3$  based alloys is improved by introducing PN junctions.” *ACS Appl. Mater. Interfaces*,



10(27), 23277–23284.

Wang, Z., Wang, G., Wang, R., Zhou, X., Chen, Z., Yin, C., Tang, M., Hu, Q., Tang, J., and Ang, R. (2018b). “Ga-doping-induced carrier tuning and multiphase engineering in n-type PbTe with enhanced thermoelectric performance.” *ACS Appl. Mater. Interfaces*, 10(26), 22401–22407.

Xiong, F., Bae, M. H., Dai, Y., Liao, A. D., Behnam, A., Carrion, E. A., Hong, S., Ielmini, D., and Pop, E. (2013). “Self-aligned nanotube-nanowire phase change memory.” *Nano Lett.*, 13(2), 464-469.

Yamanaka, S., Ishimaru, M., Charoenphakdee, A., Matsumoto, H., and Kurosaki, K. (2009). “Thermoelectric characterization of (Ga,In)<sub>2</sub>Te<sub>3</sub> with self-assembled two-dimensional vacancy planes.” *J. Electron. Mater.*, 38(7), 1392–1396.

Yan, X., Zheng, W., Liu, F., Yang, S., and Wang, Z. (2016). “Thickness effects for thermoelectric property of antimony telluride nanoplatelets via solvothermal method.” *Sci. Rep.*, 6, 37722.

Yuan, Y., Liu, C., Su, J., Cheng, L., Fang, J., Zhang, X., Sun, Y., Wu, Y., Zhang, H., and Li, J. (2018). “Structural and optical properties of Ti-doped InTe thin films.” *J. Phys. Chem. C*, 122(11), 6267–6272.

Zahab, A. A., Abd-Lefdil, M., and Cadene, M. (1990). “Electrical conductivity, optical absorption, and photoconductivity measurements of well oriented indium telluride thin films.” *Short Notes K103 phys. stat. sol.*, 117.

Zhang, L., Song, S., Xi, W., Li, L., He, Y., Lin, H., and Song, Z. (2015). “Local structure of AlSb<sub>2</sub>Te<sub>3</sub> thin film studied by experimental and theoretical methods.” *J. Phys. Chem. Solids*, 83, 52–57.

Zhou, J., Zhu, H., Liu, T. H., Song, Q., He, R., Mao, J., Liu, Z., Ren, W., Liao, B., Singh, D. J., Ren, Z., and Chen, G. (2018). “Large thermoelectric power factor from crystal symmetry-protected non-bonding orbital in half-Heuslers.” *Nat. Commun.*, 9(1), 1–9.

Zhou, L., Yan, S., Lu, T., Shi, Y., Wang, J., and Yang, F. (2014). “Indium telluride

nanotubes: Solvothermal synthesis, growth mechanism, and properties.” *J. Solid State Chem.*, 211, 75-80.

## PUBLICATIONS

### **PUBLICATIONS IN INTERNATIONAL JOURNALS:**

1. Sowjanya, V., Kasturi, V. B. and Shivakumar, G. K. (2016). "Structural, electrical and optical properties of stoichiometric In<sub>2</sub>Te<sub>3</sub> thin films." *Ceram Int.*, 43, 3748-3751. doi.org/10.1016/j.ceramint.2016.12.008.
2. Sowjanya, V., Kasturi, V. B. and Shivakumar, G. K. (2017). "Effect of substrate temperature and film thickness on the thermoelectric properties of In<sub>2</sub>Te<sub>3</sub> thin films." *J. Alloys Compd.*, 715, 224-229. doi.org/10.1016/j.jallcom.2017.04.312.
3. Sowjanya, V., Kasturi, V. B. and Shivakumar, G. K. (2019). "Synthesis of single-phase and stoichiometric InTe thin films for opto-electronic applications." *Superlattice Microst.*, 129, 220-225. doi.org/10.1016/j.spmi.2019.03.007. doi.org/10.1016/j.spmi.2019.03.007.
4. Sowjanya, V., Kasturi, V. B. and Shivakumar, G. K. (2019). "Enhanced thermoelectric power of Al and Sb doped In<sub>2</sub>Te<sub>3</sub> thin films." *Mater. Sci. Semiocond. Process.*, 93, 366-370. doi.org/10.1016/j.mssp.2019.01.025.
5. Sowjanya, V., Kasturi, V. B. and Shivakumar, G. K. (2019). "Drastic increase in thermoelectric power factor of mixed Sb<sub>2</sub>Te<sub>3</sub>- In<sub>2</sub>Te<sub>3</sub> thin films." *Superlattice Microst.*, 131, 15-20. doi.org/10.1016/j.spmi.2019.05.036.

### **CONFERENCE PROCEEDINGS:**

1. Sowjanya, V., Kasturi, V. B. and Shivakumar, G. K. (2018). " Effect of annealing and substrate temperatures on the structural properties of In<sub>2</sub>Te<sub>3</sub> thin films." *Advanced. Science Letters.*, 24(8), 5611-5613. doi.org/10.1166/asl.2018.12160

# Vallem Sowjanya

Ph.+91 9964295899

Email: [v.sowjanya1199@gmail.com](mailto:v.sowjanya1199@gmail.com)

---

---

## Academic Qualifications:

2011-2013 M.Sc. (Condensed matter Physics)

Sri Venkateswara University, Tirupathi,

Andhra Pradesh, India.

2014-2019 Ph.D. (Physics, Semiconductor thin films) (Pursuing)

National Institute of Technology Karnataka,

Manglore-575025, Karnataka, India.

## Skills and Activities:

*Skills:* Physical vapour deposition, Material Characterization; X-ray Diffraction (XRD), Scanning Electron Microscopy (SEM), Transmission Electron Microscopy (TEM), Optical and Electrical properties, Thermoelectric properties.

*Softwares:* Origin and Image-J

*Languages:* Telugu, English and Kannada

---

---

## Papers published in International Journals:

1. Sowjanya, V., Kasturi, V. B. and Shivakumar, G. K. (2016). "Structural, electrical and optical properties of stoichiometric  $\text{In}_2\text{Te}_3$  thin films." *Ceram Int.*, 43, 3748-3751. doi.org/10.1016/j.ceramint.2016.12.008.
2. Sowjanya, V., Kasturi, V. B. and Shivakumar, G. K. (2017). "Effect of substrate temperature and film thickness on the thermoelectric properties of

- In<sub>2</sub>Te<sub>3</sub> thin films.” *Journal of Alloys and Compounds.*,715, 224-229.  
doi.org/10.1016/j.jallcom.2017.04.312.
3. Sowjanya, V., Kasturi, V. B. and Shivakumar, G. K. (2018).” Effect of annealing and substrate temperatures on the structural properties of In<sub>2</sub>Te<sub>3</sub> thin films.” *Advanced. Science Letters.*, 24(8), 5611-5613.  
doi.org/10.1166/asl.2018.12160
  4. Sowjanya, V., Kasturi, V. B. and Shivakumar, G. K. (2019). “Synthesis of single-phase and stoichiometric InTe thin films for opto-electronic applications.” *Superlattice Microst.*, 129, 220-225.  
doi.org/10.1016/j.spmi.2019.03.007. doi.org/10.1016/j.spmi.2019.03.007.
  5. Sowjanya, V., Kasturi, V. B. and Shivakumar, G. K. (2018).” Enhanced thermoelectric power of Al and Sb doped In<sub>2</sub>Te<sub>3</sub> thin films.” *Materials Science in Semiconducting Processing.*, 93, 366-370.  
doi.org/10.1016/j.mssp.2019.01.025
  6. Sowjanya, V., Kasturi, V. B. and Shivakumar, G. K. (2019). “ Drastic increase in thermoelectric power factor of mixed Sb<sub>2</sub>Te<sub>3</sub>- In<sub>2</sub>Te<sub>3</sub> thin films.” *Superlattice Microst.*, 131, 15-20. doi.org/10.1016/j.spmi.2019.05.036.
  7. Sowjanya, V., Kasturi, V. B. and Shivakumar, G. K. (2019). “ A significant enhancement in thermoelectric power factor of In<sub>2</sub>Te<sub>3</sub> thin films by doping.” *J. Mater. Sci.: Mater. Electron.* (Under review).

**Research papers presented in national and International conferences:**

Sowjanya, V., Kasturi, V. B. and Shivakumar, G. K. (2016).” Preparation and characterization of In<sub>2</sub>Te<sub>3</sub> thin films.” CAMP-2016, MIT, Karnataka, India.

Sowjanya, V., Kasturi, V. B. and Shivakumar, G. K. (2016). “Effect of annealing and substrate temperatures on structural properties of In<sub>2</sub>Te<sub>3</sub> thin films.” ICNAN-2016, VIT, Vellore, Tamil Nadu, India.

### **Workshops attended:**

1. TEQIP-II sponsored workshop on “**Research Methodology and Structural equation modelling.**” NITK, Surathkal, Karnataka, India, held on 16<sup>th</sup> November, 2014.
2. Two-day Workshop on “**Scanning Probe Microscopy and High Resolution Transmission Electron Microscopy and Scanning Probe Microscopy.**” PSG Institute of advanced studies, Coimbatore, Tamil Nadu, India, during 21<sup>st</sup>-22<sup>th</sup> August 2015.
3. MHRD sponsored Global initiative for academic networks (GIAN)-workshop on “**Novel Functional Materials for Energy Conversion.**” MHRD, NITK, Surathkal, Karnataka, India, During 4<sup>th</sup>-7<sup>th</sup> October, 2016.
4. Workshop on “**Nano-Structured Materials and their Application in Catalysis & Fuel Cells (NMCF-2016).**” Department of Chemical Engineering, NITK, Surathkal, Karnataka, India, during 29<sup>th</sup> September to 1<sup>st</sup> October, 2016.

---

---

### **Awards:**

Gold medal in M. Sc. Physic

---

---

### **Permanent Address:**

D/O V. Santi Reddy,  
Chinnadudyala (V&P), Muddanur (M),  
Kadapa (D), Pin:516380, AP, India.

### **Current Address:**

House no. 123, 14<sup>th</sup> main, 6<sup>th</sup> cross, BTM layout,  
1<sup>st</sup>stage, Bangalore-560029, KA, India.